Optical tweezers in concentrated colloidal dispersions | Manipulating and imaging individual particles

Optical tweezers in concentrated colloidal dispersions | Manipulating and imaging individual particles

---

Een pincet van licht in geconcentreerde colloïdale dispersies | Manipulatie en afbeelden van individuele deeltjes

(Met een samenvatting in het Nederlands)

Proefschrift ter verkrijging van de graad van doctor aan de Universiteit Utrecht op gezag van de Rector Magnificus, Prof. dr. W.H. Gispen, ingevolge het besluit van het College voor Promoties in het openbaar te verdedigen op maandag 22 november 2004 des namiddags te 16.15 uur.

door **Dirk Leo Joep Vossen**
geboren op 29 januari 1975 te Weert

Promotor **Prof. dr. Alfons van Blaaderen**

Verbonden aan de Faculteit Natuur- en Sterrenkunde van de Universiteit Utrecht

The work described in this thesis is part of the research program of the "Stichting Fundamenteel Onderzoek der Materie (FOM)", which is financially supported by the "Nederlandse Organisatie voor Wetenschappelijk Onderzoek (NWO)".

It was initiated at the

FOM Institute for Atomic and Molecular Physics (AMOLF), Kruislaan 407, 1098 SJ Amsterdam, The Netherlands,

and was completed at

Universiteit Utrecht

Debye Institute, Utrecht University, Princeton Plein 5, 3584 CC, Utrecht, The Netherlands.

A digital version of this thesis can be downloaded from http://www.colloid.nl

ISBN 90-393-3881-7

Contents

1. Introduction 12

1.1 Introduction to optical tweezers 13

1.2 Theory of optical tweezers 14

1.2.1 The Rayleigh regime ($R << \lambda$) 15

1.2.2 The ray optics regime ($R >> \lambda$) 16

1.2.3 The Mie regime 16

1.2.4 Additional forces on a particle in optical tweezers 17

1.3 Basic optical tweezers design 17

1.4 Position control of optical tweezers 19

1.5 Trapping and manipulating particles using optical tweezers 21

1.6 Measuring and exerting forces using optical tweezers 22

1.7 Colloidal particles and optical tweezers 23

1.8 Layout of the rest of this thesis 26

References 26

2. Optical tweezers and confocal microscopy for simultaneous three-dimensional manipulation and imaging in concentrated colloidal dispersions 30

2.1 Introduction 31

2.2 Experimental 33

2.2.1 Upright, inverted, and counterpropagating optical tweezers arrays 33

2.2.2 Arrays of tweezers in more than one plane using one objective 36

2.2.3 Imaging modes 38

2.2.4 Colloidal dispersions 39

2.3 Dynamic arrays of optical tweezers 40

2.4 Optical trapping and decoupled confocal imaging 43

2.5 Arrays of tweezers in more than one plane using one objective 45

2.6 Optical tweezers in concentrated dispersions 46

2.6.1 Tweezers-induced crystallization in concentrated colloidal dispersions 46

2.6.2 Manipulation of (core-shell) tracer particles in a concentrated dispersion 48

2.7 Counterpropagating tweezers 50

2.8 Discussion and outlook 51

References 53

3. Patterning surfaces using optical tweezers and critical point drying 56
3.1 Introduction 57
3.2 Experimental details 58
3.3 Results and discussion 60
3.4 Conclusions and outlook 66
References 66

4. Combined optical tweezers/ion beam technique to tune colloidal masks for nanolithography 68
4.1 Introduction 69
4.2 Experimental details 69
4.3 Results and discussion 71
4.4 Conclusions and outlook 76
References 77

5. Chemical modification of colloidal masks for nanolithography 80
5.1 Introduction 81
5.2 Experimental details 82
5.3 Results and discussion 83
5.4 Conclusions and outlook 87
References 87

6. Colloidal crystallization induced by optical gradient forces exerted by optical tweezers 90
6.1 Introduction 91
6.2 Experimental details 92
6.2.1 Optical tweezers and independent three-dimensional imaging 92
6.2.2 Colloidal dispersions 93
6.3 Results and discussion 95
6.3.1 Optical gradient forces induced near a wall 95
6.3.2 Optical gradient forces induced in the bulk 98
6.3.3 Mixtures of tracer and host spheres 100
6.4 Conclusions and outlook 102
References 103

7. Colloidal crystallization induced via single particle control with optical tweezers 106
7.1 Introduction 107
7.2 Experimental details 109
7.3 Results and discussion 111
7.4 Conclusions and outlook 119
References 121

8. Defect formation induced by a particle driven through a three-dimensional colloidal crystal 122
8.1 Introduction 123
8.2 Experimental details 123
8.3 Results and discussion 125
8.4 Conclusions and outlook 129
References 130

Summary 132

Samenvatting 136

Dankwoord 140

Curriculum Vitae 142

List of publications 143

1 Introduction

Using a laser beam that is focused down to a diffraction-limited spot, particles with a size ranging from several nanometers up to tens of micrometers can be trapped and manipulated. These so-called optical tweezers have been used in a wide variety of (interdisciplinary) fields and their use is expanding fast. Recent improvements allow for new exciting and promising applications. In this chapter we will give an overview of the history, the theory, some basic design considerations, and some (recent) applications of optical tweezers. Colloidal dispersions and their applications are introduced, both as a model system and for designing advanced materials. We then show how a mixture of core-shell colloidal particles allows simultaneous three-dimensional trapping and imaging of individual particles inside a concentrated dispersion. Finally, an overview of the rest of this thesis is given.

1.1 Introduction to optical tweezers

In the late sixties of the twentieth century, Arthur Ashkin realized that a slightly focused laser beam could draw objects, with a refractive index higher than the surrounding medium, towards the center of the beam.[1, 2] On the optical axis, the particles were confined and propelled in the direction of light propagation. He demonstrated optical guiding of particles suspended in a liquid and in air and trapped particles by balancing the radiation pressure with the gravitational forces in an inverted geometry. He also showed three-dimensional confinement of particles using counterpropagating laser beams.[1] The single-beam gradient optical tweezers were first demonstrated in 1986 by Ashkin, Chu, and coworkers.[3] Since then, there has been a continuous stream of new developments and applications. Over the last few years, the technique has become mature, and optical tweezers are an important tool in fields like biology, physical chemistry, and (bio)physics.[4-7]

A single-beam gradient trap can be created by focusing a laser beam to a diffraction-limited spot using a high numerical aperture (NA) objective. The strong light gradient near the focus creates a potential well, in which a particle with a refractive index higher than that of the surrounding medium is trapped in three-dimensions. Dielectric particles, small metal particles as well as living materials, with sizes ranging from several nanometers to tens of micrometers, can be trapped and manipulated using optical tweezers. If there is no difference in refractive index between the particle and its surroundings, there are no optical forces exerted on the particle. If the refractive index of the particle is lower than that of the medium, the particle is expelled from the trapping beam.

The physics behind optical tweezers has been known for a long time. In 1619, Johannes Kepler explained that a comets tail always points away from the sun because of the radiation pressure of sunlight. At the end of the nineteenth century, James Clerk Maxwell predicted theoretically that light can exert a force on matter. In 1908, Mie calculated the light scattered by a spherical isotropic particle illuminated by a plane wave.[8] Although Lorentz, Debye, and others also worked on the problem, the solution is now commonly known as Mie theorie. Mie extended the work of Rayleigh on scattering of small particles to explain the colors of gold sols. Some of these sols, which were prepared by Faraday, are still stable today. The existence of radiation pressure was demonstrated experimentally in the first decade of the twentieth century by Peter Lebedev in a series of experiments that showed

that parallel plates in vacuum rotated when they were illuminated with light.[8]

The first demonstration of the single-beam gradient trap or optical tweezers opened up many new and exciting experiments. Ashkin and Chu had also been working on trapping and manipulating atoms.[9] In 1997, Steven Chu received the Nobel Prize in Physics "for development of methods to cool and trap atoms with laser light". Ashkin continued working on optical tweezers, and by showing that it is possible to trap living cells while keeping them alive, he introduced a new noninvasive technique for manipulation in biology. Biologists were the first to realize and use the potential of optical tweezers for handling and manipulating small particles. Only later on, physicists and chemists "rediscovered" the optical tweezers and extended their use further.

In this thesis we focus on the use of optical tweezers acting on colloidal particles. There are many excellent review papers that give an overview of optical tweezers, the theory of optical tweezers, their construction, their application, and recent developments.[4, 7, 10, 11]

1.2 Theory of optical tweezers

For a particle in a tightly focused laser beam, the forces on the particle can be decomposed into a "gradient force" in the direction of highest light intensity, and a "scattering force" directed along the optical axis. Note, that this separation in two forces is artificial as momentum is transferred from the trapping laser beam to the particle by scattering of laser light. However, the distinction between a gradient and a scattering force is intuitively simple and under certain conditions correct.

A particle is trapped at the point where the gradient and scattering forces balance, if the maximal restoring force of the trap is large enough to overcome the effective weight and thermal fluctuations of the particle. The calculation of optical forces on a particle is relatively straightforward in the regimes where a particle is either much smaller[12] (Rayleigh) or much larger[13] (ray optics) than the wavelength used for trapping. The general calculation of the optical forces on a particle in a trap is more challenging.[14] Quantitative calculations are still lagging behind experiment, and for most applications the optical tweezers are experimentally characterized and calibrated before they are used for quantitative measurements.

Each photon in the trapping beam has an energy of $h\lambda$ and a momentum of h/λ. A particle can gain momentum from a trapping beam

through refraction, reflection, or absorption of photons. If totally absorbed by an object, a light beam of power P exerts a force on the object of

$$F = \frac{n_m P}{c}, \qquad (1.1)$$

in which n_m is the refractive index of the surrounding medium and c is the speed of light in vacuum. The efficiency of an optical trap can be described in terms of a dimensionless quantity Q, where the force generated by the trapping beam on the particle is given by

$$F = Q\frac{n_m P}{c}. \qquad (1.2)$$

1.2.1 The Rayleigh regime ($R >> \lambda$)

When the radius (R) of a particle is much smaller than the wavelength of the trapping laser, the optical forces on the particle can be calculated by treating the particle as an induced point dipole that scatters light elastically. The trapping light exerts a scattering force on the induced dipole as it absorbs and reradiates light from the trapping beam. The scattering force exerted on the particle is given by

$$F_{scatt} = \frac{158\pi^5 R^6}{3\lambda^4}\left(\frac{m^2 - 1}{m^2 + 2}\right)^2 \frac{n_m I_o}{c}, \qquad (1.3)$$

in which R is the radius of the particle, λ is the wavelength of the trapping laser in the surrounding medium and m is the ratio of the refractive indices of the particle and the surrounding medium, n_m is the refractive index of the surrounding medium, I_o is the intensity of the field, and c is the speed of light in vacuum. The scattering force acts in the direction of the light beam and pushes particles along the optical axis. The scattering force depends strongly on the size of a particle and on the wavelength of the trapping laser.

If the induced dipole is in an electromagnetic field with an intensity gradient, it experiences a (Lorenz) force, which is given by

$$F_{grad} = \frac{2\pi n_m R^3}{c}\left(\frac{m^2 - 1}{m^2 + 2}\right) \nabla I_o, \qquad (1.4)$$

The gradient force is directed towards the region with highest light intensity and accounts for trapping in the lateral as well as in the axial direction. In the Rayleigh regime, the scattering force increases stronger with the radius (R) of the particle than the gradient force and therefore the optical trap becomes unstable for larger particles.

1.2.2 The ray optics regime ($R >> \lambda$)

When the radius (R) of a particle is much larger than the wavelength of the trapping laser, the forces on a particle can be described using ray optics, as was done by Ashkin in 1992.[15] When a light ray, traveling in a medium with refractive index n_m, impinges on a dielectric sphere with refractive index n_p, the light ray is refracted according to Snell's law. The light ray is again refracted when it leaves the particle. The momentum of the light ray is changed because of refraction by the particle. This change in momentum is transferred to the particle because momentum is conserved. A light beam is described as a collection of light rays and each individual ray is weighted according to its intensity. The contributions of all rays are summed to calculate the total optical force on a particle. When a particle has a refractive index higher than the surrounding medium ($n_p / n_m > 1$) and is in an intensity gradient, the gradient force on a particle is in the direction of the highest intensity. The particle is confined (trapped) in all directions in a three-dimensional intensity gradient. In the calculations, the light scattered and reflected from the surface of a particle can be taken into account too. The external rays of a light beam contribute relatively much more to the gradient force, while the central rays contribute more to the scattering force.

1.2.3 The Mie regime

While the description of optical forces is simple in the two limiting cases described above, optical tweezers are almost always used to trap particles that have a size comparable to the wavelength of the trapping light. The scattering of a plane wave by a spherical particle can be calculated exactly using Mie theorie. The problem is to calculate the scattering of the electromagnetic field near the focus of a high NA objective. Only recently, theories have been developed to calculate the optical forces on particles in an optical trap. A general and powerful approach is to solve the Maxwell equations numerically using a finite-difference-time-domain (FDTD) method or a finite-element method (FEM).[16] These methods are relatively slow as they

discretize the volume of the particle and some of its surroundings. Maia Neto *et al.* have developed a theory applicable to spherical particles. They used a Debye-type integral description of the electromagnetic field near the focus and Mie scattering to calculate the force on a particle.[14, 17] The T-matrix formalism has also been used to calculate forces on anisotropic particles in focused (higher-order) laser beams.[18]

1.2.4 additional forces on a particle in optical tweezers

Not only optical forces act on a particle in an optical trap, but also other forces can be present. When absorption occurs, either by the solvent or by the particle, heating of the sample can occur. Although most particles used in optical tweezers are transparent and have low absorption, there is always some heating in the sample. Peterman *et al.* measured a temperature increase of 8 K/W, for 500 nm diameter silica particles trapped in water using 1064 nm laser light.[19] In our refractive index matching experiments in core-shell mixtures, we found that we could estimate the local heating by changing the matching conditions as a function of temperature (chapter 7). Other forces that act on the particles are the thermal fluctuations, which give rise to Brownian motion, and buoyant forces when particles are not density matched by the solvent.

1.3 Basic optical tweezers design

Building a simple optical tweezers system is relatively straightforward. Practical and basic systems for undergraduate laboratories, costing a few thousand dollars, have been described.[20] Optical tweezers are now also commercially available. Arryx, Cell Robotics, and PALM Microlaser Technologies are a few companies that manufacture optical tweezers systems. Many different types of more advanced optical tweezers have been described in the literature (see also chapter 2). [4, 7, 10]

Some properties of the trapping laser are important to consider: a high power and single mode output, a good pointing stability, and low power fluctuations. Infrared lasers are often used in biological samples. Laser light with a wavelength between 900 and 1200 nm has relatively low absorption and scattering in biological material and therefore, damage to the sample is limited. For combination of optical trapping with confocal microscopy, as in our setup (chapter 2), the wavelength of the trapping laser has to be separated from the excitation and emission wavelengths of the fluorescent dyes used for confocal imaging. Many different lasers have

been used for optical trapping: (diode-pumped) Nd:YAG, Nd:YLF, or Nd:YVO_4, but also Ar-ion, HeNe, diode, vertical cavity surface emitting, and even femtosecond lasers.[4, 7, 10, 11]

To create the high intensity gradients required for three-dimensional optical trapping, high NA objectives are needed. Lower NA objectives will confine particles on the optical axis, but they will not trap a particle near the focus. A high transmittance of the trapping laser light is also important. As trapping performance is sensitive to aberrations,[21] especially along the optical axis, often plan apochromat oil immersion lenses are used. These objectives provide excellent optical trapping performance and high-resolution imaging when they are used in samples with a small or no refractive index mismatch between the solvent and the microscope cover slip (as in chapters 2, 6, 7, and 8). In many applications, however, the refractive index mismatch between the solvent and the cover slip is large and it introduces aberrations that depend strongly on the distance from the cover slip.[21] In these samples, water immersion lenses are much more suited as they are specially designed to minimize aberrations in aqueous samples. For trapping, and imaging, of particles in a solvent that has a refractive index close to silica (chapter 2), glycerol immersion objectives minimize aberrations.

Many optical tweezers systems are based on modified commercial microscopes. An inverted microscope is often used because buoyant forces on a particle can counteract the scattering force to obtain better trapping along the optical axis in this geometry. In almost all optical tweezers systems, the objective used for trapping is also used for imaging. The laser is coupled into the objective using a dichroic mirror that is chosen so that it reflects the trapping laser and transmits the light used for imaging. To create space for the dichrioc mirror, the revolver holding the objectives is often replaced by a custom-built holder for the objective. Brightfield imaging, differential interference contrast (DIC) and (epi-) fluorescence imaging in combination with a charge-coupled device CCD camera are often used for imaging. Confocal imaging allows for higher resolution, compared to conventional microscopy, as well as three-dimensional imaging of the sample because pinholes are used in front of the light source and detector.[22] When one objective is used for trapping and imaging, the trapping and imaging planes are coupled to each other.

Optical tweezers systems are normally built on a vibration isolation table to reduce mechanical vibration in the setup. Furthermore, optical

tweezers systems are designed with robust solid parts and with the beam path not too far from the surface of the optical table. When high accuracy measurements are needed, the beam path can be enclosed to exclude air currents as a source of instability.

1.4 Position control of optical tweezers

A laser beam that is collimated parallel to the optical axis, and is focused using an, infinity corrected, high NA objective, creates an optical trap in the middle of the focal plane of the objective. When the angle of incidence of the trapping beam at the back focal plane is changed, the optical trap is translated in the trapping plane. When the collimated beam is made divergent, its focus is deeper in the sample. The trapping plane is then behind the front focal plane, the imaging plane, of the objective. A convergent beam is focused before the focal plane of the objective. Combining rotation and change in divergence of the trapping beam in the back focal plane results in three-dimensional position control over the optical tweezers in the sample. Note that only for a collimated laser beam, the trapping plane and focal (or imaging) plane coincide. When the trapping beam is divergent or convergent, the two planes are separated in the axial direction.

Maybe the simplest design to control the position of an optical trap in the sample is by having a collimated laser beam incident on lens *L1*, which is imaged onto the back aperture of the microscope objective using lens *L2*. Because the back focal plane of the microscope objective and *L1* are in conjugate planes, a displacement of *L1* orthogonal to the optical axis results in a displacement of the optical trap in the trapping plane, orthogonal to the optical axis. A translation of *L1* along the optical axis changes the divergence of the laser beam in the back focal plane, resulting in an optical trap deeper in the sample. Having lens *L1* on an *xyz* translation stage is a simple, robust, and easy to use method for position manipulation of optical tweezers. It is possible to create several conjugate planes, and each plane can be used to manipulate the trap position in the sample.

Apart from simply moving a lens in a plane conjugate to the back focal plane of the objective, more sophisticated methods have been developed to control the position of the optical trap in the sample. Most of them are able to control the position of an optical trap in a single plane, while some of them can also change the axial position of the trapping plane.

When several trapping beams enter the back aperture of the microscope objective simultaneously, multiple optical traps are created. Using more than one trapping laser or by splitting a laser beam in several beam paths, multiple tweezers have been created. Although conceptually simple, the number of optical traps that can be created is limited. Several more advanced methods have been developed to create multiple (or arrays of) optical tweezers starting from a single laser beam. In all methods, the active devices are placed in a plane conjugate to the back focal plane of the microscope objective. There are two different approaches: methods that time-share and methods that intensity-share the trapping beam between different positions in the sample.

Using galvano-scanning mirrors, arrays of optical traps have been created. [23] It is a low-cost option for slow-scanning applications. Feedback corrected piezoelectric systems have also been used to create arrays of optical tweezers using scanning mirrors.[24] Due to the mechanical inertia of the mirrors, the maximum number of optical traps demonstrated is in the order of ten.

Acousto-optic deflectors (AODs) have been used to create large two-dimensional arrays of traps that could be changed dynamically.[4] The AODs contain a crystal, in which a sound wave sets up a density variation that can diffract the trapping laser beam. The frequency and the amplitude of the sound wave determine the diffraction angle and efficiency, respectively. Large arrays of optical tweezers can be created that can be changed dynamically. The method is described in detail in chapter 2. In combination with a Pockells cell, an electro-optic modulator, AODs can also be used to create arrays of optical traps in two planes separated in the direction along the axis (chapters 2 and 7).

Interference of specially designed light beams[25, 26] has also been used to create arrays of optical tweezers, although large patterns can be made, the flexibility and control of single traps are limited.

Furthermore, it is possible to diffract the trapping laser beam using a diffractive optical element.[27-31] Some of them, the holographic optical tweezers, have attracted a lot of attention. They were first introduced by Fournier and coworkers using fixed diffractive optical elements.[27] Recent advances in computer-controlled spatial light modulators make it possible to change the diffractive patterns in time. Sequences of diffraction patterns can be used to change the position of the trap in time. Many different methods

have been demonstrated, each having its advantages. Large arrays, changeable in time, can be created. It is also possible to create three-dimensional arrays of optical tweezers. The limited resolution of the spatial light modulators and the time it takes to compute a hologram are some of the disadvantages of the method.

Finally, the generalized phase contrast method converts a pattern of phase modulation from an spatial light modulator directly into an intensity pattern in the front focal plane of the objective.[31] The technique is somewhat related to phase contrast microscopy. The method is much faster than the holographic method as no holograms have to be calculated. However, only traps in two dimensions are created. The generalized phase contrast method has been used in combination with counterpropagating beams to create three-dimensional traps that can be manipulated in three-dimensions.[32]

1.5 Trapping and manipulating particles using optical tweezers

Optical tweezers are often used to trap and manipulate colloidal particles. Often, the colloidal particles are used as a handle for manipulation of materials that are too small to be trapped or imaged directly, e.g., molecular motors, proteins, microtubules, or lipid vesicles. As a force transducer, optical tweezers operate in a much lower force regime than macroscopic force transducers like an atomic force microscope (AFM), as an AFM has a cantilever with a relatively high mass and stiffness.

Recent developments have broadened the kind of forces that can be exerted onto small objects to include bending,[33] torques,[34, 35] and stretching.[36] Recently, optical tweezers have been used in microfluidics and in lab-on-a-chip applications. In these miniaturized chemical labs, activities like transport of materials, mixing, and analysis are done on a single chip. Optical tweezers and colloids have been used to create valves, pumps, and mixers.[7, 37] Another application of manipulation of colloidal particles is in fractionation of particles using an extended optical potential in two- or three-dimensions.[7, 38] In this technique, a mixture of particles is made to flow over an optical potential landscape, and by tuning the optical potential, colloidal particles can be sorted and selected on their size or refractive index.

Finally, optical tweezers have been used extensively to manipulate or modify nano-objects. For example, optical tweezers have been used to create structures of trapped particles (see also chapter 3). Tweezers have also

been used, as optical scissors or optical scalpels, to cut and modify biological materials. Two-photon polymerization has been used to fabricate parts of micromachines. These parts where then trapped and set into rotation by the radiation pressure of the optical trap. Metal particles that are too large to trap in a single-beam gradient trap, as the scattering force is too large, can be manipulated using alternative schemes such as rapid beam scanning[39] and the use of light beams with a phase singularity,[40] or counterpropagating optical tweezers (chapter 2).

1.6 Measuring and exerting forces using optical tweezers

Optical forces are ideally suited for measuring forces in systems with length scales between several nanometers up to several micrometers, as the forces that can be exerted are up to hundreds of pN with a sub-pN resolution. In general, a colloidal particle is first trapped using optical tweezers. Then, the optical potential is calibrated, determining the stiffness of the trap. This can, for example, be done by measuring the power spectrum of a particle in the trap (chapter 2), but other methods have also been developed.[11] When a force is exerted on the particle, either directly or by something attached to the particle, the particle will move from its equilibrium position in the optical trap. By measuring the displacement of the particle in the calibrated trap, the force on the particle can be determined. The restoring force acting on the particle in the optical trap is linear for small displacements of the particle from the center of the trap, e.g., less than 100nm. Using a quadrant photo diode, the particle position can be determined with nanometer accuracy at high speed (tens of kHz). Alternatively, video microscopy in combination with particle tracking routines can be used to determine the particle position with 10 nm accuracy at video rate.

In many different biological systems, optical tweezers have been used to exert and measure forces. For example, the 8 nm large, individual steps taken by molecular motors have been recorded as they walked along a microtubule fixed to a substrate.[41] Optical tweezers have also used to study the mechanical properties of proteins and (bio)polymers.[7, 11]

Also have optical tweezers been used to measure interactions between colloidal particles.[5, 7] Grier and coworkers measured interactions between charged colloidal particles.[42, 43] Two colloidal particles were trapped close together and then released. The position coordinates of the particles after they were released from the traps, were recorded and by repeating trapping

and releasing the particles many times at different distances, they measured the interaction between the charged particles.[42] Using line tweezers, a one-dimensional effective optical potential, interactions were measured with better confinement of the particle in the trapping plane.[44] A single colloidal particle was trapped and its thermal fluctuations were used to measure the optical potential of the line tweezers. After characterizing the potential, a second particle was added and the position of the two particles on the line was recorded. Using this sensitive technique, the effective depletion interaction of a binary mixture of 1100 nm and 83 nm particles was determined.[44] Brunner *et al*. used line tweezers to measure three-particle interactions between highly charged particles.[45] Recently, optical tweezers have also been used to probe hydrodynamic interactions between colloidal particles.[46]

1.7 Colloidal particles and optical tweezers

Colloidal particles, with a size between a few nanometers and several micrometers, undergo Brownian motion due to collisions of the particle with solvent molecules. Colloids are tunable in size, shape, as well as in chemical composition. The interparticle interactions can be tuned from charged-sphere like to hard-sphere like by adding salt to the dispersion. The typical time and length scales of a colloidal dispersion make colloids suitable for experiments in real-time and real-space. Particle synthesis and labeling of particles with fluorescent dyes have made it possible to perform quantitative three-dimensional analysis on a single particle level using confocal microscopy.[47]

Colloids have, like atoms, a well-defined thermodynamic temperature and, therefore, colloidal systems are used as a model system in condensed matter.[48-50] They are used as a model system for atomic and biological systems, and they are used to test statistical mechanical theories. Examples are experiments investigating the glass transition[51] and nucleation and growth of colloidal crystals.[50, 52] Because of their ability to self-organize, colloids are also used in the development of advanced materials like photonic crystals.[53]

As described above, optical tweezers are often used to trap and manipulate colloidal particles. When used as a force transducer, it is convenient to be able to extert large forces on the particle. For silica and polystyrene particles, mostly used as force transducers, the maximal force that can be exerted on the particles by optical tweezers is sometimes not

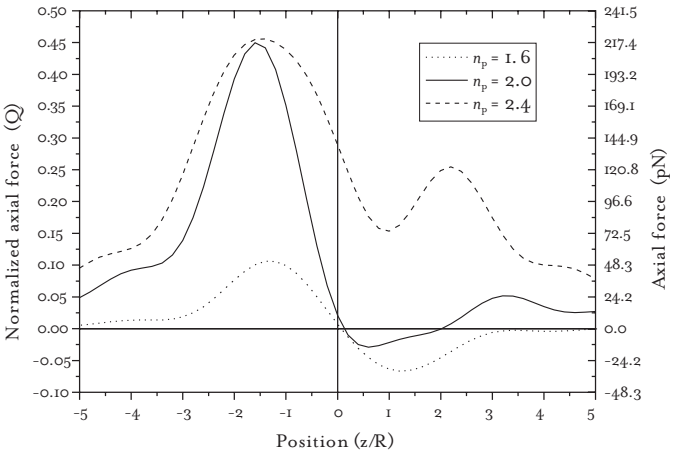

Figure 1.1

Calculated normalized axial force Q optical force on a 500 nm radius particles in a solvent with a refractive index of n_m = 1.45 (SiO_2) versus the normalized position of the particle along the optical axis. The dotted, solid, and dashed lines are for a particle with refractive index n_p of 1.6 (polystyrene), 2.0 (our ZnS particles), and 2.4, respectively. The wavelength of the trapping laser was 1064 nm, and the numerical aperture of the objective was 1.4. The axis on the right side shows the axial force on the particles for a laser power of 100 mW. The forces were calculated using the theory described in Ref. 14.

large enough. To be able to exert larger forces on the particles, we developed ZnS-SiO_2 core-shell particles (see also chapter 2). We expected that the high refractive index ZnS core would allow for a higher trapping force. The SiO_2 shell would allow all the surface chemistry used in applications, like in biology. To our surprise, we found that ZnS-SiO_2 core-shell particles with a radius larger than ~ 100 nm, could not be trapped stably in water. Slightly smaller particles, with an 81 nm ZnS core and a 1-100 nm SiO_2 shell, could be trapped.

Using the force calculation procedure of Maia Neto and Nuzzenzveig,[14] we calculated the optical force on 500 nm radius particles with different refractive indices. The medium surrounding the particles has a refractive index of n_m = 1.45, similar to that of SiO_2. *Figure 1.1* shows the calculated normalized axial force Q on a particle, as defined in formula 1.2, versus its normalized position on the optical axis. The laser beam is traveling from left to right and the focus of the beam is at zero. A positive Q indicates a force in the direction along the optical axis. The dotted, solid, and dashed lines are for particles with refractive indices n_p of 1.6, 2.0, and 2.4, respectively. The particle with a refractive index of n_p = 2.4 shows no stable trapping and this

particle will be propelled along the optical axis. The particle with n_p = 2.0 (our ZnS particles) can be trapped, although not very stable as there is only a small restoring force. The particle with n_p = 1.6 (polystyrene) is predicted to be trapped stably close to the focus and with a relatively large restoring force. The trapping wavelength used in the experiments and calculations was 1064 nm, and the numerical aperture of the microscope objective was 1.4. The axis on the right shows the force on the particles for a 100 mW trapping laser.

Although optical tweezers have been used to investigate several interesting phenomena in strongly interacting dispersions, all applications have been limited to systems that were either (almost) two-dimensional[48, 54] or had a low particle concentration.[26, 55]

To successfully use optical tweezers in concentrated colloidal dispersions, two problems have to be addressed. First of all, some way of selectively trapping and manipulating particles without affecting other particles has to be found. And secondly, imaging all individual particles in three-dimensions is desirable.

We solved both problems by synthesizing mixtures of two types of particles and dispersing them in a solvent mixture. The mixture consists of a small amount of tracer particles that have a high refractive index core and a low refractive index shell and a large amount of host spheres that have the same refractive index as the shell of the tracer particles. Because of their high-index core, the tracer particles can be trapped using the optical tweezers. The host spheres are refractive index matched by the solvent and no optical forces are exerted on the host spheres. The high index core of the tracer particles and the fluorescently labeled core of the host particles can be imaged simultaneously, using reflection and fluorescence confocal microscopy. The core-shell structure has additional advantages: the interparticle interactions between the tracer and host spheres is the same, optically induced interparticle forces are reduced because the high refractive index cores remain further separated, and distortions in three-dimensional trapping arrays are minimized because of the smaller scattering unit in the tracer particles. Finally, due to the high refractive index of the solvent mixtures, aberrations are much reduced or even absent because there is no longer a dielectric mismatch between the solvent and the sample wall. Both trapping and imaging are much better compared to a water-based system, even when water immersion lenses are used.

1.8 Layout of the rest of this thesis

The remainder of this thesis is organized as follows. The next chapter describes the combined optical tweezers and confocal microscopy setup used for independent three-dimensional trapping and imaging of individual particles. We also introduce specially synthesized mixtures of core-shell colloidal particles for manipulation in concentrated dispersions.

Next, in chapters 3 to 5, optical tweezers and colloids are used for creating arrays of nanoparticles on surfaces. In chapter 3, we describe how optical tweezers can be used to pattern surfaces with colloids. In chapter 4, optical tweezers are used to create two-dimensional structures of colloidal particles that are then used as masks for colloidal lithography. Ion beam deformation is used to modify the masks of colloids. In chapter 5, chemical methods are presented to further modify the colloidal masks for nanolithography.

Finally, in chapters 6 to 8, optical tweezers and the confocal microscope are used for the study of crystallization and melting in colloidal dispersions using a core-shell model system that can also be density matched with the solvent. In chapter 6, a single optical trap is used to crystallize two- and three-dimensional colloidal dispersions. Arrays of optical tweezers are used in chapter 7 to trap core-shell particles that act as nuclei for homogeneous and heterogeneous nucleation in concentrated colloidal dispersions. In chapter 8, we trap a single particle and drive it through a three-dimensional colloidal crystal.

Acknowledgements

We gratefully acknowledge Krassimir Velikov for synthesis of the ZnS-SiO_2 particles and Alexander Moroz for writing the computer code which we used to calculate the optical forces on the core-shell particles using the theory given in Ref. 14.

References

1 *A. Ashkin, Acceleration and trapping of particles by radiation pressure, Phys. Rev. Lett. 24, 156 (1970).*
2 *A. Ashkin and J. M. Dziedzic, Optical levitation by radiation pressure, Appl. Phys. Lett. 19, 283 (1971).*
3 *A. Ashkin, J. M. Dziedzic, J. E. Bjorkholm, and S. Chu, Observation of a single-beam gradient force optical trap for dielectric particles, Opt. Lett. 11, 288 (1986).*
4 *K. Visscher, S. P. Gross, and S. M. Block, Construction of multiple-beam optical traps with nanometer-resolution position sensing, IEEE Journal of Selected Topics in Quantum Electronics 2, 1066 (1996).*
5 *D. G. Grier, Optical tweezers in colloid and interface science, Curr. Opin. Colloid Interface Sci. 2, 264 (1997).*

6 K. Dholakia, G. Spalding, and M. MacDonald, Optical tweezers: the next generation, Phys. World 15, 31 (2002).
7 D. G. Grier, A revolution in optical manipulation, Nature 424, 810 (2003).
8 V. Lembessis, P.N. Lebedev and light radiation pressure, Europhysics News 32, 16 (2001).
9 A. Ashkin, Trapping of atoms by resonance radiation pressure, Phys. Rev. Lett. 40, 729 (1978).
10 S. M. Block, Making light work with optical tweezers, Nature 360, 493 (1992).
11 K. C. Neuman and S. M. Block, Optical trapping, Rev. Sci. Instrum. 75, 2787 (2004).
12 Y. Harada and T. Asakura, Radiation forces on a dielectric sphere in the Rayleigh scattering regime, Opt. Commun. 124, 529 (1996).
13 A. Ashkin, in Methods in Cell Biology, edited by M. P. Sheetz (Academic Press, San Diego, 1998), Vol. 55, p. 1.
14 P. A. M. Neto and H. M. Nussenzveig, Theory of optical tweezers, Europhys. Lett. 50, 702 (2000).
15 A. Ashkin, Forces of a single-beam gradient laser trap on a dielectric sphere in the ray optics regime, Biophysical Journal 61, 569 (1992).
16 D. A. White, Numerical modeling of optical gradient traps using the vector finite element method, Journal of Computational Physics 159, 13 (2000).
17 A. Mazolli, P. A. M. Neto, and H. M. Nussenzveig, Theory of trapping forces in optical tweezers, Proceedings of the Royal Society of London Series a-Mathematical Physical and Engineering Sciences 459, 3021 (2003).
18 T. A. Nieminen, H. Rubinsztein-Dunlop, N. R. Heckenberg, and A. I. Bishop, Numerical modelling of optical trapping, Computer Physics Communications 142, 468 (2001).
19 E. J. G. Peterman, F. Gittes, and C. F. Schmidt, Laser-induced heating in optical traps, Biophysical Journal 84, 1308 (2003).
20 J. Bechhoefer and S. Wilson, Faster, cheaper, safer optical tweezers for the undergraduate laboratory, American Journal of Physics 70, 393 (2002).
21 A. Rohrbach and E. H. K. Stelzer, Trapping forces, force constants, and potential depths for dielectric spheres in the presence of spherical aberrations, Appl. Optics 41, 2494 (2002).
22 J. B. Pawley, Handbook of biological confocal microscopy (Plenum Press, New York, 1995).
23 K. Sasaki, M. Koshioka, H. Misawa, N. Kitamura, and H. Masuhara, Pattern-formation and flow-control of fine particles by laser-scanning micromanipulation, Opt. Lett. 16, 1463 (1991).
24 C. Mio, T. Gong, A. Terray, and D. W. M. Marr, Design of a scanning laser optical trap for multiparticle manipulation, Rev. Sci. Instrum. 71, 2196 (2000).
25 M. M. Burns, J.-M. Fournier, and J. A. Golovchenko, Optical matter: crystallization and binding in intense optical fields, Science 249, 749 (1990).
26 M. P. MacDonald, L. Paterson, K. Volke-Sepulveda, J. Arlt, W. Sibbett, and K. Dholakia, Creation and manipulation of three-dimensional optically trapped structures, Science 296, 1101 (2002).
27 J.-M. Fournier, M. M. Burns, and J. A. Golovchenko, in Proc. SPIE, edited by S. A. Benton, (1995), Vol. 2406, p. 101.
28 E. R. Dufresne and D. G. Grier, Optical tweezer arrays and optical substrates created with diffractive optics, Rev. Sci. Instrum. 69, 1974 (1998).
29 Y. Hayasaki, M. Itoh, T. Yatagai, and N. Nishida, Nonmechanical optical manipulation of microparticle using spatial light modulator, Opt. Rev. 6, 24 (1999).
30 J. Liesener, M. Reicherter, T. Haist, and H. J. Tiziani, Multi-functional optical tweezers using computer-generated holograms, Opt. Commun. 185, 77 (2000).
31 R. L. Eriksen, V. R. Daria, and J. Gluckstad, Fully dynamic multiple-beam optical tweezers, Opt. Express 10, 597 (2002).
32 P. J. Rodrigo, V. R. Daria, and J. Gluckstad, Real-time three-dimensional optical micromanipulation of multiple particles and living cells, Opt. Lett. 29, 2270 (2004).
33 K. Visscher, G. J. Brakenhoff, and J. J. Krol, Micromanipulation by multiple optical traps created by a single fast scanning trap integrated with the bilateral confocal scanning laser microscope, Cytometry 14, 105 (1993).
34 M. E. J. Friese, T. A. Nieminen, N. R. Heckenberg, and H. Rubinsztein-Dunlop, Optical alignment and spinning of laser-trapped microscopic particles, Nature 394, 348 (1998).
35 L. Paterson, M. P. MacDonald, J. Arlt, W. Sibbett, P. E. Bryant, and K. Dholakia, Controlled rotation of optically trapped microscopic particles, Science 292, 912 (2001).
36 J. Guck, R. Ananthakrishnan, T. J. Moon, C. C. Cunningham, and J. Kas, Optical deformability of soft biological dielectrics, Phys. Rev. Lett. 84, 5451 (2000).

37 A. Terray, J. Oakey, and D. W. M. Marr, Microfluidic control using colloidal devices, Science 296, 1841 (2002).
38 M. P. MacDonald, G. C. Spalding, and K. Dholakia, Microfluidic sorting in an optical lattice, Nature 426, 421 (2003).
39 K. Sasaki, M. Koshioka, H. Misawa, N. Kitamura, and H. Masuhara, Optical trapping of a metal-particle and a water droplet by a scanning laser-beam, Appl. Phys. Lett. 60, 807 (1992).
40 H. He, M. E. J. Friese, N. R. Heckenberg, and H. Rubinsztein-Dunlop, Direct observation of transfer of angular-momentum to absorptive particles from a laser-beam with a phase singularity, Phys. Rev. Lett. 75, 826 (1995).
41 K. Svoboda, Direct observation of kinesin stepping by optical trapping interferometry, Nature 365, 721 (1993).
42 J. C. Crocker and D. G. Grier, Microscopic measurement of the pair interaction potential of charge-stabilized colloid, Phys. Rev. Lett. 73, 352 (1994).
43 J. C. Crocker and D. G. Grier, When like charges attract: the effects of Geometrical confinement on Long-Range Colloidal Interactions, Phys. Rev. Lett. 77, 1897 (1996).
44 J. C. Crocker, J. A. Matteo, A. D. Dinsmore, and A. G. Yodh, Entropic attraction and repulsion in binary colloids probed with a line optical tweezer, Phys. Rev. Lett. 82, 4352 (1999).
45 M. Brunner, J. Dobnikar, H. H. von Grunberg, and C. Bechinger, Direct measurement of three-body interactions amongst charged colloids, Phys. Rev. Lett. 92, 078301 (2004).
46 S. Henderson, S. Mitchell, and P. Bartlett, Position correlation microscopy: probing single particle dynamics in colloidal suspensions, Colloid Surf. A-Physicochem. Eng. Asp. 190, 81 (2001).
47 A. van Blaaderen and P. Wiltzius, Real-space structure of colloidal hard-sphere glasses, Science 270, 1177 (1995).
48 M. Brunner, C. Bechinger, W. Strepp, V. Lobaskin, and H. H. von Grunberg, Density-dependent pair interactions in 2D colloidal suspensions, Europhys. Lett. 58, 926 (2002).
49 A. van Blaaderen, J. P. Hoogenboom, D. L. J. Vossen, A. Yethiraj, A. van der Horst, K. Visscher, and M. Dogterom, Colloidal epitaxy: Playing with the boundary conditions of colloidal crystallization, Faraday Discuss. 123, 107 (2003).
50 A. Yethiraj and A. van Blaaderen, A colloidal model system with an interaction tunable from hard sphere to soft and dipolar, Nature 421, 513 (2003).
51 W. K. Kegel and A. van Blaaderen, Direct observation of dynamical heterogeneities in colloidal hard-sphere suspensions, Science 287, 290 (2000).
52 U. Gasser, E. R. Weeks, A. Schofield, P. N. Pusey, and D. A. Weitz, Real-space imaging of nucleation and growth in colloidal crystallization, Science 292, 258 (2001).
53 A. van Blaaderen, K. P. Velikov, J. P. Hoogenboom, D. L. J. Vossen, A. Yethiraj, R. P. A. Dullens, T. van Dillen, and A. Polman, in Photonic crystals and light localization in the 21st century, edited by C. M. Soukoulis (Kluwer, 2001), p. 239.
54 P. T. Korda and D. G. Grier, Annealing thin colloidal crystals with optical gradient forces, J. Chem. Phys. 114, 7570 (2001).
55 J. Leach, G. Sinclair, P. Jordan, J. Courtial, M. J. Padgett, J. Cooper, and Z. J. Laczik, 3D manipulation of particles into crystal structures using holographic optical tweezers, Opt. Express 12, 220 (2004).

2 Optical tweezers and confocal microscopy for simultaneous three-dimensional manipulation and imaging in concentrated colloidal dispersions

A setup is described for simultaneous three-dimensional manipulation and imaging inside a concentrated colloidal dispersion using (time-shared) optical tweezers and confocal microscopy. The use of two microscope objectives, one above and one below the sample, enables imaging to be completely decoupled from trapping. The instrument can be used in different imaging and trapping (inverted, upright, and counterpropagating) modes. Optical tweezers arrays, dynamically changeable and capable of trapping several hundreds of micrometer-sized particles, were created using acousto-optic deflectors. Several schemes are demonstrated to trap three-dimensional colloidal structures with optical tweezers. One combined a Pockels cell and polarizing beam splitters to create two trapping planes at different depths in the sample, in which the optical traps could be manipulated independently. Optical tweezers were used to manipulate collections of particles inside concentrated colloidal dispersions, allowing control over colloidal crystallization and melting. Furthermore, we show that selective trapping and manipulation of individual tracer particles inside a concentrated dispersion of host particles is possible as well. The tracer particles had a core-shell geometry with a high refractive index material core and a lower index material shell. The host particles consisted of the same material as the lower index shells and were fluorescently labeled. The tracer particles could be manipulated without exerting forces on the host particles because the mixture was dispersed in a solvent with the same refractive index as that of the host particles. Using counterpropagating tweezers strongly scattering particles that could not be trapped by conventional single-beam optical tweezers were trapped and manipulated.

2.1 Introduction

Since the invention of optical tweezers by Ashkin and coworkers[1, 2] optical tweezers have found widespread use in fields like biology, physical chemistry, and (bio)physics.[3-6] An optical trap can be created by focusing a laser beam to a diffraction-limited spot using a high numerical aperture (NA) objective. The strong light gradient near the focus creates a potential well, in which a particle with a refractive index higher than that of the surrounding medium is trapped. The forces on a particle can be decomposed into a "gradient force" in the direction of highest light intensity and a "scattering force" directed along the optical axis. The particle is trapped at the point where these two force contributions balance, if the maximal restoring force of the trap is large enough to overcome effective weight and thermal fluctuations of the particle. The general calculation of the optical forces on a particle in a trap is a challenging problem.[7] This task is simpler in the regimes where a particle is either much smaller[8] (Rayleigh) or much larger[9] (ray optics) than the wavelength used for trapping. Dielectric particles, small metal particles as well as living materials, with sizes ranging from several nanometers to tens of micrometers, can be trapped and manipulated in a single-beam gradient trap as long as the scattering force is not too large. If there is no difference in refractive index between the particle and its surroundings, there are no direct optical forces exerted on the particle. If the refractive index of the particle is lower than that of the medium, the particle is expelled from the trapping beam. However, alternative schemes such as rapid beam scanning[10] and the use of light beams with a phase singularity,[11] have been invented to manipulate particles in this situation. Recent developments have broadened the kind of forces that can be exerted on small objects to include bending,[12] torques,[13, 14] and stretching.[15]

To manipulate more than one particle at once, a number of methods have been developed to create and manipulate planar arrays of optical traps using galvano[16] or piezoelectric[17] scanning mirrors, acousto-optic deflectors (AODs),[3] (computer generated) diffractive optical elements,[18-21] interference of specially designed light beams,[22, 23] or the generalized phase contrast method.[24]

Around the same time the single-beam optical tweezers were pioneered, the confocal microscope was reinvented after it was first demonstrated at the end of the 1950s.[25, 26] At present, confocal microscopy is widely used in biology and medicine, and its use in chemistry, physics,

and materials science is increasing.[27-29] In confocal microscopy the sample is illuminated with a diffraction-limited spot while detection occurs by imaging the focal region with the same objective onto a pinhole aperture. Only a thin section of the sample contributes to the signal, thus out-of-focus stray light is efficiently reduced by the detection pinhole. By scanning the beam in the sample a three-dimensional image can be build up. Besides the sectioning capability the use of pinholes also leads to an increase in resolution compared to conventional microscopy.[30]

Because of their tunability, in size, shape, as well as in chemical composition, and their ability to self-organize, colloids find applications in the development of advanced materials like photonic crystals.[31] In addition, colloidal systems are used as a model system in condensed matter.[32-34] Colloids have, like atoms, a well-defined thermodynamical temperature, their interaction potential is tunable, and the time and length scales involved are experimentally accessible. Recent developments in particle synthesis and labeling of particles with fluorescent dyes opened up the possibility to perform quantitative three-dimensional analysis using confocal microscopy on a single particle level.[35] Examples are experiments investigating the glass transition[36] and nucleation and growth of crystals[34, 37] in colloidal dispersions. Optical tweezers have been used to manipulate colloidal particles, to pattern substrates with two- and three-dimensional structures,[38, 39] and to measure double layer repulsions,[40] depletion,[41] and hydrodynamic interactions.[42] However, as selective manipulation in a concentrated dispersion was not possible until now, all applications have been limited to systems that were either (almost) two-dimensional[32, 43] or had a very low particle concentration.[23, 44]

Combining the powerful techniques of optical tweezers and confocal microscopy opens up series of new experiments. For example, three-dimensional structures can be created with optical tweezers that can be imaged and studied in detail in three dimensions. In addition, their effect on other particles, which are not trapped, can be analyzed in three dimensions. The setup described in this chapter is designed to use optical tweezers and independently image the sample using confocal microscopy because it uses two microscope objectives on each side of the sample.

The simplest way of combining optical tweezers with a confocal microscope is by using the same objective to image and trap. However, this makes it impossible to use the three-dimensional scanning ability, and

only one plane is imaged.[45] Hoffmann and coworkers implemented optical trapping and three-dimensional imaging using one objective and fast scanning compensating optics to keep the tweezers at a fixed position.[46] The use of two independent microscope objectives for trapping and imaging was pioneered by Visscher and coworkers,[12, 47] although trapping was limited to a two dimensional plane. In this article we also use two microscope objectives, one above and one below the sample, to decouple imaging and trapping completely. Samples could be imaged quantitatively in three dimensions without affecting optical trapping performance. AODs were used to create large two-dimensional arrays of traps that could be changed dynamically. Three-dimensional arrays of traps were created by fast switching between two beam paths using AODs, a Pockels cell, and polarizing beam splitters.

We extended the use of optical tweezers in soft condensed matter systems to concentrated dispersions, both on individual particles using core-shell tracers and on collections of particles. We induced crystallization in a concentrated dispersion and demonstrated that selective trapping of core-shell tracer particles inside a concentrated dispersion of index matched host particles in combination with three-dimensional imaging is possible. Some preliminary results were described in Ref. 33. Using counterpropagating beams[1, 48] we trapped high refractive index particles that were not stably trapped in a single-beam gradient trap.

The remainder of this chapter is organized as follows. The next section describes the setup used to create the different trapping and imaging modes and it describes the colloidal dispersions used. In section 2.3 we demonstrate the flexibility, accuracy, and speed of AODs to create large arrays of optical traps which can be changed dynamically. In Sections 2.4 and 2.5 decoupled trapping and imaging, and arrays of tweezers created in more than one plane are demonstrated. How optical tweezers can be used in concentrated colloidal dispersions is demonstrated in section 2.6 while section 2.7 shows the use of counterpropagating tweezers for trapping high index particles. We end with conclusions and an outlook.

2.2 Experimental

2.2.1 upright, inverted, and counterpropagating optical tweezers arrays

Figure 2.1 shows a schematic drawing of the setup. We use a diode-pumped Nd:YVO_4 laser (Spectra Physics; Millennia IR; 10 W; cw) with a wavelength

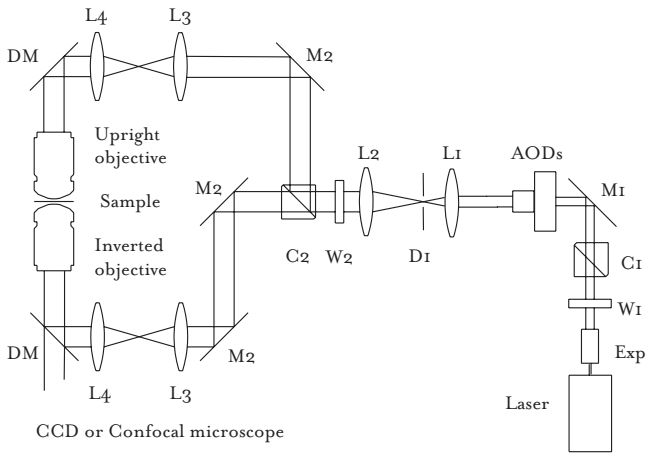

Figure 2.1
Schematic diagram of the setup used to create inverted, upright, and counterpropagating optical tweezers. Two objectives allowed imaging to be completely decoupled from trapping. AODs were used for beam steering and the creation of arrays of tweezers.

of 1064 nm and a TEM_{00} mode profile. The wavelength was chosen such that it is well separated from the excitation and emission wavelengths of the fluorescent dyes used in the confocal microscopy modes. This wavelength also minimizes absorption and scattering in biological materials. The laser beam is expanded six times using a beam expander (*EXP*, Melles Griot). The beam is attenuated using a half-lambda zero-order wave plate (*W1*, Newport), which rotates the vertically polarized laser light, in combination with a polarizing beam splitter cube *(C1)*. The horizontally polarized fraction is directed into a beam dump.

Using a gimbaled mirror (*M1*; Newport), the vertically polarized beam is coupled into two AODs (IntraAction Corp.; DTD-276HB2; 6 x 6 mm^2 aperture). In the AODs a diffraction grating is set up by a sound wave propagating through the TeO_2 crystals. The laser beam is deflected at specific angles and intensities that depend on the frequency and the amplitude of the sound wave in the crystal, respectively. We corrected, if needed, for the diffraction efficiency of the AODs not being constant over the frequency range by either adjusting the amplitude of the signal to the AODs or by changing the relative time spent by the laser beam at a certain frequency.

A synthesizer board and amplifier (both IntraAction Corp.) allow for fast and accurate control over the position as well as the stiffness of the optical trap. The synthesizer board was controlled using a *LabVIEW* (National Instruments) program, which addressed a C++ program when faster

switching was needed. The beam is scanned quickly from point to point in the sample using the AODs to create arrays of tweezers with great control over the position of the traps. We also used direct digital synthesizers (Novatech Instruments Inc.; DDS8m 100 MHz) to create multiple traps without timesharing the laser beam. Two frequencies were applied simultaneously to the AODs, resulting in a corresponding number of diffracted beams. With this procedure, the beams are not time-shared and can be modulated independently although the intensities are interrelated.

The two AODs are each fitted on a four-axis kinematic stage (New Focus) for better alignment. As the AODs diffract the incoming laser into multiple beams, a diaphragm *(D1)* is used to select the (1,1) order for trapping. By careful alignment of the AODs with respect to the incoming laser beam, up to 60% of the light of the original undiffracted beam can be transferred into the (1,1) order.

The deflected beam is broadened further using a telescope with lenses *L1* (f = 120 mm) and *L2* (f = 250 mm). All lenses are achromat doublets and were obtained from Melles Griot while the mirrors and beam-splitting cubes were from Newport. All components have an antireflection coating for 1064 nm. The combination of the telescope and the beam expander broadens the laser beam 12 times to a width of $2\omega_0$ = 5.6 mm, equal to the back aperture of the 100x objective.

Switching between different trapping modes is done using a half-lambda wave plate *W2* combined with a polarizing beam splitter cube *C2*. Rotation of the wave plate determines the fraction of the beam diverted to the upper or the lower beam paths, thereby switching between inverted and upright trapping modes. When both paths are used at the same time, inverted and upright single-beam optical traps can be created at different heights in the sample. Dual-beam counterpropagating optical tweezers can be created when the inverted and upright tweezers are aligned on top of each other. Depending on whether the lower or the upper beam path is used, the scattering force augments or counteracts gravity.

Mirrors (*M2*) and the 1:1 telescope lenses (*L3* and *L4*, both f = 80 mm) guide the beam to the microscope. The lenses *L3* are placed on *xyz* stages fitted with micromanipulators. The lenses *L3* as well as the AODs are positioned in planes conjugate to the back focal plane of the objectives. This allows for manipulation of the optical traps in the front focal plane of the objective by changing the angle at which the beam enters the back aperture

of the microscope objective. The lenses *L3* are achromat doublet lenses to minimize aberrations. Also the displacement of these lenses from the optical axis is small and we have not seen any notable change in trap efficiency when lenses *L3* were moved. For optimal two-dimensional position control, the AODs are aligned such that the plane between the two AODs is conjugate to the backfocal planes of the two objectives. The distance between the centers of the AODs is 32 mm.

Two dichroic mirrors (*DM*, ChromaTech) are attached to the body of an inverted microscope (Leica, DMIRB). The mirrors reflect the 1064 nm laser beam into the back aperture of the objectives while they allow imaging in the visible. The revolver of the microscope is replaced with a block holding the inverted objective, and the condenser is replaced by the upper microscope objective. This upright objective is mounted on an *xyz* translation stage, fitted with microscrews (Newport), for manipulation and alignment. The upright objective can be used as a condenser for imaging as well as for trapping. We used 100x (0.7-1.4 NA), 63x (1.4 NA), and 40x (1.4 NA) oil immersion objectives and a 20x (0.7 NA) air objective. All objectives were plan apochromats and were obtained from Leica.

A high-resolution piezo stage (Physik Instrumente, P-730.4C, accuracy better than 0.5 nm when operated in a closed loop circuit) is mounted on the body of the microscope, providing the ability to move the sample with high accuracy. The power of the laser was measured using a broadband power meter (Melles Griot). The setup was built on a vibration isolation table (Melles Griot).

2.2.2 Arrays of tweezers in more than one plane using one objective

To create multiple traps in different planes and to image the sample in three dimensions simultaneously, the laser beam was split into two beams, which were recombined after changing their relative divergence. As the (z axis) position of the trapping plane is determined by the divergence (or convergence) of the beam at the back focal plane of the objective, we were able to create traps in two different planes in the sample. Switching between these planes can be done using a Pockels cell, which rotates the polarization of the laser beam, combined with a polarizing beam splitting cube. Synchronizing the Pockels cell with the AODs creates independent arrays of optical tweezers.

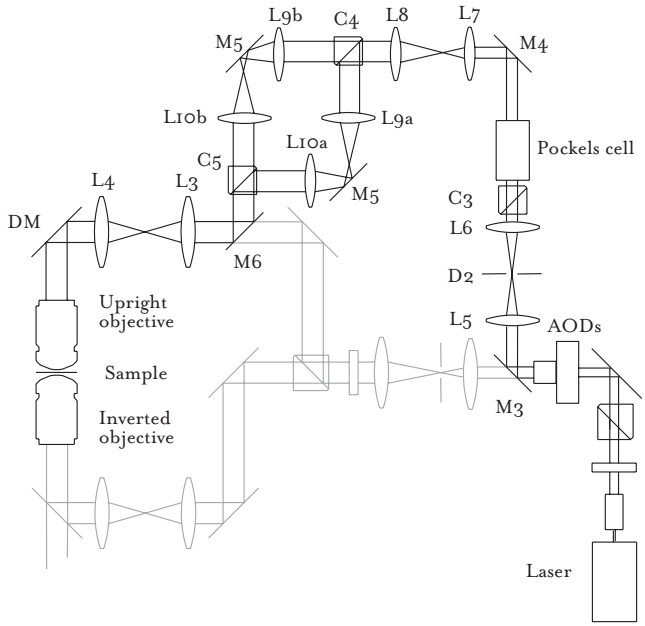

Figure 2.2
Setup used for the creation of arrays of tweezers in two trapping planes. A Pockels cell and beam splitting cubes (C4 and C5) were used to switch between the planes. The Pockels cell and the AODs were synchronized to create different arrays of traps in each plane. The upright objective was used for trapping, while the inverted objective was used for imaging. The part of the setup drawn in light gray was not used when two trapping planes were created.

Figure 2.2 shows the setup used for creating arrays of tweezers in two separate planes. A mirror (*M3*) after the AODs reflects the beam into a 1:1 telescope formed by two lenses (*L5* and *L6*, both f = 120 mm). A polarizing beam splitting cube (*C3*) is placed in front of the Pockels cell (Conoptics; 360-50 LA) to remove any horizontal component of the polarization introduced by the AODs. A personal computer with an analog output board (NuDAQ PCI-6208V) controls the angle of rotation of the polarization induced by the Pockels cell. The computer also contains the synthesizer board that generates the acoustic signals for the AODs. Both boards are controlled and synchronized using a *LabVIEW* program to create independent arrays in each trapping plane. For increased speed, the *LabVIEW* program calls a *C++* program to write the data to the two boards.

After the Pockels cell and a mirror (*M4*), the lenses *L7* and *L8* (f = 65 and 140 mm) expand the beam to overfill the back aperture of the objective. A polarizing beam splitter cube (*C4*) splits the laser beam into two separate paths. In each of the paths the beam passes through a 1:1 telescope formed by a pair of lenses (*L9a,b* and *L10a,b* all f = 90 mm). The

lenses *L9a,b* are positioned in a plane conjugate to the back focal plane of the upright objective. The lens *L9a* is mounted on an *xyz* translation stage allowing displacement of the traps created in the sample with path *a* with respect to the traps created with path *b*. After recombination of the two beams using a polarizing beam splitter cube (*C5*), the combined beam is coupled into the microscope with the mirrors *M5*, *M6* and lenses *L3* and *L4*. A movement of lens *L3* results in a collective displacement of the traps created with paths *a* and *b*. The lenses *L3* and *L9a,b* as well as the Pockels cell and the AODs are all in planes conjugate to the back focal plane of the upright objective. Because of the length of the Pockels cell (75 mm) and the small aperture (5 x 5 mm^2), the modulator is placed with its center at a plane conjugate to the back focal plane of the objective. The mirrors *M3* and *M6* are placed on flippers (New Focus) to move them out the beam path when this part of the setup was not used.

2.2.3 imaging modes

The inverted objective is used for imaging while both the inverted and upright objectives can be used for trapping. The sample can be imaged in brightfield, differential interference contrast (DIC), epifluorescence, and reflection microscopy using mercury or halogen light sources. For DIC imaging, a polarizer and Wollaston prism are placed below the inverted objective in addition to an analyzer and a prism placed above the upright objective. The sample is imaged with a charge coupled device (CCD) camera (UNIQ, UP-600), which is read out by a home build frame grabber using a programmable coprocessor (SiliconSoftware, microEnable). The images (540 x 480 pixels, 10 bit grayscale) can be stored digitally on an array of hard disks (Promise tech., Fasttrak 100) at a rate of 20 Hz for full images and up to 50 Hz for smaller regions. For position detection in real-time, the frame grabber is programmed to determine the gray-value center of mass of particles separated by at least a line of pixels on the CCD. An infrared filter (Schott) is used to block the trapping beam from the CCD camera.

For confocal imaging we use a commercial confocal scan head (Leica TCS NT) attached to the side port of the inverted microscope. The confocal microscope excites the sample using a mixed-gas Kr-Ar laser, and the fluorescence is detected using photomultiplier tubes. To image the sample in three dimensions, the lower objective is mounted on a microscope objective scanner (Physik Instrumente, Pifoc P-721.20) operated in closed loop mode, while the sample is kept stationary. The software of the confocal

microscope controls the piezo driver electronics. For imaging of the fluorescently labeled silica particles described in the next section, the 488 nm line of the Kr-Ar laser was used in combination with cutoff filters. The silica-coated polystyrene particles were imaged in reflection mode using a second photomultiplier tube. Only in the upright mode and at high powers was the trapping laser detected by the photomultiplier tubes. In that case an infrared filter was used to block the trapping laser from the imaging channels that were used in the visible. Image analysis was done using routines similar to those described in Refs. 35 and 49.

2.2.4 colloidal dispersions

Colloidal silica particles with a core-shell geometry were synthesized using the so-called Stöber growth process, modified to incorporate a fluorescent dye and followed by a seeded growth. This method and particle characterization are described in more detail elsewhere.[50-52] We used two sizes of silica particles with average diameters of 1384 and 1050 nm and polydispersities of 1.5% and 3%, respectively. The diameters of the cores were determined to be 386 and 400 nm, respectively, and the cores were labeled with the fluorescent dye fluorescein isothiocyanate (FITC). We will refer to the fluoresceine labeled silica particles as FITC-SiO_2. ZnS particles were synthesized following a procedure described elsewhere.[53] The ZnS particles had an average diameter of 500 nm and a polydispersity of 10%. The index of refraction of the ZnS particles was estimated to be $n_d^{20} = 2.0$.[53]

Recently, we developed a method to synthesize core-shell particles with a polystyrene core and a silica shell.[54] Polyvinyl pyrrolidone (PVP) was absorbed onto polystyrene (PS) particles with a diameter of 772 nm (estimated refractive index $n_d^{20} = 1.6$), and then a silica shell was grown onto the PVP-coated PS particles in several growth steps. The final diameter of the particles was determined to be 975 nm with a polydispersity of less than 3%. We will refer to the polystyrene-silica core-shell particles as PS-SiO_2. The densities of the particles used are not important for the trapping experiments in this article as optical forces exceed gravitational force by far. The densities of the particles used are stated in cited references.

The particles were dispersed in ethanol (Merck, analytical grade), dimethyl formamide (DMF; Merck, analytical grade), or a mixture of DMF and dimethylsulfoxide (DMSO; Merck, analytical grade). All chemicals were used as received.

In order to match the refractive index of the FITC-SiO_2 particles, we made a series of solvent mixtures with different relative composition of DMF and DMSO but with a constant concentration of silica particles. For each mixture the transmission was measured at a wavelength of 1064 nm using a spectrometer (Perkin Elmer). A mixture with a volume ratio of DMF: DMSO = 18% : 82% was found to index match the particles at 1064 nm. Using an Abbe refractometer (Atago, 3T), the refractive index of the matching mixture was measured to be n_d^{20} = 1.4675. For the trapping experiments on particles in a concentrated dispersion, a small amount of PS-SiO_2 particles was added to a concentrated dispersion of FITC-SiO_2 particles. The mixture was then transferred to a refractive index matching mixture of DMF and DMSO in several centrifugation (not exceeding 120 g) and redispersion steps.

Samples with a thickness of 10-15 µm were made by sandwiching a drop of dispersion between a larger and a smaller microscope cover slip (Chance; No. 1; thickness 150 µm). The samples were sealed with candle wax. Thin samples were clamped on all sides to prevent them from bending when the objectives were moved. Thicker samples were made in 0.1 x 2 x 50 mm^3 capillaries (VitroCom; wall thickness 100 µm) that were closed by melting. The optical quality of the microscope cover slips is better than that of the capillaries.

2.3 Dynamic arrays of optical tweezers

Figure 2.3 shows an array of 20 x 20 time-shared optical traps holding 1.4 µm FITC-SiO_2 particles. The inverted objective (63x; 1.4 NA) was used for trapping as well as for imaging. The array was scanned at a frequency of 96 Hz using the AODs. The particles were dispersed in ethanol in a 100 µm thick capillary. The tweezers array was shifted up slightly with respect to the imaging plane. The (untrapped) particles next to the array were just below the imaging plane. Some traps held more than one particle while some traps on the edge of the pattern were not filled. The total laser power used to create the 400 traps was 1.0 W at the back focal plane of the trapping objective.

When time-sharing a laser beam, the beam has to be scanned fast enough over the different positions in the sample for a particle to behave like it was trapped in a non-time-shared optical trap. In a single non-time-shared optical trap, a particle experiences a harmonic potential if its displacements from the center of the trap are not too large. The power

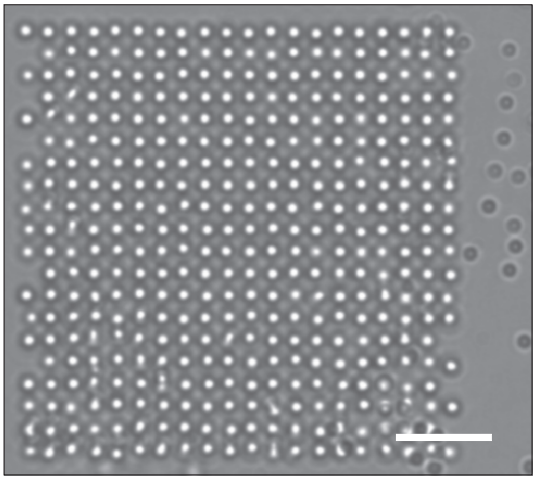

Figure 2.3
Transmission microscopy image of 1.4 µm diameter FITC-SiO_2 particles trapped in a time-shared array of 400 optical tweezers. The inverted objective was used for trapping as well as for imaging. Using the AODs the array was scanned at 96 Hz, well above the roll-off frequency of the particles in the traps. The particles on the right of the image were not trapped and were below the imaging plane. The scale bar is 10 µm.

spectrum of a particle's displacement in a harmonic potential is given by a Lorenzian[55]

$$S_x(f) = \frac{k_b T}{\lambda \pi^2 (f_c^2 + f^2)}, \qquad (2.1)$$

in which k_b is Boltzmann's constant, T is temperature, and λ the viscous drag coefficient. For an isolated sphere of radius R in a solvent with dynamic viscosity λ, the viscous drag coefficient is given by $\gamma = 2\pi\eta R$. The roll-off frequency f_c is given by:

$$f_c = \frac{\kappa}{2\pi\gamma}, \qquad (2.2)$$

in which κ is the trap stiffness. For frequencies above f_c, the particle shows free diffusive behavior in the trap while for frequencies below f_c the optical trap confines the motion of the particle. Each trap in the array of tweezers in *Figure 2.3* was addressed 96 times per second. The point-to-point scan-frequency was 38.4 kHz. Using a quadrant photodiode on our setup as described elsewhere,[3] we measured the power spectrum of a 1.4 µm diameter silica particle trapped in an optical trap created with a power of 2.5 mW at the back focal plane of the trapping objective. From this, the roll-off frequency was determined to be 10 Hz, which is well below the 96 Hz at which the

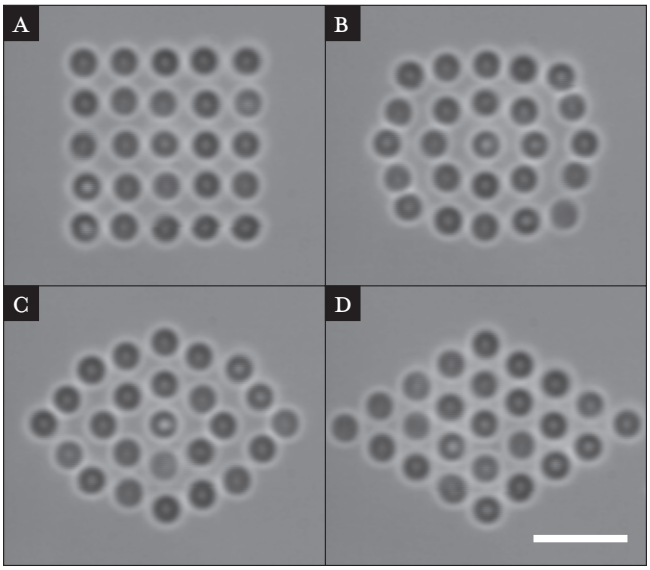

Figure 2.4
(a) Transmission microscopy image of 1.4 µm diameter FITC-SiO_2 particles in a time-shared array of 25 traps with square symmetry. The inverted objective was used for trapping as well as for imaging. Using the AODs, the pattern was dynamically changed in a few seconds without losing particles via intermediate patterns (b) and (c) to an array with triangular symmetry (d). The scale bar is 5 µm.

array in *Figure 2.3* was scanned. Already hundreds of traps can be created by time-sharing the AODs in a low viscosity solvent like ethanol for micron-size particles, and increasing the viscosity and thus lowering f_c, would allow even larger arrays to be made.

The maximum speed at which the position of an optical trap can be changed is determined by the width of the laser beam and the speed of the sound wave in the crystal. This is because the sound wave in the crystal has to be uniform in frequency over the laser beam to deflect the beam completely into a certain direction. In our setup it takes around 4.5 µs to change the direction in which the beam is diffracted, which sets the upper limit for point-to-point movement of the trap to 220 kHz. The maximum scanning speed can be increased by decreasing the width of the laser beam at the AODs and expanding the beam further after the AODs to keep the back focal plane of the objective overfilled.

Figure 2.4a shows 25 FITC-SiO_2 particles (1.4 µm diameter) trapped in a 5 x 5 square symmetric pattern using the inverted microscope objective (100x; 1.4 NA). The particles were dispersed in ethanol. The pattern was then changed in a few seconds, without losing particles from the trap, via intermediate stages *(Figures 2.4b* and *2.4c)* into the triangular pattern shown in *Figure 2.4d.* A *LabVIEW* program was used to switch between the different arrays of tweezers in a few seconds.

The maximum displacement of the trap in the sample is determined by the maximum deflection angle of the beam at the AODs, by the optics in the setup, and by the magnification of the microscope objective used. We used the (1,1) order of the diffracted beam after the AODs. For this order, a centerfrequency of 25 MHz on the AODs deflects the beam 45 mrad with respect to the zeroth order undiffracted beam. The position of the trap in the sample changes when the frequency on the AODs is changed around the centerfrequency. The accessible frequency interval ranges from 16 to 34 MHz corresponding to a deflection between −15 and +15 mrad of the beam at the AODs. The deflection angle at the back aperture of the objectives was reduced by a factor of 2.2 because of the telescope behind the AODs. The resulting maximum displacement of the optical traps in the sample was found to be 28, 45, and 71 μm in both the x and y direction for the 100x, 63x, and 40x objectives, respectively. For these objectives, the trapping force is comparable as they all have an NA of 1.4.

Compared to other techniques to time-share optical tweezers, for example scanning mirrors,[16] AODs are fast and flexible. Even mirrors mounted on piezo scanners[17] have a scan rate of a few kHz, while the AODs can be used at hundreds of kHz. Other techniques that intensity-share the beam, like diffractive optical elements[18, 19] in combination with computer addressed spatial light modulators,[20, 21] are very flexible although their computational process is complex and time consuming. Multiple tweezers generated with the generalized phase contrast method[24] are much faster than holographic optical tweezers but they only trap in two dimensions.

The AODs can also be used to create multiple tweezers without time-sharing the laser beam. We used digital synthesizers to generate two frequency signals, which were combined as input for one of the AODs, while the other AOD had a single frequency as input. The laser beam was diffracted at different angles, and this was used to create multiple tweezers in the sample. Arrays of tweezers are possible using this approach although the intensities of the beams are interrelated, and higher order frequencies might appear. All arrays of tweezers in the remainder of this chapter are created by time-sharing the laser beam.

2.4 Optical trapping and decoupled confocal imaging

The two microscope objectives on each side of the sample allow optical trapping and simultaneous three-dimensional imaging in the sample. To

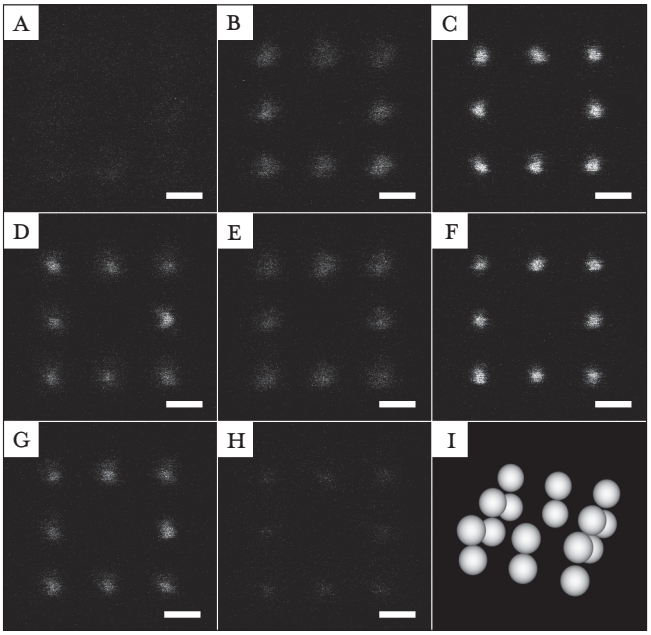

Figure 2.5
(a–h) Fluorescence confocal images of a three-dimensional structure of colloidal particles created with a two-dimensional time-shared array of optical tweezers. Eight time-shared optical traps held two 1.4 µm diameter FITC-SiO_2 particles each. The particles aligned on top of each other in the propagation direction of the laser beam. The height difference between each subsequent image was 546 nm with (a) below and (h) above the structure. The upright objective was used for trapping while the inverted objective was used for imaging. Only the fluorescent cores of the particles were imaged and image (i) was computer generated after determination of the particle coordinates from the confocal images. The scale bars are 2 µm.

demonstrate this independent trapping and imaging, we created a three-dimensional structure of colloidal particles. The upright objective (100x; 1.4 NA) was used to create an array of eight optical traps. Each trap was filled with two 1.4 µm diameter FITC-SiO_2 particles. The pair of particles in each trap was distributed along the propagation direction of the beam and formed a three-dimensional structure. This method was recently demonstrated, although not by imaging in three dimensions, by MacDonald and coworkers.[23] Using the inverted objective (63x; 1.4 NA) we imaged the sample in confocal mode. Starting below the structure and ending above it, we scanned through the two layers of particles.

Figure 2.5a shows a plane below the structure with almost no fluorescence signal detected. Moving upwards, the eight particles in the lower plane were imaged *(Figures 2.5b* and *2.5c)*. Between the two trapping planes *(Figures 2.5d* and *2.5e)* some fluorescence from the particles was detected. Moving further upwards, the particles in the second layer were imaged *(Figure 2.5f)*. Finally, *Figure 2.5h* shows a plane just above the structure. Because the

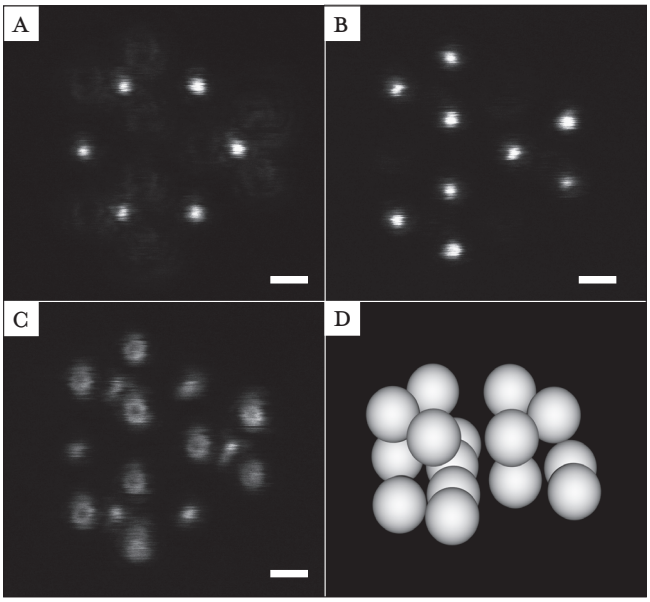

Figure 2.6
Fluorescence confocal images of particles trapped in a three-dimensional array of tweezers created by synchronizing the Pockels cell and the AODs.
(a) Six particles were trapped in the upper plane and
(b) nine in the lower plane.
(c) Between the two trapping planes fluorescence from particles in both planes was detected. The height difference between the two trapping planes was 1.7 µm. The upright objective was used for trapping while the inverted objective was used for imaging. The 1.4 µm diameter FITC-SiO_2 particles were dispersed in ethanol, and only their fluorescent cores were imaged.
(d) An image was computer generated on the basis of the confocal data.
The scale bars are 1 µm.

particles have a fluorescent core and non-fluorescent shell only the cores were imaged. The separation between the imaging planes in *Figure 2.5* was determined to be 546 nm.[56] From the confocal images we determined the three-dimensional coordinates of the particles, which we used to computer generate an image of the structure created by the optical traps (*Figure 2.5i*).

2.5 Arrays of tweezers in more than one plane using one objective

We created two trapping planes, each with a different configuration of traps, using an (100x; 1.4 NA) upright objective. The three-dimensional array was then filled with 1.4 µm diameter FITC-SiO_2 particles. The particles were dispersed in ethanol in a 10 µm thick sample. The lower objective (100x; 1.4 NA) was used for imaging. *Figure 2.6a* shows a confocal image of the upper plane in which six particles were trapped. The nine particles in the lower plane were imaged in *Figure 2.6b*. The distance between the trapping planes was determined to be 1.7 µm.[56] When the confocal microscope was focused

between the two trapping planes, both the upper and the lower plane were vaguely imaged *(Figure 2.6c)*. From the confocal images we determined the position coordinates of the particles in the trapping array and generated an artificial image of the three-dimensional structure created *(Figure 2.6d)*.

2.6 Optical tweezers in concentrated dispersions

2.6.1 Tweezers-induced crystallization in concentrated colloidal dispersions

A 100 µm thick capillary was filled with 1.4 µm diameter FITC-SiO_2 particles dispersed in DMF. The particles have a higher density than DMF ($\Delta\rho$ = 1.05 g/cm^3) and after sedimentation, a height-dependent concentration profile formed at the bottom of the capillary. The number of particles in the sample was chosen such that the bottom layer of the sediment was still fluid-like. The sample was imaged with the confocal microscope using the inverted objective (100x; 1.4 NA). *Figure 2.7a* shows an image of the bottom layer. Only the fluorescent cores of the particles were visible, and, as can be seen, the particles were in the liquid state just below the freezing transition. The interparticle distance was 1.9 µm, slightly larger than the diameter of the spheres, due to a small charge on the particles. *Figure 2.7c* shows a scan through the sample orthogonal to the bottom layer and parallel to gravity. The sediment was only a few micrometers thick.

The beam was then focused into the sample from above (upright mode) using a low numerical aperture objective (20x; 0.7 NA). With this low NA, three-dimensional trapping is not possible and the particles are pushed against the bottom of the sample cell. The focal plane of the upright objective was 33 µm below the bottom layer of the sediment. *Figure 2.7b* shows the bottom layer of the sample 15 min after the upright tweezers were turned on. The dispersion had crystallized due to the light field in the sample. The crystalline area extended over a few hundred micrometers. The defect lines in the crystal can be attributed to small aggregates in the dispersion from which they originate. *Figure 2.7d* shows an image scan parallel to gravity. The thickness of the sediment increased in comparison with the situation without tweezers *(Figure 2.7c)*. The laser beam is visible in *Figure 2.7d* as no infrared filter was used in front of the photomultiplier tubes. The laser power used was measured to be 0.58 W at the back focal plane of the objective. When the tweezers were turned off the crystal melted, and the sample returned to a fluid state.

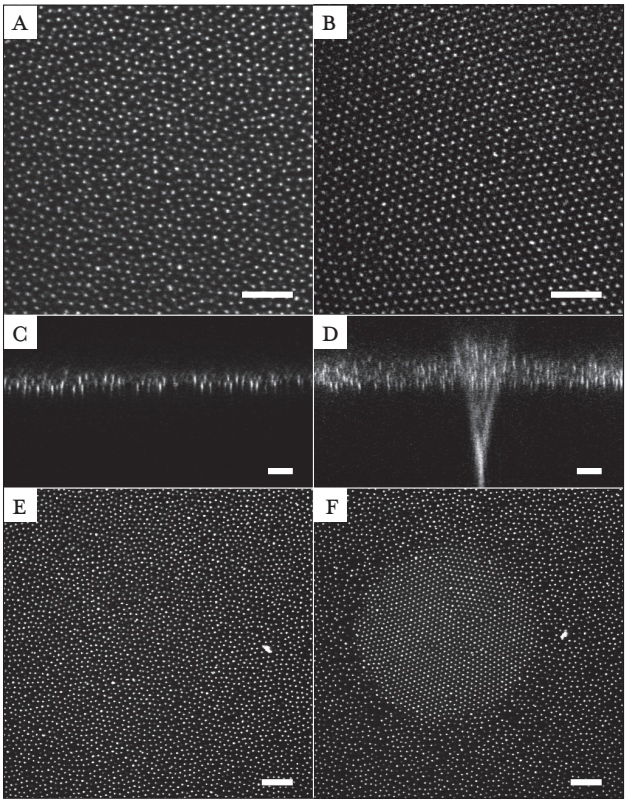

Figure 2.7
Fluorescence confocal images of 1.4 µm diameter FITC-SiO_2 particles dispersed in DMF.
(a) In the absence of the optical tweezers the particles were in the bottom layer in a liquid state.
(b) The bottom layer became crystalline when the trap was turned on, in the upright mode, using a low numerical aperture objective (20x; 0.7 NA). The crystal layer extended over hundreds of micrometers
(c) A scan of the sample perpendicular to the bottom layer and in the absence of the field. The sediment was a few particles thick
(d) With the tweezers turned on the sediment became thicker. The trapping beam was imaged and the focus of the trap was 33 µm below the bottom plane of the sample. The size of the optical trap was diffraction limited and in the order a few particle diameters.
(e) Bottom layer of a dispersion of 1.4 µm diameter FITC-SiO_2 particles in ethanol.
(f) A crystal formed when the laser was focused using a high numerical aperture objective (100x; 1.4 NA) in upright trapping mode.
The scale bars are 10 µm.

We also used a high numerical aperture objective (100x; 1.4 NA) to focus the laser in a dispersion of 1.4 µm diameter FITC-SiO_2 particles dispersed in ethanol. *Figure 2.7e* shows a confocal image of particles in the fluid phase in the bottom layer of the sample before the laser was turned on. When the upright tweezers were turned on, a crystallite formed in the colloidal fluid *(Figure 2.7f)*. The interparticle distance in the crystal was 1.6 µm. The diameter of the crystallite increased with the laser power used. For this experiment, the power at the back focal plane was measured to be 0.5 W. When the tweezers were turned off the crystallite melted within a few seconds and the sample returned to its original state.

The optical force on the particles in the bottom plane is proportional to the gradient of the intensity of the light field. The focused laser light applies an optical pressure towards the focal point. As particles were pushed towards the focal point, the concentration increased locally, and the thickness of the sediment increased. A steady state was achieved when the optical, the osmotic, and the gravitational pressure balanced. When the local pressure in the sample exceeded the pressure at the freezing transition, the colloidal fluid crystallized. Although the size of the focal spot was diffraction limited and in size only a few particle diameters, the gradient force far away from the focus was still large enough to crystallize the sample. Recently, Sullivan and coworkers reported crystallization of concentrated dispersions induced by increasing the volume fraction locally with gradients in electric fields.[57] Optical tweezers-induced crystallization can be viewed as a high-frequency analog of their technique. Crystallization of the layer of colloidal particles was not observed when the tweezers were operated in the inverted mode as no equilibrium situation was achieved and particles were pushed around through the sample. We are currently investigating these processes in more detail.

2.6.2 manipulation of (core-shell) tracer particles in a concentrated dispersion

To demonstrate selective optical trapping in a concentrated dispersion, we dispersed a mixture of PS-SiO_2 tracer and FITC-SiO_2 host particles in a solvent mixture of DMF and DMSO with the same refractive index as SiO_2 at 1064 nm. The diameters of the particles were 975 and 1050 nm, respectively. The concentration of the samples was chosen such that, after the dispersion had sedimented in the 100 µm thick capillary, a thin sediment formed which was either liquid-like or crystalline in the bottom layer. We created a 3 x 3 square array of optical tweezers with different spacings between the traps in the bottom layer in the dispersion. Eight traps were filled with tracer particles, and one trap was left empty. The upright objective (63x; 1.4 NA) was used for trapping, while the inverted objective (100x; 1.4 NA) was used for imaging.

Figure 2.8 shows combined fluorescence and reflection confocal images of the trapped tracer particles surrounded by host particles. The tracer particles are displayed in black while the hosts are displayed in light gray. The images were averaged over multiple frames with a time step of

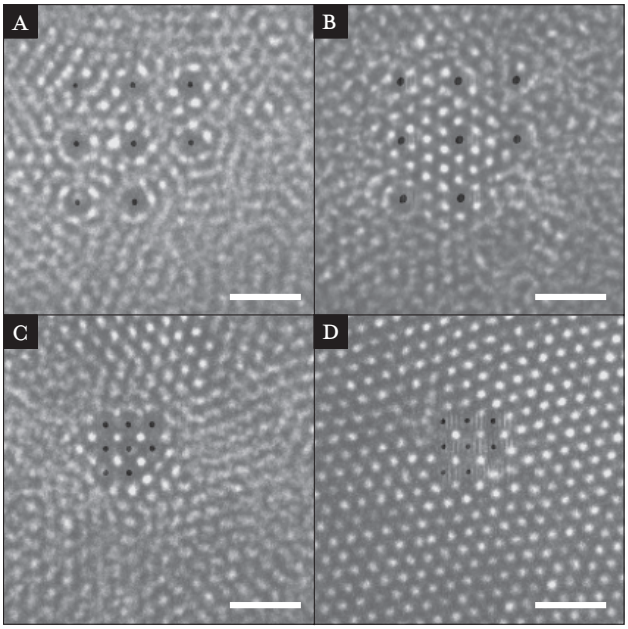

Figure 2.8
Combined confocal reflection and fluorescence images of a mixture of PS-SiO_2 tracer particles (black) and FITC-SiO_2 host particles (light gray). The mixture was dispersed in a fluid matching the refractive index of the host particles. The tracer particles were trapped in a 3 x 3-array of optical tweezers. The upright objective was used for trapping while the inverted objective was used for imaging. The lattice spacing of the templates was (a) 4.1 µm, (b) 4.1 µm, (c) 1.6 µm, and (d) 1.8 µm. The template of tracer particles induced structure in the host dispersion. Images were averaged over (a) 20, (b) and (c) 10, and (d) 4 images with 1.7 seconds between the frames. Immobile particles were imaged sharply while moving particles became blurred. Only the cores of both tracer and host particles were imaged. Note that only eight of the nine traps were occupied and that no host particles are drawn towards nor expelled from the empty trap, demonstrating that optical forces on the host particles are negligible.
The scale bars are 5 µm.

1.7 s between the frames. Because of the averaging, mobile particles were blurred in the images, while particles that were not moving were imaged sharply. *Figure 2.8a* was averaged over 20 images and shows an open structure with a separation between the traps of 4.1 µm. The concentration of the surrounding host particles was below the freezing point, and they were in the liquid state. In the array with trapped tracer particles, the host particles showed some ordering but did not crystallize. *Figure 2.8b* (averaged over ten frames) shows an array with the same trap separation as in *Figure 2.8a*, but here the host spheres crystallized with a hexagonal symmetry in the array with tracer particles. The host particles surrounding the array were still clearly liquid-like. *Figures 2.8c* and *2.8d* (averaged over ten and four frames, respectively) show arrays with smaller trap separations of 1.6 and 1.8 µm. In *Figure 2.8c* host spheres penetrate the array of tracer particles, resulting

in an ordered structure with square symmetry while the surrounding host spheres were still liquid-like. *Figure 2.8d* shows that also in a crystalline layer the tracer particles can be trapped in an array that is incommensurate with the crystal lattice. The hexagonal layer incorporated the different symmetry of the trapped structure although some defect lines originate from the trapped structure. At the position of the empty trap in the 3 x 3 array can be seen that the force on the host particles was negligible compared to their thermal energy. If the host particles were either under or over matched by the solvent mixture, the optical forces on the host particles would either pull them towards or expel them from the trap.

The high index core of the tracer particles allowed them to be manipulated in a concentrated dispersion of refractive-index matched host particles. The core-shell morphology of the tracer particles has several other advantages. Because the shell of the core-shell particles is of the same material as the host particles, all particles in the mixture have the same surface properties and thus the same interparticle interaction. Furthermore, the optically induced forces between trapped particles are decreased, as only the cores are trapped, and the forces decay strongly with interparticle distance.[22, 58] Finally, the core-shell geometry is advantageous for trapping in three-dimensional arrays of optical traps (as in Sections 2.4, 2.5, and 7.3) as the scattering unit of a particle is smaller, thus giving less distortion of the laser field behind the particle.

2.7 Counterpropagating tweezers

Counterpropagating optical tweezers[1, 48] have the advantage over single-beam traps that they can trap strongly scattering particles. The scattering force on a particle is cancelled due to symmetry of the two beams along the optical axis. At the same time, the gradient force is added resulting therefore in stronger confinement of the particle in all directions compared to a single-beam trap.

To demonstrate such a counterpropagating trap, we trapped a 0.5 µm ZnS particle dispersed in ethanol. The high refractive index (n_d^{20}= 2.0) meant that the particle could not be trapped in a conventional single-beam gradient trap. *Figure 2.9a* shows on the left the ZnS particle in a counterpropagating trap. The trap was created using both the inverted and upright objective (both 100x, 1.4 NA). The laser power was divided equally between the lower and the upper beam path. The particle on the right in *Figure 2.9a* is a 1.4 µm FITC-SiO_2 particle stuck to the lower sample wall. To

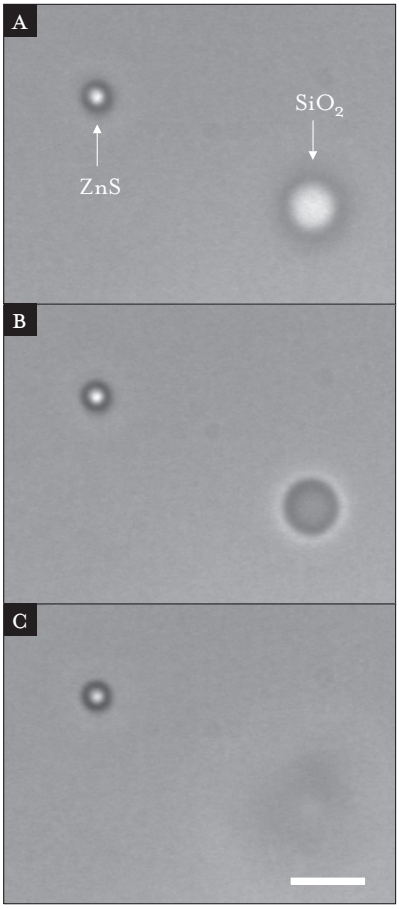

Figure 2.9
(a) A 0.5 µm diameter ZnS particle (left) trapped in counterpropagating optical tweezers next to a 1.4 µm diameter FITC-SiO_2 particle (right) that was stuck to the surface of the sample cell. The ZnS particle was trapped in three dimensions as can be seen in
(b) and (c) where the sample was moved down with respect to the trapping plane. The ZnS particle was trapped and therefore stayed in focus, while the FITC-SiO_2 particle moved out of the focal plane. It was not possible to trap the ZnS particle using single-beam optical tweezers.
The scale bar is 2 µm.

demonstrate that the ZnS particle was indeed trapped in three dimensions in the counterpropagating trap, we moved the stage down in *Figures 2.9b* and *2.9c*. As can be seen, the ZnS particle stayed in focus while the FITC-SiO_2 particle moved out of focus. We could shift the position of the ZnS particle with respect to the imaging plane by changing the relative power in the upper and lower beam paths. It should be noted that earlier counterpropagating traps used low NA lenses (and therefore radiation pressure) for trapping. As we use high NA objectives, particles are trapped by the gradient force.

2.8 Discussion and outlook

The setup described in this chapter was developed to both manipulate and image individual colloidal particles in three dimensions in concentrated

colloidal dispersions. We have shown that the combination of confocal microscopy and time-shared optical tweezers allows independent three-dimensional imaging and manipulation of the dispersion. At present we are exploring, with the setup, the stability of three-dimensional arrangements of particles[23] and optically induced forces between non-core-shell particles[59] on a quantitative level.

By choosing AODs to time-share the laser beam we have shown that it is possible to create large arrays of hundreds of optical traps and change them dynamically, because AODs can be scanned at hundreds of kHz. These arrays of tweezers were used to create two- and three-dimensional structures of particles. Arrays of tweezers in two planes were created using a Pockels cell and polarizing beam splitters. Such an approach does not make it possible to move particles in three dimensions, but is one of the fastest methods to create and dynamically change the symmetry of two independent two-dimensional arrays of optical tweezers.

In addition, we have shown that selective trapping and manipulation of individual tracer particles is possible if a concentrated system of host and tracer particles is used and the tracer particles have a core-shell geometry with a high refractive index material core and a lower index material shell. We have shown that when the host particles consist of the same material as the lower index shells, the tracer particles can be manipulated without exerting forces on the host particles. By fluorescently labeling the (cores of the) host particles it is possible to follow the effects of the trapped spheres on the bulk dispersion on a single particle level in three dimensions. The optically trapped particles experience a local potential by which they can be brought out of equilibrium.

In combination with the use of the earlier mentioned arrays of tweezers it is possible to study crystal nucleation (as is also shown in chapter 7). With our setup the umbrella-sampling scheme that uses a local potential to allow the possibility to probe unlikely events such as crystal nucleation in computer simulations,[60] can now be implemented experimentally.

Also without the use of a tracer-host system we have shown that it is possible to crystallize and melt colloidal dispersions using optical forces (see also chapter 6). In this case forces are exerted on collections of particles. By changing the numerical aperture of the lens the geometry of the volume on which forces are exerted can be changed. This technique bears strong resemblances with the use of gradients of low-frequency electric fields to

manipulate the density of the colloidal dispersion.[57] In combination with a tracer-host system, this technique to manipulate the concentration can be used to study the critical nucleus size in a colloidal fluid close to crystallization as well.

Finally, by using counterpro pagating traps high refractive index particles could be manipulated that could not be trapped in three dimensions with conventional single-beam optical tweezers. Recently, we have developed a method to create structures of colloidal particles on surfaces using single-beam optical tweezers (see also chapter 3).[38, 39] Using the setup in counterpropagating mode allows particles with a high refractive index to be incorporated in such two- and three-dimensional structures giving the possibility to create or dope photonic materials with high index particles.

Acknowledgements

This work has been performed together with Astrid van der Horst and Marileen Dogterom. We would like to thank Joop van Dorsselaer, Henk Neerings, Sjoerd Wouda, and Hans Wisman for help in designing and constructing the setup, Krassimir Velikov for synthesis of the ZnS particles, and Jacob Hoogenboom, Cendrine Faivre-Moskalenko, Alexander Moroz, Myrthe Plaisier, and Koen Visscher for useful discussions. Koen Visscher is also thanked for his assistance with the first experiments using the Pockels cell, which were performed in his lab by Astrid van der Horst.

REFERENCES

1 *A. Ashkin, Acceleration and trapping of particles by radiation pressure, Phys. Rev. Lett. 24, 156 (1970).*
2 *A. Ashkin, J. M. Dziedzic, J. E. Bjorkholm, and S. Chu, Observation of a single-beam gradient force optical trap for dielectric particles, Opt. Lett. 11, 288 (1986).*
3 *K. Visscher, S. P. Gross, and S. M. Block, Construction of multiple-beam optical traps with nanometer-resolution position sensing, Journal of Selected Topics in Quantum Electronics 2, 1066 (1996).*
4 *D. G. Grier, Optical tweezers in colloid and interface science, Curr. Opin. Colloid Interface Sci. 2, 264 (1997).*
5 *K. Dholakia, G. Spalding, and M. MacDonald, Optical tweezers: the next generation, Phys. World 15, 31 (2002).*
6 *D. G. Grier, A revolution in optical manipulation, Nature 424, 810 (2003).*
7 *P. A. M. Neto and H. M. Nussenzveig, Theory of optical tweezers, Europhys. Lett. 50, 702 (2000).*
8 *Y. Harada and T. Asakura, Radiation forces on a dielectric sphere in the Rayleigh scattering regime, Opt. Commun. 124, 529 (1996).*
9 *A. Ashkin, in Methods in Cell Biology, edited by M. P. Sheetz (Academic Press, San Diego, 1998), Vol. 55, p. 1.*
10 *K. Sasaki, M. Koshioka, H. Misawa, N. Kitamura, and H. Masuhara, Optical trapping of a metal-particle and a water droplet by a scanning laser-beam, Appl. Phys. Lett. 60, 807 (1992).*
11 *H. He, M. E. J. Friese, N. R. Heckenberg, and H. Rubinsztein-Dunlop, Direct observation of transfer of angular-momentum to absorptive particles from a laser-beam with a phase singularity, Phys. Rev. Lett. 75, 826 (1995).*

12 K. Visscher, G. J. Brakenhoff, and J. J. Krol, Micromanipulation by multiple optical traps created by a single fast scanning trap integrated with the bilateral confocal scanning laser microscope, Cytometry 14, 105 (1993).
13 M. E. J. Friese, T. A. Nieminen, N. R. Heckenberg, and H. Rubinsztein-Dunlop, Optical alignment and spinning of laser-trapped microscopic particles, Nature 394, 348 (1998).
14 L. Paterson, M. P. MacDonald, J. Arlt, W. Sibbett, P. E. Bryant, and K. Dholakia, Controlled rotation of optically trapped microscopic particles, Science 292, 912 (2001).
15 J. Guck, R. Ananthakrishnan, T. J. Moon, C. C. Cunningham, and J. Kas, Optical deformability of soft biological dielectrics, Phys. Rev. Lett. 84, 5451 (2000).
16 K. Sasaki, M. Koshioka, H. Misawa, N. Kitamura, and H. Masuhara, Pattern-formation and flow-control of fine particles by laser-scanning micromanipulation, Opt. Lett. 16, 1463 (1991).
17 C. Mio, T. Gong, A. Terray, and D. W. M. Marr, Design of a scanning laser optical trap for multiparticle manipulation, Rev. Sci. Instrum. 71, 2196 (2000).
18 J.-M. Fournier, M. M. Burns, and J. A. Golovchenko, in Proc. SPIE, edited by S. A. Benton, 1995, Vol. 2406, p. 101.
19 E. R. Dufresne and D. G. Grier, Optical tweezer arrays and optical substrates created with diffractive optics, Rev. Sci. Instrum. 69, 1974 (1998).
20 Y. Hayasaki, M. Itoh, T. Yatagai, and N. Nishida, Nonmechanical optical manipulation of microparticle using spatial light modulator, Optical Review 6, 24 (1999).
21 J. Liesener, M. Reicherter, T. Haist, and H. J. Tiziani, Multi-functional optical tweezers using computer-generated holograms, Opt. Commun. 185, 77 (2000).
22 M. M. Burns, J.-M. Fournier, and J. A. Golovchenko, Optical matter: crystallization and binding in intense optical fields, Science 249, 749 (1990).
23 M. P. MacDonald, L. Paterson, K. Volke-Sepulveda, J. Arlt, W. Sibbett, and K. Dholakia, Creation and manipulation of three-dimensional optically trapped structures, Science 296, 1101 (2002).
24 R. L. Eriksen, V. R. Daria, and J. Gluckstad, Fully dynamic multiple-beam optical tweezers, Opt. Express 10, 597 (2002).
25 M. Minsky, (U.S. Patent 301467, 1961).
26 J. K. Stevens, L. R. Mills, and J. E. Trogadis, Three-dimensional confocal microscopy: Volume investigation of biological systems (Academic Press, San Diego, 1994).
27 M. H. Chestnut, Confocal microscopy of colloids, Curr. Opin. Colloid Interface Sci. 2, 158 (1997).
28 A. van Blaaderen, Quantitative real-space analysis of colloidal structures and dynamics with confocal scanning light microscopy, Progr Colloid Polym Sci 104, 59 (1997).
29 A. D. Dinsmore, E. R. Weeks, V. Prasad, A. C. Levitt, and D. A. Weitz, Three-dimensional confocal microscopy of colloids, Appl. Optics 40, 4152 (2001).
30 J. B. Pawley, Handbook of biological confocal microscopy (Plenum Press, New York, 1995).
31 A. van Blaaderen, K. P. Velikov, J. P. Hoogenboom, D. L. J. Vossen, A. Yethiraj, R. P. A. Dullens, T. van Dillen, and A. Polman, in Photonic crystals and light localization in the 21st century, edited by C. M. Soukoulis (Kluwer, 2001), p. 239.
32 M. Brunner, C. Bechinger, W. Strepp, V. Lobaskin, and H. H. von Grunberg, Density-dependent pair interactions in 2D colloidal suspensions, Europhys. Lett. 58, 926 (2002).
33 A. van Blaaderen, J. P. Hoogenboom, D. L. J. Vossen, A. Yethiraj, A. van der Horst, K. Visscher, and M. Dogterom, Colloidal epitaxy: Playing with the boundary conditions of colloidal crystallization, Faraday Discuss. 123, 107 (2003).
34 A. Yethiraj and A. van Blaaderen, A colloidal model system with an interaction tunable from hard sphere to soft and dipolar, Nature 421, 513 (2003).
35 A. van Blaaderen and P. Wiltzius, Real-space structure of colloidal hard-sphere glasses, Science 270, 1177 (1995).
36 W. K. Kegel and A. van Blaaderen, Direct observation of dynamical heterogeneities in colloidal hard-sphere suspensions, Science 287, 290 (2000).
37 U. Gasser, E. R. Weeks, A. Schofield, P. N. Pusey, and D. A. Weitz, Real-space imaging of nucleation and growth in colloidal crystallization, Science 292, 258 (2001).
38 J. P. Hoogenboom, D. L. J. Vossen, C. Faivre-Moskalenko, M. Dogterom, and A. van Blaaderen, Patterning surfaces with colloidal particles using optical tweezers, Appl. Phys. Lett. 80, 4828 (2002).
39 D. L. J. Vossen, J. P. Hoogenboom, K. Overgaag, and A. van Blaaderen, in Materials Research Society Symposium Proceedings, edited by L. Merhari, Boston, (2002), Vol. 705.

40 J. C. Crocker and D. G. Grier, Microscopic measurement of the pair interaction potential of charge-stabilized colloid, Phys. Rev. Lett. 73, 352 (1994).

41 J. C. Crocker, J. A. Matteo, A. D. Dinsmore, and A. G. Yodh, Entropic attraction and repulsion in binary colloids probed with a line optical tweezer, Phys. Rev. Lett. 82, 4352 (1999).

42 S. Henderson, S. Mitchell, and P. Bartlett, Position correlation microscopy: probing single particle dynamics in colloidal suspensions, Colloid Surf. A-Physicochem. Eng. Asp. 190, 81 (2001).

43 P. T. Korda and D. G. Grier, Annealing thin colloidal crystals with optical gradient forces, J. Chem. Phys. 114, 7570 (2001).

44 J. Leach, G. Sinclair, P. Jordan, J. Courtial, M. J. Padgett, J. Cooper, and Z. J. Laczik, 3D manipulation of particles into crystal structures using holographic optical tweezers, Opt. Express 12, 220 (2004).

45 A. Resnick, Design and construction of a space-borne optical tweezer apparatus, Rev. Sci. Instrum. 72, 4059 (2001).

46 A. Hoffmann, G. M. Z. Horste, G. Pilarczyk, S. Monajembashi, V. Uhl, and K. O. Greulich, Optical tweezers for confocal microscopy, Appl. Phys. B-Lasers Opt. 71, 747 (2000).

47 K. Visscher and G. J. Brakenhoff, Single beam optical trapping integrated in a confocal microscope for biological applications, Cytometry 12, 486 (1991).

48 S. B. Smith, Y. J. Cui, and C. Bustamante, Overstretching B-DNA: The elastic response of individual double-stranded and single-stranded DNA molecules, Science 271, 795 (1996).

49 J. C. Crocker and D. G. Grier, Methods of digital video microscopy for colloidal studies, J. Colloid Interface Sci. 179, 298 (1996).

50 A. van Blaaderen and A. Vrij, Synthesis and characterization of colloidal dispersions of fluorescent, monodisperse silica spheres, Langmuir 8, 2921 (1992).

51 N. A. M. Verhaegh and A. van Blaaderen, Dispersions of rhodamine-Labeled silica spheres - synthesis, characterization, and fluorescence confocal scanning laser microscopy, Langmuir 10, 1427 (1994).

52 H. Giesche, Synthesis of monodispersed silica powders II. Controlled growth reaction and continuous production process, J. Eur. Ceramic Soc. 14, 205 (1994).

53 K. P. Velikov and A. van Blaaderen, Synthesis and characterization of monodisperse core-shell colloidal spheres of zinc sulfide and silica, Langmuir 17, 4779 (2001).

54 C. Graf, D. L. J. Vossen, A. Imhof, and A. van Blaaderen, A general method to coat colloidal particles with silica, Langmuir 19, 6693 (2003).

55 F. Gittes and C. F. Schmidt, in Methods in Cell Biology, edited by M. P. Sheetz (Academic Press, San Diego, 1998), Vol. 55, p. 129.

56 S. W. Hell and E. H. K. Stelzer, in Handbook of biological confocal microscopy, edited by J. B. Pawley (Plenum Press, New York, 1995).

57 M. Sullivan, K. Zhao, C. Harrison, R. H. Austin, M. Megens, A. Hollingsworth, W. B. Russel, Z. D. Cheng, T. Mason, and P. M. Chaikin, Control of colloids with gravity, temperature gradients, and electric fields, J. Phys. Cond. Matter 15, S11 (2003).

58 M. I. Antonoyiannakis and J. B. Pendry, Mie resonances and bonding in photonic crystals, Europhys. Lett. 40, 613 (1997).

59 R. C. Gauthier and M. Ashman, Simulated dynamic behavior of single and multiple spheres in the trap region of focused laser beams, Appl. Optics 37, 6421 (1998).

60 S. Auer and D. Frenkel, Prediction of absolute crystal-nucleation rate in hard-sphere colloids, Nature 409, 1020 (2001).

3 Patterning surfaces using optical tweezers and critical point drying

A method for patterning substrates with colloidal particles in any designed two-dimensional structure is described. Optical tweezers are used to bring particles from a reservoir to a surface that carries a surface charge opposite to that of the particles. Chemical surface modification and polyelectrolyte coating of either the substrate or the colloids make the method generally applicable. Using this technique, large two-dimensional patterns can be fabricated, with full control over the position of each individual particle. Subsequently, the structures can be dried without distortions due to surface tension forces using critical point drying. As examples we show positioning of 79 nm radius metallodielectric particles, and we show two-dimensional patterns that have been used to direct three-dimensional epitaxial crystal growth. The method is inexpensive, relatively fast, and can be fully automated. We show some first results of three-dimensional structures created by repeating the procedure of patterning in a layer-by-layer fashion.

3.1 Introduction

Colloidal particles are the building blocks for materials that find applications in a wide variety of research. The typical particle sizes, ranging from several nanometers up to a few micrometers, and the possibility to control their morphology and chemical properties make colloids interesting for photonic,[1-3] electronic,[4,5] magnetic and sensor[6,7] applications. Two-dimensional arrangements of colloids on substrates are of great interest for most of these applications. Several recent examples include the use of colloidal mono-layers as microlens arrays[2, 8] and arrays of closely spaced metal nanoparticles that can serve as subwavelength plasmon-mode waveguides.[3, 9, 10] Arrays of colloidal particles have also been used to create other nanostructures, e.g., by using them as masks for lithography,[11] as is shown in chapters 4 and 5.

The techniques used for arranging colloids in two-dimensional patterns vary from template-directed self-assembly[1, 2, 12, 13] and patterning of self-assembled monolayers,[14] to direct single-particle patterning.[15-17] Clearly, this last category of methods offers the highest level of control over pattern structure, but the techniques reported so far are limited in the range of particle sizes, particle morphologies, and substrates that they can process.

To our knowledge, Misawa and coworkers were the first to use optical trapping of micron-sized polymeric particles to assemble larger structures.[18] They described a technique to position polymeric particles on polymeric substrates using optical tweezers and single-particle photothermal fixation.[15] Mio *et al.* used local photopolymerization and time-shared optical tweezers to fix particles arranged in a desired structure against a glass substrate.[17] These techniques were limited in either particle type or pattern size. Other methods that have been developed use an atomic force microscope or a micro-robot in a scanning electron microscope.[16] Both methods need particle-tip contact, limiting the particle sizes that can be handled or spatial resolution that can be obtained. Furthermore, the last method needs to be operated at high vacuum.

In this chapter, we describe a method to create large, two-dimensional patterns of colloids on substrates using optical tweezers.[19, 20] Surfaces and particles are given an opposite charge, if necessary, and optical tweezers are then used to select, trap, position, and stick particles to the desired position on the surface. The method gives full control over the structure on a single particle level. The particles are bound to the oppositely charged

substrates through electrostatic interaction. A wide variety of techniques for chemical and physical surface modification is available, allowing a large variety of particle sizes and morphologies to be used. We demonstrate our technique for micron- and submicron-sized particles, and we will show that it is possible to direct three-dimensional crystallization of colloidal particles using two-dimensional patterns as templates. For many applications it is necessary to dry the patterned structures before further processing. Drying by solvent evaporation easily distorts the structures, because surface tension forces can become much larger than the forces keeping the particles fixed to the surface. To remove the structures from the solvent without distortions, critical point drying is used.[20] We will show how, by repeated patterning and drying, three-dimensional structures can be built in a layer-by-layer fashion.

3.2 Experimental details

In our setup, optical tweezers are created by focusing an infrared laser beam (Spectra Physics; 10 W; wavelength 1064 nm) to a diffraction-limited spot using a high numerical aperture (NA) microscope objective (100x; oil immersion; 1.4 NA) on an inverted microscope (Leica DM IRB). The position of the tweezers in the sample is controlled using acousto-optic deflectors (IntraAction) or by moving the sample using a high-accuracy (< 0.5 nm) piezo microscope stage (Physik Instrumente). Apart from the possibility to position particles in a single-particle trap like in the examples shown below, large arrays of optical tweezers can also be used to position hundreds of particles simultaneously. The sample can be imaged in normal brightfield mode or in differential interference contrast (DIC) microscopy and a charge-coupled device (CCD) camera or by confocal microscopy (Leica TCS NT). The setup is described in detail in chapter 2 as well as in Ref. 21.

Figure 3.1 shows a schematic drawing of the sample cells used. The sample cell consists glass cover slip (Chance; No. 1) on the bottom and a glass substrate on top, spaced approximately 10 μm apart. For particles with high enough buoyancy, sedimentation of particles in suspension naturally forms a reservoir at the bottom glass plate of the sample. Alternatively, in the case of particles with low buoyancy, a laterally displaced reservoir of particles in the sample was used. The optical tweezers are used to trap particles in the reservoir and bring them to the top substrate at the desired

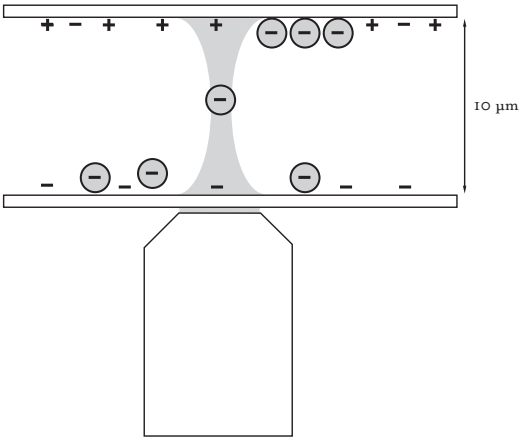

Figure 3.1
Schematic drawing (not to scale) of the sample cell used for patterning surfaces using optical tweezers. The sample cell consists of a colloidal suspension sandwiched between two cover slips of which the top one has an opposite charge from that of the colloids. Particles are freely diffusing on the bottom wall, acting as a reservoir, and are brought up using the optical tweezers.

position. Alternatively, the optical trap can be focused at the upper surface of the sample cell. The particles are then guided upwards and immobilized at the upper plate. Leaving the beam focused at the top substrate until a particle is positioned and then rapidly switching its position allows for faster positioning, although one cannot discriminate between different types of particles. Because image processing of the trapped sphere can take place at any stage of the patterning procedure, the process can be fully automated. A feedback loop can be built in the system for increased positioning accuracy.

In the present chapter, we used particles that can be trapped stably in three dimensions using a single-beam optical trap, but we want to remark that when the trap is positioned at the top surface, only two-dimensional stable trapping is required as in "laser-driven particle propagation".[22] The high intensity gradient needed for three-dimensional stable trapping used in this chapter improves the accuracy for positioning particles that can only be trapped stably in two dimensions.

The silica and metallodielectric particles shown in the examples below were all synthesized using procedures described in the literature.[23-25] Particles were suspended in ethanol or water, and particle concentrations were chosen such that if all particles were sedimented, they would cover approximately 20% of the bottom glass plate. A typical concentration was $10^7\,ml^{-1}$. Electrostatic interactions are used to immobilize particles on the top substrate. When the natural surface charges of either substrate or particles in suspension are too low or not of opposite sign, they can be changed by surface modification. Our glass cover slips were coated with a

layer of 3-aminopropyltriethoxysilane (APS; Fluka),[23, 26] which renders the glass surface positively charged. To this end, the glass cover slips were placed in a mixture of 140 ml ethanol (Merck; absolute grade) and 4.5 ml ammonia (Sigma; 25 wt-%). Then, 23.0 ml APS was added, followed by thorough mixing of the suspension. The coating reaction was allowed to proceed for one hour under gentle stirring using a magnetic bead stirrer. The coated cover slips were rinsed several times with ethanol and dried in air. We have also coated substrates and particles with a layer of adsorbed polyelectrolytes of a few nanometer thick. We used poly(allylamine hydrochloride) (PAH; Aldrich) or poly(styrene sodium sulfonate) (PHS; Aldrich) using a layer-by-layer assembly technique.[27, 28] This technique has proven to work for a large variety of particles and surfaces, including organic, inorganic, hybrid, and uncharged colloids. For a review see Ref. 29.

The samples were dried using a critical point dryer (Emscope CPD 750), which was filled with ethanol. After closing the chamber, the sample was carefully flushed with liquid carbondioxide for 10 min. after which the sample was left for 10 min. to ensure mixing of ethanol and liquid CO_2. These steps of flushing and soaking were repeated, typically two times, until no ethanol came out of the sample chamber. After the replacement of ethanol with liquid carbondioxide, the sample chamber of the critical point dryer was heated, increasing the temperature and pressure above the critical point of CO_2 (T_c = 31.5 °C; P_c = 75 bar). With the carbon dioxide in its supercritical state, the sample was let to equilibrate for 10 minutes, after which the chamber was slowly depressurized taking care that the temperature stayed constant and above the critical temperature. For the positioning of a next layer, the sample was kept at 80 °C for one night and the structure was recoated as described above. Scanning Electron Microscopy (SEM, Philips XL30 SFEG) with an acceleration voltage of 2 kV was used to image the dried structures.

3.3 Results and discussion

Figure 3.2 shows a differential interference contrast (DIC) image of 153 silica particles, with 700 nm radius, patterned on a 3-APS coated glass cover slip. The particles have been positioned with the symmetry of a (1100)-plane of a hexagonally close-packed crystal. The accuracy of positioning, the root-mean-square deviation of the actual versus the designated position, was determined with image processing to be 73 nm. Note that in solution, particle

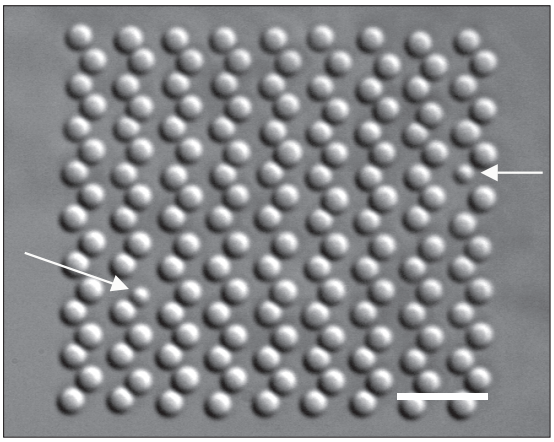

Figure 3.2
DIC microscopy image of a pattern of 153 silica particles (700 nm radius) arranged on a hcp (1100) lattice on a substrate, in suspension. The arrows indicate two smaller particles that have been incorporated as defects in the pattern.
The scale bar is 5 μm.

excursions in the optical trap are limited to within several nanometers only. When the position of the trap is moved towards the glass surface, particle excursions increase due to reflections affecting the optical potential gradient in the trap. The accuracy of positioning can be improved considerably by reducing reflections at the surface by refractive-index matching the glass interface, as described in chapters 6-8. Or, alternatively, the accuracy can be improved by using counterpropagating optical tweezers, as described in chapter 2, to create a symmetric and stiffer trap over the interface.

As an illustration of how defects or different types of particles can be incorporated into a structure, two smaller particles have been placed in the structure as indicated by the white arrows in *Figure 3.2*. Using our technique, incorporation of a different particle type into a structure is easier to achieve than when immobilizing larger assemblies of particles at once, e.g., using time-shared optical tweezers in combination with photopolymerization.[17] Furthermore, the use of electrostatic attraction between particles and substrate allows for a wider range of particles and substrates to be used than with single-particle photothermal fixation[2] or local photopolymerization.[30]

The variety of particles that can be manipulated with optical tweezers is enormous. Materials that can be trapped include inorganic dielectric, metallic, and biological materials. Particle sizes range from several nanometers to tens of micrometers. Structures that we made using this method include particles that are interesting for photonic applications like

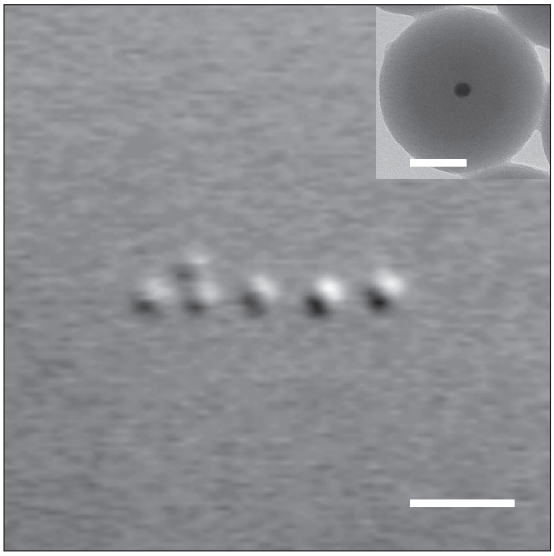

Figure 3.3
Metallodielectric core-shell particles consisting of a 7.5 nm radius gold core coated with a silica shell with outer radius 79 nm, arranged in a line pattern. The interparticle spacing is 1 µm. A sixth particle has been placed above the second particle from the left. The image was taken in DIC. The inset shows a TEM image of the particles used, with the gold core clearly visible.
Scale bars in the image and the inset are 2 µm and 50 nm, respectively.

high-refractive index (ZnS) core-silica shell particles, metallic core-silica shell particles, fluorescently labeled particles, and small (several nanometers large) gold particles.[19] As described in the experimental section we also used the techniques developed by Decher and coworkers to coat the particles or the substrate with polyelectrolytes. The combination of optical tweezers and a simple coating step makes this a very general and powerful method for creating large two-dimensional patterns. During the whole procedure of particle capture and positioning, image processing of the trapped sphere can take place, so that the process can be automated.

Apart from the micron-sized silica particles shown in *Figure 3.2*, we have also applied our method to 7.5 nm radius gold particles coated with a silica shell with an outer radius of 79 nm (see the TEM-image in the inset in *Figure 3.3*). Arrangements of functional particles in this size range in plasmon wire structures have been suggested as a route to high efficiency, sub-wavelength waveguides.[3, 9] Because of their smaller size compared to the 700 nm silica particles, a sample cell containing a particle concentration gradient was used, where particles were trapped in the high-concentration part of the sample and then moved towards the other end containing the patterned region. In *Figure 3.3*, a line pattern of the metallodielectric core-shell particles is shown. The pattern consists of 5 particles spaced 1 µm apart, with a sixth particle arranged above the second one from the left.

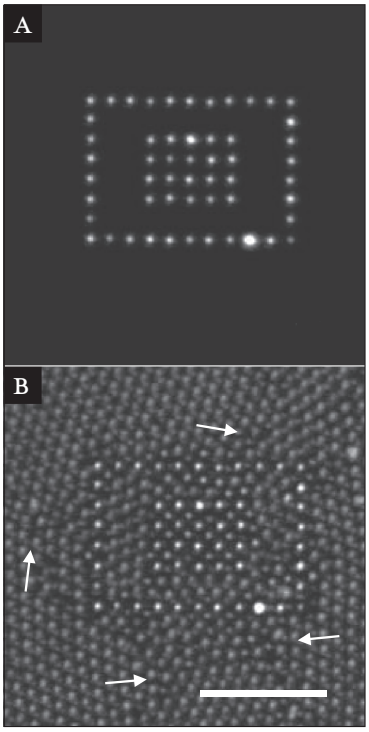

Figure 3.4
Fluorescence confocal microscopy images of
(a) a pattern of 1 μm diameter silica particles labeled with RITC and
(b) after addition of FITC labeled (dark gray) particles. The image in (b) has been taken with the focus in between the first and the second layer such that particles from both the first and the second layer can be seen in the central square.
The scale bar is 10 μm.

This demonstrates the range of particle sizes for which this technique can be used as well as its applicability to patterning with particles with a functional morphology.

This two-dimensional 'do-it-yourself' organization can be used to direct three-dimensional self-organization by colloidal epitaxy. First, we patterned a structure consisting of a rectangular array of four by five particles surrounded by a rectangle of particles with equal interparticle spacing. The patterned 500 nm radius silica particles have a 100 nm radius core labeled with rhodamine isothiocyanide (RITC). *Figure 3.4a* shows a confocal microscopy image of this structure. After patterning, the sample cell was washed with water to remove excess particles, inverted and a small amount of particles with the same outer radius of 500 nm but with a 200 nm radius fluoresceine isothiocyanide (FITC) core was added. *Figure 3.4b* shows both the initially patterned particles in light gray and the added FITC particles in dark gray, 16 hours after addition. The added FITC particles have crystallized in hexagonal sheets parallel to the glass wall, as is observed for a flat silica wall on which particles are free to diffuse. This is probably due to the fact that the

APS-coated surface lost most of its positive surface charge by exposure to CO_2 in water (H_2CO_3) during the washing step. These FITC particles are slightly out-of-focus, causing the hexagonal lattice to be blurred, so that the particles in the second layer above the square pattern could also be imaged. These particles are clearly visible as dark gray particles in between the light gray particles and follow the square symmetry of the pattern, showing that a small grain can locally direct epitaxial growth. Similarly, the pattern could be made containing built-in defects, like in *Figure 3.2*, in order to study the relaxation of defects in three-dimensional epitaxy. In *Figure 3.4b* effects of the pattern on the in-plane crystallization can also be observed. First of all, the distance between the array and the rectangular boundary has a clear impact on the ordering of particles in between. By varying this distance and the boundary structure, the influence of confinement and boundary conditions on two-dimensional colloidal crystallization can be examined in a systematic way. Secondly, defect-lines in the surrounding hexagonal crystal, indicated by the arrows in *Figure 3.4b*, originate from the pattern. This again shows how, using such patterns, the role of defects in two- and three-dimensional crystal growth can be examined. A thorough understanding of defect formation and the ability to manipulate defects is critical for the use of colloidal structures in photonic as well as many other applications.

All structures fabricated with our method are made in a wet environment. For most purposes, however, removal of the liquid is necessary. Drying by solvent evaporation destroys the structures because surface tension forces become very large for small structures and these forces can easily overcome the forces keeping the particles attached to the surface. We use critical point drying to dry the structure without surface tension forces.

Figure 3.5a shows a two-dimensional structure of 700 nm radius silica particles that was created using optical tweezers and then dried using critical point drying. The separation between the particles was 1.6 µm. *Figure 3.5b* shows a pattern of particles with a 2.4 µm interparticle spacing. Once a structure of particles is dried, it can be slightly sintered, recoated and patterned again. By repeating these steps it is possible to create three-dimensional structures in a layer-by-layer fashion. *Figure 3.5c* shows a structure made using this method. Although these are only first results, they demonstrate that the method can be used to make large, three-dimensional structures. For example, by placing layers of particles on top of the cubic structures

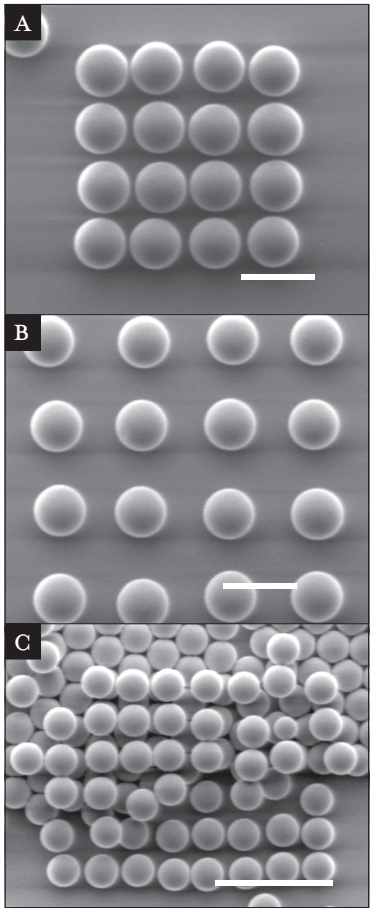

Figure 3.5
SEM images of structures of 1.4 μm diameter silica particles dried using critical point drying. The distances between the particles are (a) 1.6 μm and (b) 2.5 μm. (c) A second layer of particles, with square symmetry, was patterned on top of a hexagonally close-packed layer of particles.
The scale bars are 2 μm, 2 μm, and 5 μm, respectively.

shown in *Figure 3.5a*, an FCC crystal structure can be made. By using particles of different composition, for example silica and polystyrene, and afterwards burning away the polystyrene particles, a diamond structure can be made.[31] A photonic crystal with a diamond structure requires a relatively low contrast to achieve a band gap and was considered impossible to make with colloids. Clearly, this method can also be combined with (directed) self-organization as well, for instance to dielectrically dope a photonic crystal in the bulk at specific lattice sites. For example, by positioning particles on top of a crystal and subsequent further growth, e.g., by controlled drying as described by Velikov *et al*.[32], defects can be created inside a three-dimensional crystal.

3.4 Conclusions and outlook

A method was demonstrated that enables fabrication of large patterns of a wide variety of (functional) colloidal particles on coated substrates using optical tweezers. The accuracy of positioning was significantly below the particle size. Defects or impurities can be completely avoided or, if desired for a specific application, built into the structures at any desired position. This makes the procedure suitable for fabrication of photonic, electronic, and magnetic materials. We have shown the application of such patterns in colloidal epitaxy, showing the possibility both to locally manipulate self-assembly as well as to study the evolution of defects in two- and three-dimensional crystallization. The structures can be dried without distortions using critical point drying. By repeating the patterning procedure, three-dimensional structures can be build in a layer-by-layer fashion.

Acknowledgements

This work has been performed together with Jacob Hoogenboom, Karin Overgaag, Cendrine Faivre-Moskalenko, and Marileen Dogterom. We would like to thank Peter Vergeer and Christina Graf for synthesis and characterization of the RITC-SiO_2 and metallodielectric particles, respectively, and Damir Fific and Wijnand Takkenberg for valuable support with the critical point drying.

References

1 *A. van Blaaderen, From the de-Broglie to visible wavelengths - manipulating electrons and photons with colloids, MRS Bulletin 23, 39 (1998).*

2 *Y. Lu, Y. D. Yin, and Y. N. Xia, A self-assembly approach to the fabrication of patterned, two- dimensional arrays of microlenses of organic polymers, Adv. Mater. 13, 34 (2001).*

3 *S. A. Maier, M. L. Brongersma, P. G. Kik, S. Meltzer, A. A. G. Requicha, and H. A. Atwater, Plasmonics - A route to nanoscale optical devices, Adv. Mater. 13, 1501 (2001).*

4 *M. J. Hostetler and R. W. Murray, Colloids and self-assembled monolayers, Curr. Opin. Colloid Interface Sci. 2, 42 (1997).*

5 *A. N. Shipway, E. Katz, and I. Willner, Nanoparticle arrays on surfaces for electronic, optical, and sensor applications, ChemPhysChem 1, 18 (2000).*

6 *J. H. Holtz and S. A. Asher, Polymerized colloidal crystal hydrogel films as intelligent chemical sensing materials, Nature 389, 829 (1997).*

7 *O. D. Velev and E. W. Kaler, In situ assembly of colloidal particles into miniaturized biosensors, Langmuir 15, 3693 (1999).*

8 *M. H. Wu and G. M. Whitesides, Fabrication of arrays of two-dimensional micropatterns using microspheres as lenses for projection photolithography, Appl. Phys. Lett. 78, 2273 (2001).*

9 *S. I. Bozhevolnyi, J. Erland, K. Leosson, P. M. W. Skovgaard, and J. M. Hvam, Waveguiding in surface plasmon polariton band gap structures, Phys. Rev. Lett. 86, 3008 (2001).*

10 C. L. Haynes and R. P. Van Duyne, Nanosphere lithography: A versatile nanofabrication tool for studies of size-dependent nanoparticle optics, J. Phys. Chem. B 105, 5599 (2001).

11 F. Burmeister, W. Badowsky, T. Braun, S. Wieprich, J. Boneberg, and P. Leiderer, Colloid monolayer lithography- A flexible approach for nanostructuring of surfaces, Appl. Surf. Sci. 145, 461 (1999).

12 J. Aizenberg, P. V. Braun, and P. Wiltzius, Patterned colloidal deposition controlled by electrostatic and capillary forces, Phys. Rev. Lett. 84, 2997 (2000).

13 K. M. Chen, X. Jiang, L. C. Kimerling, and P. T. Hammond, Selective self-organization of colloids on patterned polyelectrolyte templates, Langmuir 16, 7825 (2000).

14 X. M. Lin, R. Parthasarathy, and H. M. Jaeger, Direct patterning of self-assembled monolayers by electron beams, Appl. Phys. Lett. 78, 1915 (2001).

15 J. Won, T. Inaba, H. Masuhara, H. Fujiwara, K. Sasaki, S. Miyawaki, and S. Sato, Photothermal fixation of laser-trapped polymer microparticles on polymer substrates, Appl. Phys. Lett. 75, 1506 (1999).

16 H. T. Miyazaki, H. Miyazaki, K. Ohtaka, and T. Sato, Photonic band in two-dimensional lattices of micrometer-sized spheres mechanically arranged under a scanning electron microscope, J. Appl. Phys. 87, 7152 (2000).

17 C. Mio and D. W. M. Marr, Tailored surfaces using optically manipulated colloidal particles, Langmuir 15, 8565 (1999).

18 H. Misawa, K. Sasaki, M. Koshioka, N. Kitamura, and H. Masuhara, Laser manipulation and assembling of polymer latex particles in solution, Macromolecules 26, 282 (1993).

19 J. P. Hoogenboom, D. L. J. Vossen, C. Faivre-Moskalenko, M. Dogterom, and A. van Blaaderen, Patterning surfaces with colloidal particles using optical tweezers, Appl. Phys. Lett. 80, 4828 (2002).

20 D. L. J. Vossen, J. P. Hoogenboom, K. Overgaag, and A. van Blaaderen, in Materials Research Society Symposium Proceedings, edited by L. Merhari, Boston, (2002), Vol. 705.

21 D. L. J. Vossen, A. van der Horst, M. Dogterom, and A. van Blaaderen, Optical tweezers and confocal microscopy for simultaneous three-dimensional manipulation and imaging in concentrated colloidal dispersions, Rev. Sci. Instrum. 75, 2960 (2004).

22 T. N. Buican, M. J. Smyth, H. A. Crissman, G. C. Salzman, C. C. Stewart, and J. C. Martin, Automated single-cell manipulation and sorting by light trapping, Appl. Optics 26, 5311 (1987).

23 A. van Blaaderen and A. Vrij, Synthesis and characterization of colloidal dispersions of fluorescent, monodisperse silica spheres, Langmuir 8, 2921 (1992).

24 H. Giesche, Synthesis of monodispersed silica powders II. Controlled growth reaction and continuous production process, J. Eur. Ceramic Soc. 14, 205 (1994).

25 L. M. Liz-Marzan, M. Giersig, and P. Mulvaney, Langmuir 12, 4329 (1996).

26 D. L. J. Vossen, M. J. A. de Dood, T. van Dillen, T. Zijlstra, E. van der Drift, A. Polman, and A. van Blaaderen, Novel method for solution growth of thin silica films from tetraethoxysilane, Adv. Mater. 12, 1434 (2000).

27 G. Decher, J. D. Hong, and J. Schmitt, Buildup of ultrathin multilayer films by a self-assembly process, III. consecutively alternating adsorption of anionic and cationic polyelectrolytes on charged surfaces, Thin Solid Films 210, 831 (1992).

28 F. Caruso, R. A. Caruso, and H. Mohwald, Nanoengineering of inorganic and hybrid hollow spheres by colloidal templating, Science 282, 1111 (1998).

29 F. Caruso, Nanoengineering of particle surfaces, Adv. Mater. 13, 11 (2001).

30 S. Ito, H. Yoshikawa, and H. Masuhara, Optical patterning and photochemical fixation of polymer nanoparticles on glass substrates, Appl. Phys. Lett. 78, 2566 (2001).

31 F. Garcia-Santamaria, C. Lopez, F. Meseguer, F. Lopez-Tejeira, J. Sanchez-Dehesa, and H. T. Miyazaki, Opal-like photonic crystal with diamond lattice, Appl. Phys. Lett. 79, 2309 (2001).

32 K. P. Velikov, C. G. Christova, R. P. A. Dullens, and A. van Blaaderen, Layer-by-layer growth of binary colloidal crystals, Science 296, 106 (2002).

4 Combined optical tweezers/ion beam technique to tune colloidal masks for nanolithography

A method is presented to control the in-plane ordering, size, and interparticle distance of nanoparticles fabricated by evaporation through a mask of colloidal particles. The use of optical tweezers combined with critical point drying gives single-particle position control over the colloidal particles in the mask. This extends the geometry of the colloidal masks from (self-organized) hexagonal to any desired symmetry and spacing. Control over the mask hole size is achieved by MeV ion irradiation, which causes the colloids to expand in the in-plane direction, thus shrinking the size of the holes. After modification of the mask, evaporation at different angles with respect to the mask gives additional control over structure and interparticle distance, allowing nanoparticles of different materials to be deposited next to each other. We demonstrate large arrays of metal nanoparticles with dimensions in the 15-30 nm range, with complete control over the interparticle distance and in-plane ordering.

4.1 Introduction

Arrays of nanoparticles can find applications in photonic, electronic, magnetic and sensor devices.[1-5] For example, lines of metal nanoparticles were shown to work as sub-wavelength plasmon-mode waveguides.[6] Conventional methods used to fabricate structures of nanoparticles (like electron beam lithography) are complex, expensive, or time consuming. An alternative method to create arrays of small particles on a substrate is nanosphere lithography (NSL). This technique was pioneered in the early 1980s[7, 8] and was further developed by several groups.[9, 10] In NSL, a self-organized layer of colloidal spheres is used as a mask for a lithographic step like illumination, deposition, or etching. When used as a deposition mask, an array of particles is left on the substrate after removal of the colloidal mask. NSL is a simple, fast, and inexpensive method to create large arrays of particles on a substrate. Typical feature sizes after removal of the mask are 100 nm and above. Arrays of metallic nanoparticles created with NSL were used to study plasmonic resonances[11] and to fabricate plasmonic sensors.[12] Surfaces patterned with colloidal masks have also been used for catalysing the growth of nano-fibers (e.g., of carbon[13] and ZnO[14]) and for selective protein adsorption.[15] More complex structures of particles can be created using multiple depositions at different angles[16] or by rotating the sample during deposition.[17]

Nanosphere lithography has two major disadvantages.[9, 10] Firstly, control over the geometry of the mask of colloidal particles is limited since it is created by self-organization: for a single layer the structure is hexagonal close-packed. Secondly, the size of the colloidal particles in the mask determines both the size and the interparticle spacing of the nanoparticles.

In this chapter we present a combination of two methods to resolve these limitations of nanosphere lithography: we create colloidal masks with arbitrary geometry using optical tweezers, and tune the shape of the mask using ion irradiation. In this way, the in-plane ordering as well as the size and interparticle distance of nanoparticles formed by evaporation through the mask can be controlled.

4.2 Experimental details

Silica particles with a diameter of 1.0 μm or 1.4 μm, and a polydispersity less than a few percent, were synthesized using a Stöber growth process and subsequent growth steps using methods described in detail elsewhere.[18-20]

The size and polydispersity were determined using scanning electron microscopy (SEM) on several hundreds of particles. Analytical grade ethanol, ammonia solution (29 wt-%), and 3-aminopropyl triethoxysilane from Merck were used as received. Glass microscope cover slips (diameter 19 mm, Chance No. 1, thickness 150 µm) and Si(100) wafers were used as substrates, as received.

Scanning electron microscopy was performed on a FEI XL30 SFEG microscope operated with an acceleration voltage in the range 1-15 keV. Holes in colloidal masks were characterized by measuring the three long axes of the hole's triangular shape. An average over five holes was taken. The holes were measured at least five or six rows away from the edge of a domain.

Glass or silicon substrates were immersed in a mixture of 170 ml ethanol and 4.5 ml ammonia. Then 23.5 ml 3-aminopropyl triethoxysilane was added and the substrate was left to react for 1.5 hours under stirring. The substrate was then taken from the mixture and rinsed with ethanol. A sample cell was prepared by sandwiching a drop of colloidal dispersion between an uncoated glass microscope cover slip and a coated substrate. Optical tweezers were used to position negatively charged colloidal particles, taken from a reservoir at the bottom of the sample, on the coated, positively charged, substrate.[21] The samples were dried from ethanol in a critical point drier (Bal-tec; CPD 030).[22] The patterning and drying are described in detail in chapter 3. The optical tweezers setup is described in detail in chapter 2 as well as in Ref. 23.

Hexagonal close-packed masks were made by self-organization of colloidal particles on an uncoated substrate. A drop of particles in dispersion was put on a glass or silicon substrate, and the solvent was left to evaporate slowly.

A 1 MV van de Graaff accelerator and a 6 MV tandem accelerator were used to irradiate colloidal masks with 4 MeV Xe^{4+} and 30 MeV Cu^{5+} ions, respectively. The sample was clamped on a copper substrate and cooled to 90 K using liquid nitrogen. The base pressure during irradiation was $5 \cdot 10^{-7}$ mbar. The average penetration depth in colloidal silica of 4 MeV Xe and 30 MeV Cu was calculated to be 1.7 µm and 8.6 µm, respectively, using TRIM98.[24]

A layer of metal was evaporated on the ion-beam modified colloidal masks using thermal evaporation at a base pressure of $1.3 \cdot 10^{-6}$ mbar. Alternatively, metals were deposited using electron beam evaporation at

a base pressure of $1 \cdot 10^{-8}$ mbar. During evaporation, the samples could be tilted over two orthogonal axes. After deposition, the masks were removed from the samples by sonication in ethanol. Nanoparticles were annealed in air at ambient pressure.

4.3 Results and discussion

To create masks with arbitrary geometry, glass or silicon substrates were given a positive surface charge and then patterned with negatively charged colloidal silica particles using optical tweezers.[21, 22] This allows masks to be created with complete control over the position of single particles. After patterning, the solvent was removed from the sample using critical point drying (CPD) to prevent capillary forces from distorting the structure.[22] *Figure 4.1a* shows a SEM image of a double-line array of 1.0 µm diameter silica particles on a glass substrate after patterning and drying. The average centre-to-centre distance between the colloidal particles within each line was 1.2 µm. A 10 nm thick silver layer was deposited onto the colloidal mask by thermal evaporation. The same section of the substrate is shown in *Figure 4.1b* after the mask was removed by sonication. Clearly, the mask was replicated in the silver layer on the substrate. The method can be used to create more complex masks in which colloidal particles of different size, shape, and composition can be incorporated.[23, 25]

Additional control over the dimensions of the mask can be achieved by ion irradiation. As we have shown earlier, under irradiation with an MeV ion beam, individual colloidal particles expand in the plane perpendicular to the ion beam and shrink parallel to the ion beam.[26] This plastic deformation effect can be used to tune the size and shape of the holes in the colloidal deposition mask. *Figure 4.1c* shows a SEM image of a cubic mask pattern created with optical tweezers and CPD on a glass substrate. The centre-to-centre distance between the 1.4 µm diameter silica particles was 1.6 µm. The same structure is shown at the same magnification in *Figure 4.1d* after irradiation with 4 MeV Xe ions to a fluence of $2.0 \cdot 10^{15}$ cm^{-2}. During irradiation the sample was kept at 90 K, and the ion beam was perpendicular to the substrate. Clearly, the ion beam induced deformation has dramatically shrunk the size of the holes between the colloids. The major axis of the particle just outside the structure (marked with an arrow) increased from 1.4 µm to 2.0 µm. When the deforming spheres in a mask come into contact, the deformation becomes a collective process and the final dimensions are

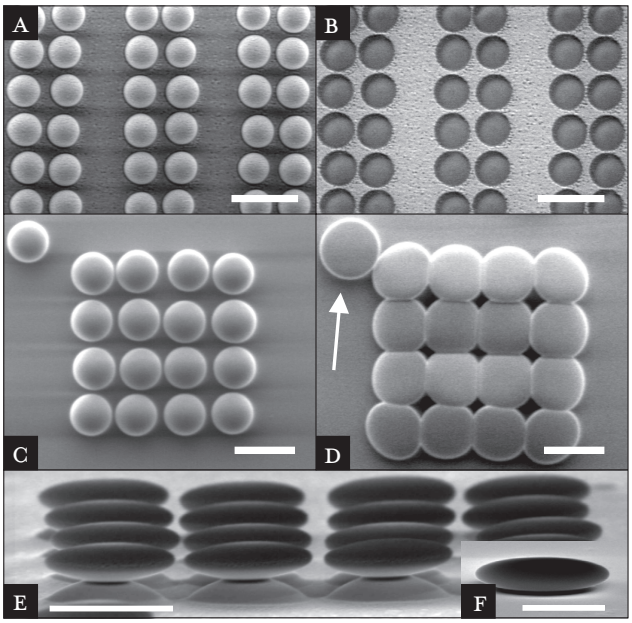

Figure 4.1
Colloidal masks made with single-particle position control using optical tweezers, and modified with 4 MeV Xe ion irradiation.
(a) SEM image of 1.0 μm diameter silica particles positioned on a glass substrate using optical tweezers. The sample was dried using critical point drying and covered with a 10 nm thick silver layer by thermal evaporation.
(b) After removal of the particles by sonication, the structure of the mask was replicated on the substrate.
(c) 1.4 μm diameter silica particles positioned in a pattern with square symmetry.
(d) Same structure after normal-incidence irradiation with 4 MeV Xe ions to a fluence of $2.0 \cdot 10^{15}$ cm^{-2} at 90 K. The in-plane expansion of the colloidal particles can be tuned by varying the ion fluence.
(e) Side-view of an array of ion-beam-deformed 1.4 μm diameter silica colloids (4 MeV, $2.0 \cdot 10^{15}$ cm^{-2}) imaged at an angle of 10° with respect to the substrate. Not only the silica particles but also the glass substrate was deformed. The size aspect ratio of the particles was 3.4.
(f) Side-view (at 10°) of an ion-beam-deformed 1.4 μm diameter silica colloid (4 MeV) on a silicon substrate. Note that the silicon substrate did not deform, while the silica particle deformed as the particles did in Figure 4.1e.
The scale bars in Figure 4.1a-e are 2 μm, the scale bar in Figure 4.1f is 1 μm.

determined by the combined deformation of interacting colloids. This can be clearly seen in *Figure 4.1d* where the shapes of the colloidal particles and the holes depend on their position in the mask. In *Figure 4.1d*, the centre-to-centre distance in the mask pattern is 1.8 μm, which is much larger than the original spacing of 1.6 μm (*Figure 4.1c*). This indicates that during irradiation the expansion of the interacting colloids caused an overall expansion of the mask domain, with colloids sliding over the substrate. For large domains, buckling of the colloidal mask was observed in some cases, which we attribute to large in-plane stresses resulting from the deformation.[27]

A more open structure of silica particles is shown in *Figure 4.1e* at a viewing angle of 10° with respect to the substrate. The colloidal mask was

irradiated with $2.0 \cdot 10^{15}$ 4 MeV Xe ions/cm^2. The size aspect ratio (major over minor diameter) of the colloidal particles in the mask increased from 1 to 3.4. From *Figure 4.1e* it can also be seen that the glass substrate deformed under irradiation, leading to the formation of a pedestal centred under each colloid. We attribute this to inhomogeneous anisotropic deformation of the substrate under the mask. For 4 MeV Xe, the energy remaining after penetration through the centre of a colloid is only 0.85 MeV. As the deformation rate increases with ion energy,[28] the driving force for in-plane expansion of the substrate surface layer under the colloids will be much smaller than under the holes (where the ion energy is 4 MeV). This can lead to a plastic shape deformation of the glass substrate that causes formation of pedestals under each colloid.

To verify this hypothesis, a glass substrate covered with 1.0 µm diameter colloidal particles was irradiated with 30 MeV Cu ions ($8.7 \cdot 10^{14}$ cm^{-2}). At this high energy, the relative energy loss through the colloids is small, so that the substrate is irradiated at a nearly uniform energy. Indeed, under these conditions the substrate was found to stay flat.

The substrate deformation observed for 4 MeV Xe irradiation can be avoided by using silicon as a substrate. Crystalline Si rapidly becomes amorphous under 4 MeV Xe irradiation, and, as we have recently shown,[29] the anisotropic deformation rate of amorphous silicon is ~10 times smaller than that of silica. Indeed, (amorphised) silicon substrates covered with 1.4 µm diameter silica colloids stayed flat for an ion fluence of $2.0 \cdot 10^{15}$ Xe cm^{-2}. *Figure 4.1f* shows a silica particle on a silicon substrate after irradiation with intermediate ion fluence. It can clearly be seen that the silicon substrate remained flat while the deformation of the silica particle is comparable to that of the particles in *Figure 4.1e*. While the formation of pedestals may be considered unwanted (and can be avoided as we have shown above), we note that ellipsoidal colloidal particles on a pedestal may find use as arrays of (coupled) optical microresonators.[30]

The dependence of the size of holes in a colloidal mask on the ion fluence was determined for a two-dimensional hexagonal lattice of close-packed 1.4 µm diameter silica particles on a silicon substrate. The mask, with crystalline domains with dimensions between 20 and 50 µm, was formed by self-organization during slow evaporation of a drop of a colloidal dispersion on a silicon substrate. During 4 MeV Xe ion irradiation the sample was gradually moved along the 2.5 x 2.5 cm^2 aperture through which the ion

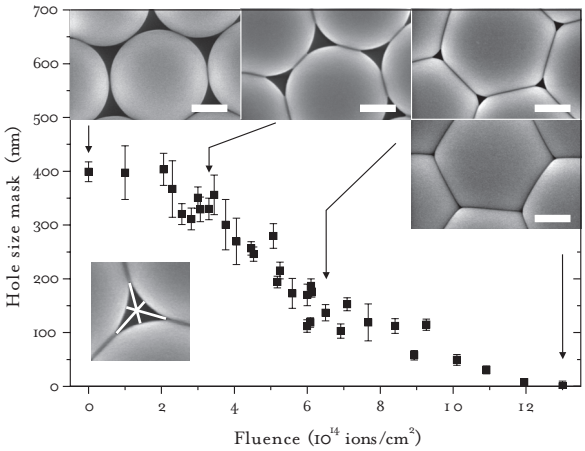

Figure 4.2
Dependence of hole size on 4 MeV Xe ion fluence. A two-dimensional hexagonal mask of 1.4 μm diameter silica particles on a silicon substrate was irradiated with 4 MeV Xe ions. The size of the holes gradually decreased until the holes were completely closed. The insets at the top of the image show SEM images of the mask at fluences of 0, $3.3 \cdot 10^{14}$, $6.5 \cdot 10^{14}$, and $13 \cdot 10^{14}$ ions/cm^2; corresponding hole sizes were 400 nm, 330 nm, 137 nm, and 0 nm, respectively. The arrows indicate the fluences at which the images were taken. The inset in the lower left corner shows how the hole size is defined.
The scale bars are 500 nm.

beam was scanned. A linearly varying ion fluence ranging from zero to $2.0 \cdot 10^{15}$ ions/cm^2 across the sample area was thus created. Hole sizes were determined at least five or six rows of particles away from the domain edges. We define the size of a hole between three colloidal particles in a hexagonal close-packed mask as the smallest distance between the point where two particles touch and a point on the surface of the third colloidal particle (see the inset in the lower left corner of *Figure 4.2*). As can be seen in *Figure 4.2*, the hole size decreases with ion fluence, as a result of the increased in-plane particle expansion. The insets in the top of *Figure 4.2* show an unirradiated section of the mask, and sections irradiated with $3.3 \cdot 10^{14}$, $6.5 \cdot 10^{14}$ and $13 \cdot 10^{14}$ ions/cm^2. The corresponding hole sizes are 400, 330, 137, and 0 nm, respectively. Small variations in hole size observed at each fluence are attributed to polydispersity in colloid size.

To demonstrate that the ion-beam-deformed colloidal mask can be used to fabricate unique nanostructures, a 30 nm thick gold layer was deposited by electron beam evaporation onto various ion irradiation-modified hexagonal masks (colloid diameter 1.4 μm, 4 MeV Xe).

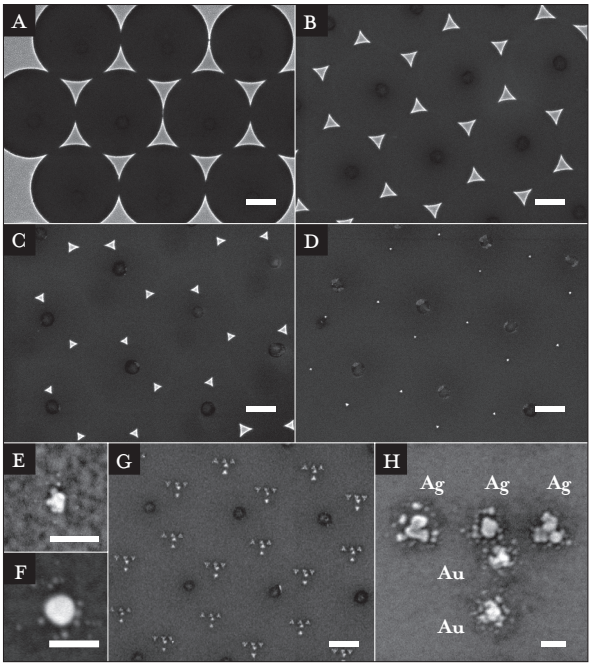

Figure 4.3
Arrays of metal nanoparticles created with an ion beam deformed mask.
(a) Hexagonal array of gold particles with a size of 400 nm, created on a glass substrate using an unmodified colloidal mask of 1.4 µm diameter silica particles.
(b) Hexagonal array of gold particles with a size of 229 nm,
(c) 119 nm, and
(d) 30 nm created with a mask modified with 4 MeV Xe ions.
(e) Image at high magnification of a Au particle with feature sizes of 15-20 nm.
(f) Image of a Au particle annealed first at 150 °C and then at 250 °C (both for 30 minutes). The particle has a more round and single droplet like shape.
(g) Array of "T" structures with three silver and two gold nanoparticles created by deposition at different angles on a modified mask.
h) Image at high magnification of a "T" structure. The size of the particles is between 50 nm and 80 nm and their spacing is ~135 nm.

The scale bars in Figure 4.3a-d and 4.3g are 500 nm; the ones in Figure 4.3e-f, and 4.3h are 50 nm.

Subsequently, the colloidal mask was removed by sonication. As a reference, *Figure 4.3a* shows a deposited pattern for an unirradiated mask. The size of these gold particles was 400 nm. *Figures 4.3b, 4.3c*, and *4.3d* show arrays of gold particles made using masks irradiated at $4.9 \cdot 10^{14}$, $7.7 \cdot 10^{14}$, and $11 \cdot 10^{14}$ ions/cm^2, respectively, leading to gold particle sizes of 229 nm, 119 nm, and 30 nm. The variation in nanoparticle size is 5-10%. A high-magnification image shows a Au dot with feature sizes between 15-20 nm *(Figure 4.3e)*. As can be seen, for these small particles, inhomogeneous particle shapes are observed, which are attributed to the nucleation and growth kinetics. Thermal annealing can remove sharp features and combine metal nanoparticles that are close together.[31] *Figure 4.3f* shows a Au particle that was annealed at 150 °C for 30 minutes and subsequently at 250 °C for another 30 minutes. The particle shows a more round shape and has become a single-droplet shaped particle.

To further demonstrate the versatility of the combination of optical tweezers and ion irradiation, more complex nanoparticle arrays were created by subsequent deposition of metals at different angles using an ion beam modified mask. *Figure 4.3g* shows an array of "T" structures made through subsequent silver and gold depositions through an ion-modified mask, where several depositions were done at two sets of orthogonal angles. Three silver particles were created by deposition of 11 nm silver at angles of -4.5, 0, and +4.5 degrees in a horizontal plane in *Figure 4.3g*. Two gold particles were made by subsequent depositions of 10.5 nm gold at angles of -4.5 and 0 degrees in a vertical plane in *Figure 4.3g*. *Figure 4.3h* shows a single "T" structure at higher magnification. The size of the core of the deposited features was in the range 30-50 nm, and the centre-to-centre interparticle spacing was ~135 nm. The spacing between the silver and closest gold nanoparticles was 62 nm. Annealing of the structure in *Figures 4.3g* and *4.3h*, composed of both silver and gold dots, was not possible due to the different annealing kinetics of the two metals. However, metal dots in more complex structures such as "T" structures composed of a single metal are expected to change shape after annealing, as shown in *Figure 4.3f* and Ref. 31. Finally, we note that during deposition the mask hole size is gradually decreasing, due to the continued deposition of metal on the colloids in the mask. Thus for very small holes, the total amount of metal that is deposited for each particle is determined by a self-limiting process.

4.4 Conclusions and outlook

In conclusion, we have provided a solution to two major limitations of nanosphere lithography. The geometry of the masks is extended from (self-organized) hexagonal close-packed to any desired symmetry using optical tweezers combined with critical point drying. In the presented experiments, colloidal particles were positioned in the mask by manual control, at a speed in the order of one particle per second. However, the process can be fully automated to achieve a higher accuracy as well an increased speed of patterning. Control over the hole size (independent of the size of the colloids in the mask) is achieved by ion irradiation, which causes an in-plane expansion of the mask, thus shrinking the size of the holes. By varying the ion fluence, the hole size can be continuously reduced to arbitrarily small size. Recently, we have shown that deformation of colloidal spheres also works with low ion energies.[28] These modified masks can be used to create

arrays of nanoparticles with sizes down to tens of nanometres. Evaporation of material at different angles with respect to the mask gives additional control over structure and interparticle distance, allowing nanoparticles of different materials to be arranged with high accuracy in a variety of geometries.

Acknowledgements
This work has been performed together with Damir Fific, Joan Penninkhof, Teun van Dillen, and Albert Polman. We gratefully acknowledge the assistance of Jan Verhoeven with metal evaporations, and Michiel de Dood, Jacob Hoogenboom, and Anna Tchebotareva for discussions.

References

1 *A. N. Shipway, E. Katz, and I. Willner, Nanoparticle arrays on surfaces for electronic, optical, and sensor applications, ChemPhysChem 1, 18 (2000).*
2 *A. L. Rogach, D. V. Talapin, E. V. Shevchenko, A. Kornowski, M. Haase, and H. Weller, Organization of matter on different size scales: Monodisperse nanocrystals and their superstructures, Advanced Functional Materials 12, 653 (2002).*
3 *F. X. Redl, K. S. Cho, C. B. Murray, and S. O'Brien, Three-dimensional binary superlattices of magnetic nanocrystals and semiconductor quantum dots, Nature 423, 968 (2003).*
4 *R. D. Schaller, M. A. Petruska, and V. I. Klimov, Tunable near-infrared optical gain and amplified spontaneous emission using PbSe nanocrystals, J. Phys. Chem. B 107, 13765 (2003).*
5 *P. Alivisatos, The use of nanocrystals in biological detection, Nature Biotechnology 22, 47 (2004).*
6 *S. A. Maier, P. G. Kik, H. A. Atwater, S. Meltzer, E. Harel, B. E. Koel, and A. A. G. Requicha, Local detection of electromagnetic energy transport below the diffraction limit in metal nanoparticle plasmon waveguides, Nature Materials 2, 229 (2003).*
7 *U. C. Fischer and H. P. Zingsheim, Submicroscopic pattern replication with visible light, J. Vac. Sci. Technol. 19, 881 (1981).*
8 *H. W. Deckman and J. H. Dunsmuir, Natural lithography, Appl. Phys. Lett. 41, 377 (1982).*
9 *J. C. Hulteen and R. P. Van Duyne, Nanosphere lithography: A materials general fabrication process for periodic particle array surfaces, J. Vac. Sci. Technol. A 13, 1553 (1995).*
10 *F. Burmeister, C. Schafle, T. Matthes, M. Bohmisch, J. Boneberg, and P. Leiderer, Colloid monolayers as versatile lithographic masks, Langmuir 13, 2983 (1997).*
11 *C. L. Haynes and R. P. Van Duyne, Nanosphere lithography: A versatile nanofabrication tool for studies of size-dependent nanoparticle optics, J. Phys. Chem. B 105, 5599 (2001).*
12 *M. D. Malinsky, K. L. Kelly, G. C. Schatz, and R. P. Van Duyne, Chain length dependence and sensing capabilities of the localized surface plasmon resonance of silver nanoparticles chemically modified with alkanethiol self-assembled monolayers, J. Am. Chem. Soc. 123, 1471 (2001).*
13 *Z. P. Huang, D. L. Carnahan, J. Rybczynski, M. Giersig, M. Sennett, D. Z. Wang, J. G. Wen, K. Kempa, and Z. F. Ren, Growth of large periodic arrays of carbon nanotubes, Appl. Phys. Lett. 82, 460 (2003).*
14 *X. Wang, C. J. Summers, and Z. L. Wang, Large-scale hexagonal-patterned growth of aligned ZnO nanorods for nano-optoelectronics and nanosensor arrays, Nano Lett. 4, 423 (2004).*
15 *R. Michel, I. Reviakine, D. Sutherland, C. Fokas, G. Csucs, G. Danuser, N. D. Spencer, and M. Textor, A novel approach to produce biologically relevant chemical patterns at the nanometer scale: Selective molecular assembly patterning combined with colloidal lithography, Langmuir 18, 8580 (2002).*

16 *C. L. Haynes, A. D. McFarland, M. T. Smith, J. C. Hulteen, and R. P. Van Duyne, Angle-resolved nanosphere lithography: Manipulation of nanoparticle size, shape, and interparticle spacing, J. Phys. Chem. B 106, 1898 (2002).*
17 *A. Kosiorek, W. Kandulski, P. Chudzinski, K. Kempa, and M. Giersig, Shadow nanosphere lithography: Simulation and experiment, Nano Lett. 4, 1359 (2004).*
18 *A. van Blaaderen and A. Vrij, Synthesis and characterization of colloidal dispersions of fluorescent, monodisperse silica spheres, Langmuir 8, 2921 (1992).*
19 *A. van Blaaderen, J. van Geest, and A. Vrij, Monodisperse colloidal silica spheres from tetraalkoxysilanes - Particle formation and growth-mechanism, J. Colloid Interface Sci. 154, 481 (1992).*
20 *H. Giesche, Synthesis of monodispersed silica powders II. Controlled growth reaction and continuous production process, J. Eur. Ceramic Soc. 14, 205 (1994).*
21 *J. P. Hoogenboom, D. L. J. Vossen, C. Faivre-Moskalenko, M. Dogterom, and A. van Blaaderen, Patterning surfaces with colloidal particles using optical tweezers, Appl. Phys. Lett. 80, 4828 (2002).*
22 *D. L. J. Vossen, J. P. Hoogenboom, K. Overgaag, and A. van Blaaderen, in Materials Research Society Symposium Proceedings, edited by L. Merhari, Boston, (2002), Vol. 705.*
23 *D. L. J. Vossen, A. van der Horst, M. Dogterom, and A. van Blaaderen, Optical tweezers and confocal microscopy for simultaneous three-dimensional manipulation and imaging in concentrated colloidal dispersions, Rev. Sci. Instrum. 75, 2960 (2004).*
24 *J. F. Ziegler, J. P. Biersack, and U. Littmark, The stopping and range of ions in solids (Pergamon, New York, 1985).*
25 *A. van Blaaderen, J. P. Hoogenboom, D. L. J. Vossen, A. Yethiraj, A. van der Horst, K. Visscher, and M. Dogterom, Colloidal epitaxy: Playing with the boundary conditions of colloidal crystallization, Faraday Discuss. 123, 107 (2003).*
26 *E. Snoeks, A. van Blaaderen, T. van Dillen, C. M. van Kats, M. L. Brongersma, and A. Polman, Colloidal ellipsoids with continuously variable shape, Adv. Mater. 12, 1511 (2000).*
27 *E. Snoeks, T. Weber, A. Cacciato, and A. Polman, MeV ion irradiation-induced creation and relaxation of mechanical-stress in silica, J. Appl. Phys. 78, 4723 (1995).*
28 *T. van Dillen, A. Polman, C. M. van Kats, and A. van Blaaderen, Ion beam-induced anisotropic plastic deformation at 300 keV, Appl. Phys. Lett. 83, 4315 (2003).*
29 *T. van Dillen, M. J. A. de Dood, J. J. Penninkhof, A. Polman, S. Roorda, and A. M. Vredenberg, Ion beam-induced anisotropic plastic deformation of silicon microstructures, Applied Physics Letters, 84, 3591 (2004).*
30 *K. J. Vahala, Optical microcavities, Nature 424, 839 (2003).*
31 *F. Burmeister, W. Badowsky, T. Braun, S. Wieprich, J. Boneberg, and P. Leiderer, Colloid monolayer lithography-A flexible approach for nanostructuring of surfaces, Appl. Surf. Sci. 145, 461 (1999).*

5 Chemical modification of colloidal masks for nanolithography

A method is presented to tune the size of the holes in colloidal masks used for nanolithography. Using a wet-chemical method, a thin layer of silica is grown on masks of silica particles. The growth mechanism of the silica coating was found to be diffusion-limited. The size of the holes can be controlled accurately using a seed dispersion and proper calibration. Modified masks were used for nanolithography: after metal deposition and mask removal, large arrays of nanoparticles had been created. Using modified arrays of large colloidal particles (1.4 μm diameter), nanoparticles with sizes ranging from 400 nm (for unmodified masks) down to tens of nanometers were created. The method is fast, simple, and inexpensive.

5.1 Introduction

In nanosphere lithography, a self-organized layer of colloidal spheres is used as a mask for a lithographic step like illumination, deposition or etching.[1-4] It is a simple, fast, and inexpensive method to pattern substrates over large areas. Arrays of metal colloids have many applications[5-7] and arrays created using colloidal masks have been used to study plasmonic resonances,[8] to fabricate plasmonic sensors,[9] to catalyze the growth of nano-fibers,[10, 11] and for selective protein adsorption.[12] Complex structures of nanoparticles can be made when the angle between the colloidal mask and the evaporation beam is adjusted[13] or when the sample is rotated during deposition.[14]

Nanosphere lithography also has a disadvantage: the size of the holes in the mask is determined by the size of the colloidal particles that form the mask. Therefore, the size of the features created using nanosphere lithography is coupled to the size of the colloidal particles in the mask.[3, 4] In chapter 4 we used optical tweezers to create masks with arbitrary geometry and ion beam irradiation to control the hole size in colloidal masks.[15]

In this chapter we present an alternative method to modify colloidal masks and use those to make arrays of noble metal nanoparticles. A wet-chemical method is used to grow a thin layer of silica on a two-dimensional close-packed layer of colloidal silica spheres on a substrate. The layer of silica decreases the size of the holes in the colloidal mask. We investigated the growth mechanism of the silica coating, and show that the size of the holes can be controlled accurately. Modified masks were used for nanolithography: after metal deposition and mask removal, large arrays of metal nanoparticles were created.[4] Using modified arrays of large colloidal particles (1.4 μm diameter), arrays of nanoparticles with a size ranging from 400 nm (for unmodified masks) down to tens of nanometers were created.

The coating method we use is based on the Stöber-method,[16] a base-catalyzed reaction of alkoxy silanes in mixtures of ethanol and ammonia, which is well-known for the synthesis of monodisperse colloidal silica particles. Catalyzed by the ammonia, tetra-ethoxysilane (TEOS) molecules first hydrolyze and then condense to form silica. In the early stage of the reaction small silica aggregates are formed. These coalesce until they, as they grow larger and acquire more surface-charge, become stable. Once stable, the aggregates grow even larger and become spherical in shape by addition of monomers and small oligomers. The final size of the colloidal spheres depends both on the number of particles formed in the early nucleation

stage as well as on the amount of TEOS added to the reaction mixture. How many particles are formed as they become stable is a complicated function of experimental conditions and is in general not accurately controllable.[17-19]

Recently, we developed a modification of this process to grow thin silica films on macroscopic surfaces.[20] The growth mechanism for the silica layers was found to be surface-reaction limited, as was also found for the original Stöber-process.[19] When a seed dispersion of colloidal spheres was added to the reaction mixture, the silica layer grown increased with the same amount as the radius of the colloidal seed particles.[20] If a well-characterized seed dispersion is used, silica layers can be grown with nanometer control over layer thickness.[20] We use this method to modify colloidal masks for nanosphere lithography.

5.2 Experimental details

Silica particles with a radius of 700 nm and a polydispersity of 2% were synthesized using the Stöber growth process and subsequent growth steps using methods described in detail elsewhere.[17-19] The size and polydispersity were determined using scanning electron microscopy (SEM) on several hundreds of particles. Analytical grade ethanol, ammonia solution (29 wt-%) and tetra-ethoxysilane (TEOS) from Merck were used as received. Si(100) wafers were used as substrates, as received.

Hexagonal close-packed masks were fabricated by self-organization of colloidal silica particles on a substrate. A drop of particles (700 nm radius) in ethanol was deposited on a glass or silicon substrate, and the solvent was left to evaporate slowly. Due to capillary forces, the particles self-organized into regions of close-packed hexagonal monolayers. The substrates with masks were then coated in a mixture of ethanol, ammonia, water, and TEOS as described in the text. Layers of Au and Ag were deposited on the colloidal masks using electron beam evaporation at a base pressure of $1 \cdot 10^{-8}$ mbar. After deposition, the masks were removed from the samples by sonication in ethanol.

Scanning electron microscopy (SEM) was performed on a FEI XL30 SFEG microscope operated with an acceleration voltage in the range 1-15 keV. We defined the size of a hole as the smallest distance between the point where two particles touch and a point on the surface of the third colloidal particle in a hexagonal close-packed mask (see the inset in *Figure 5.1a*). In determining the hole size, an average over three measurements on five holes was taken.

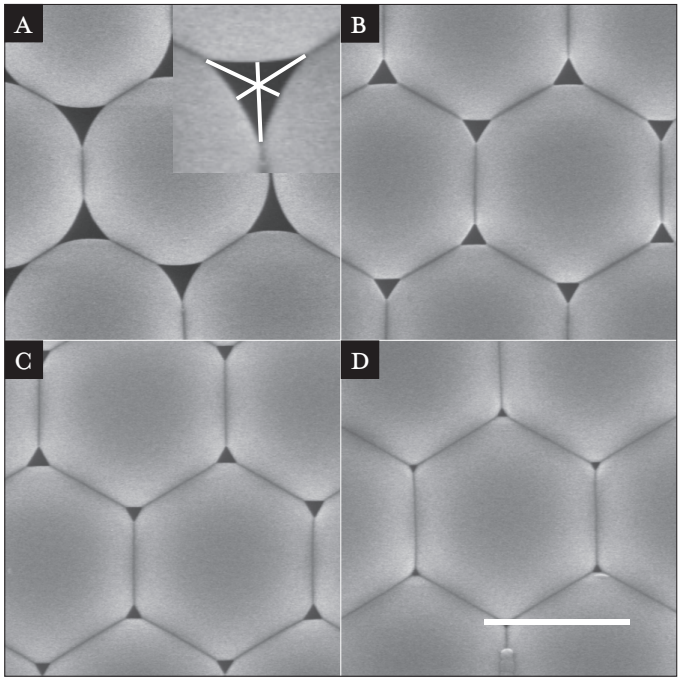

Figure 5.1
SEM images of two-dimensional close-packed colloidal masks modified by wet-chemical deposition of thin layers of silica. The silica coating was used to tune the size of the interstitial holes in the mask. The silica particles in the mask had a radius of 700 nm. The size of the holes in an uncoated mask was 400 nm.
(a) SEM image of a mask after one coating step, the size of the holes was reduced to 264 nm. The inset shows how the size of the holes is defined.
(b)-(d) Images of colloidal masks after two, three, and four coating steps, with hole sizes of 152, 104, and 55 nm, respectively.
The scale bar is 1 µm.

5.3 Results and discussion

A colloidal seed dispersion was synthesized by adding 0.360 g TEOS to a mixture of 7.867 g ethanol, 0.787 g water, and 0.715 g ammonia. After two hours of continuous stirring, colloidal silica particles had formed, and 75 µl dispersion was taken out of the reaction mixture. The radius of the newly formed spheres in the seed dispersion was determined to be 363 nm +/- 2.3 %. The number density of seed particles in the dispersion was calculated to be $2.7 \cdot 10^{11}$ ml^{-1}.

Four samples with colloidal masks were prepared as described in the experimental section. The size of the holes between the particles in the colloidal mask was measured to be 400 nm. The four samples covered with colloidal masks were then immersed in the ethanol-ammonia mixture containing the seed dispersion. Subsequently, 0.188 g TEOS was added, and after two hours of stirring, one sample and 75 µl of seed dispersion were taken out of the mixture. Then 0.178 g TEOS was added to the mixture with the seed dispersion and the three remaining samples. After two hours, again one sample and 75 µl of seed dispersion were taken out. These steps were repeated twice in which 0.083 and 0.084 g TEOS were added, respectively.

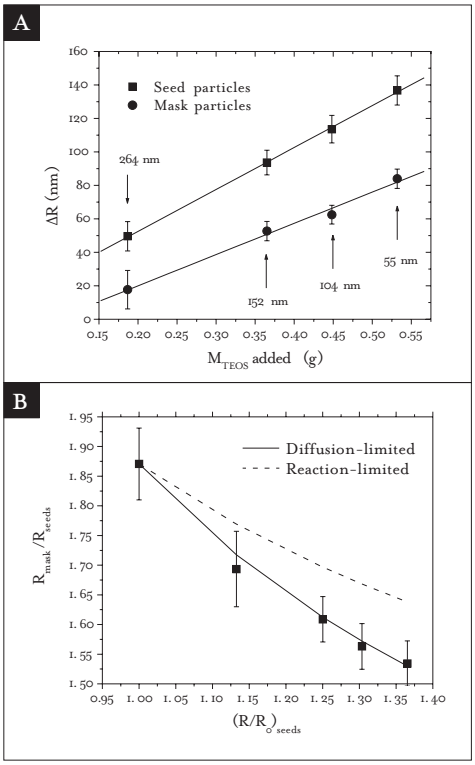

Figure 5.2
(a) The increase in size of the seed particles in the coating mixture (squares) and the colloidal particles in the mask (circles) as a function of the amount of TEOS added. The lines are linear fits through the data points. The size of both particles increased linearly, although the seed particles grew faster. For each coating step, the hole size in the mask is indicated.
(b) The ratio of the radii of the mask and seed particles versus the relative growth of the seed particles. The two curves show the expected relation for growth models where the growth of the mask particles is diffusion-limited (solid line) or reaction-limited (dashed line).

Figure 5.1a shows a SEM image at high magnification of a colloidal mask that was taken out of the reaction mixture after the first coating step. A layer of silica had grown on the mask, and the size of the holes was decreased to 264 nm. This is a 136 nm reduction of the hole size compared to an uncoated mask. After the second coating the size of the holes was reduced to 152 nm *(Figure 5.1b)*. After the third and fourth coating steps, the sizes of the holes were determined to be 104 nm *(Figure 5.1c)* and 55 nm *(Figure 5.1d)*, respectively.

During each coating step, silica was grown on the colloidal masks and also on the seed colloids in the reaction mixture. We determined the size of the seed and mask particles after each growth step. The size of the mask particles is defined as the radius of a particle in the mask at the position where it is not connected to another particle. As the masks were coated, the size of the mask particles increased and the size of the holes decreased. The data points in the graph in *Figure 5.2a* show that the radius of both the seed (square) and mask (circles) particles increased as a function of the amount

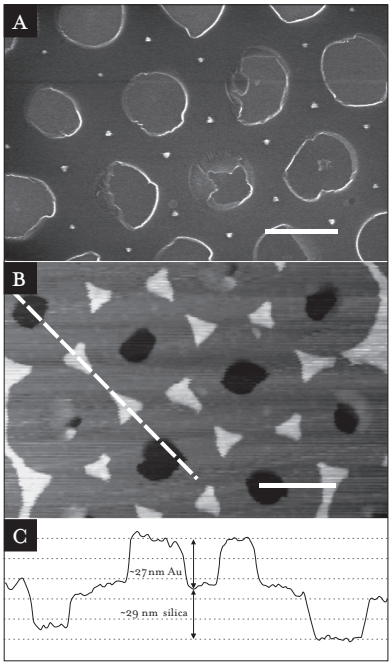

Figure 5.3
(a) SEM image of an array of gold nanoparticles created by deposition of 20 nm Au on a modified colloidal mask and subsequent mask removal by sonication of the sample. The in-plane size of the nanoparticles was 70 nm.
(b) AFM image of an array of Au particles (350 nm) on a silica layer. The holes in the silica layer are where the mask particles were during the coating.
(c) Height profile over two Au particles on the silica layer on the silicon substrate. The thickness of the Au particles was 27 nm while the silica layer had a thickness of 29 nm. The dashed line in Figure 5.3b indicates the position of the line scan.
The scale bars in (a) and (b) are 1 µm, the width of image (c) is 3.6 µm.

of TEOS added. Linear fits are drawn through the data points. The size of the seed particles increased more rapidly than the size of the particles in the mask with more TEOS added. For each growth step, the size of the holes in the mask is also indicated in the graph.

The graph in *Figure 5.2b* shows the ratio of the radii of the mask and seed particles plotted against the relative increase of the seed particles. The two curves indicate the predicted behavior for diffusion-limited (solid) and surface-reaction-limited (dashed) growth.[19, 20] In diffusion-limited growth, particle growth is proportional to the radius of a particle and not to the square of the radius as for surface-reaction-limited growth. As can be seen in *Figure 5.2b*, the growth of the particles in the masks is well described by a diffusion-limited model. Although diffusion-limited growth means that the layer thickness grown on the colloidal mask will depend on geometrical properties of the mask, which will be different for different sample geometries, accurate tuning of the size of the holes is still possible once a calibration curve is determined.

After modification, the masks were used for lithography. *Figure 5.3a* shows an array of gold nanoparticles created by deposition of 20 nm Au on a sample with a modified colloidal mask and subsequent removal of this

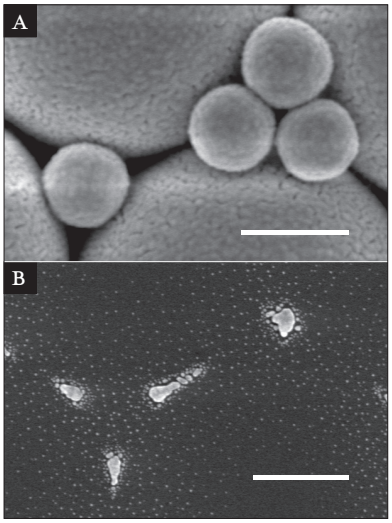

Figure 5.4
(a) SEM image at high magnification of an arrangement of small silica particles on top of larger ones. The small particles modified the size and shape of the holes between the large particles. A 20 nm thick layer of Ag was deposited on the mask.
(b) Ag particles created on the substrate by evaporation through a mask of large and small particles as in Figure 5.4a.
The scale bars are 1 µm.

mask by sonication. The size of the nanoparticles was determined to be 70 nm. The metal nanoparticles were deposited on the silica layer grown on the substrate during coating. Where the colloidal mask touched the silicon substrate, indentations in the silica film can be seen.

To investigate the height-profile of a sample, an array of Au particles was imaged using an atomic force microscope (AFM) *(Figure 5.3b)*. The Au particles had a lateral size of 350 nm. *Figure 5.3c* shows a height profile recorded on the dashed line indicated in *Figure 5.3b*. Two Au particles on the silica layer on top of the silicon substrate are visible. The height of the Au particles was 27 nm, while the silica layer had a thickness of 29 nm. For many applications the presence of silica on the substrate poses no problem. However, modification of the surface can be prevented when our coating method is used on freestanding colloidal masks that are, after coating, transferred to a substrate for lithography.[4]

Figure 5.4a shows a zoomed-in image of small silica particles on top of larger ones. The small particles modify the size and shape of the holes between the large particles. A 20 nm thick Ag layer was deposited on top of the mask. *Figure 5.4b* shows the substrate after the mask was removed. The three elongated Ag particles (on the left; oriented at 120° angles) were created through a hole in the mask that was partially blocked by a small particle. The small Ag particle on the right was deposited through a hole, which was modified by three particles in a hole in the mask. Using controlled-drying

methods,[21] large areas of binary crystals can be created that can be used as masks for nanolithography.[3, 22] Even more control over the masks is possible with optical tweezers as is shown in chapter 4.[15] Small metal particles were sometimes observed to have irregular shapes *(Figure 5.4b)*, which can be attributed to a combination of nucleation and growth kinetics and imperfect wetting of the substrate by the metal. Thermal annealing[23] makes the shapes more regular as was also shown in chapter 4.

5.4 Conclusions and outlook

In conclusion, we developed a method to modify the hole size of self-assembled colloidal masks used for lithography. A mask is coated with a thin silica layer in the presence of a seed dispersion of silica colloids. The growth mechanism of the silica coating was found to be diffusion-limited. The size of the holes can be controlled accurately using a seed dispersion and proper calibration. The modified masks were used to create arrays of metal nanoparticles. The method is inexpensive, simple, and fast. The method can be used in combination with the techniques to modify colloidal masks as described in chapter 4. We plan to use this technique to create arrays of metal nanoparticles embedded in silica by applying several silica coating steps after mask removal. When embedded in silica, high energy ion-beam irradiation can be used to deform the metal particles.[24]

Acknowledgements

This work has been performed together with Joan Penninkhof and Damir Fific. We gratefully acknowledge Albert Polman for discussions and Anna Tchebotareva for AFM imaging.

References

1 *U. C. Fischer and H. P. Zingsheim, Submicroscopic pattern replication with visible light, J. Vac. Sci. Technol. 19, 881 (1981).*
2 *H. W. Deckman and J. H. Dunsmuir, Natural lithography, Appl. Phys. Lett. 41, 377 (1982).*
3 *J. C. Hulteen and R. P. Van Duyne, Nanosphere lithography: A materials general fabrication process for periodic particle array surfaces, J. Vac. Sci. Technol. A 13, 1553 (1995).*
4 *F. Burmeister, C. Schafle, T. Matthes, M. Bohmisch, J. Boneberg, and P. Leiderer, Colloid monolayers as versatile lithographic masks, Langmuir 13, 2983 (1997).*
5 *A. N. Shipway, E. Katz, and I. Willner, Nanoparticle arrays on surfaces for electronic, optical, and sensor applications, ChemPhysChem 1, 18 (2000).*
6 *F. X. Redl, K. S. Cho, C. B. Murray, and S. O'Brien, Three-dimensional binary superlattices of magnetic nanocrystals and semiconductor quantum dots, Nature 423, 968 (2003).*
7 *P. Alivisatos, The use of nanocrystals in biological detection, Nature Biotechnology 22, 47 (2004).*

8 C. L. Haynes and R. P. Van Duyne, Nanosphere lithography: A versatile nanofabrication tool for studies of size-dependent nanoparticle optics, J. Phys. Chem. B 105, 5599 (2001).

9 M. D. Malinsky, K. L. Kelly, G. C. Schatz, and R. P. Van Duyne, Chain length dependence and sensing capabilities of the localized surface plasmon resonance of silver nanoparticles chemically modified with alkanethiol self-assembled monolayers, J. Am. Chem. Soc. 123, 1471 (2001).

10 Z. P. Huang, D. L. Carnahan, J. Rybczynski, M. Giersig, M. Sennett, D. Z. Wang, J. G. Wen, K. Kempa, and Z. F. Ren, Growth of large periodic arrays of carbon nanotubes, Appl. Phys. Lett. 82, 460 (2003).

11 X. Wang, C. J. Summers, and Z. L. Wang, Large-scale hexagonal-patterned growth of aligned ZnO nanorods for nano-optoelectronics and nanosensor arrays, Nano Lett. 4, 423 (2004).

12 R. Michel, I. Reviakine, D. Sutherland, C. Fokas, G. Csucs, G. Danuser, N. D. Spencer, and M. Textor, A novel approach to produce biologically relevant chemical patterns at the nanometer scale: Selective molecular assembly patterning combined with colloidal lithography, Langmuir 18, 8580 (2002).

13 C. L. Haynes, A. D. McFarland, M. T. Smith, J. C. Hulteen, and R. P. Van Duyne, Angle-resolved nanosphere lithography: Manipulation of nanoparticle size, shape, and interparticle spacing, J. Phys. Chem. B 106, 1898 (2002).

14 A. Kosiorek, W. Kandulski, P. Chudzinski, K. Kempa, and M. Giersig, Shadow nanosphere lithography: Simulation and experiment, Nano Lett. 4, 1359 (2004).

15 D. L. J. Vossen, D. Fific, J. Penninkhof, T. van Dillen, A. Polman, and A. van Blaaderen, Combined optical tweezers / ion beam technique to tune colloidal masks for nanolithography, Submitted (2004).

16 W. Stöber, A. Fink, and E. J. Bohn, Controlled growth of monodisperse silica spheres in the micron size range, J. Colloid Interface Sci. 26, 62 (1968).

17 H. Giesche, Synthesis of monodispersed silica powders II. Controlled growth reaction and continuous production process, J. Eur. Ceramic Soc. 14, 205 (1994).

18 A. van Blaaderen and A. Vrij, Synthesis and characterization of colloidal dispersions of fluorescent, monodisperse silica spheres, Langmuir 8, 2921 (1992).

19 A. van Blaaderen, J. van Geest, and A. Vrij, Monodisperse colloidal silica spheres from tetraalkoxysilanes - Particle formation and growth-mechanism, J. Colloid Interface Sci. 154, 481 (1992).

20 D. L. J. Vossen, M. J. A. de Dood, T. van Dillen, T. Zijlstra, E. van der Drift, A. Polman, and A. van Blaaderen, Novel method for solution growth of thin silica films from tetraethoxysilane, Adv. Mater. 12, 1434 (2000).

21 K. P. Velikov, C. G. Christova, R. P. A. Dullens, and A. van Blaaderen, Layer-by-layer growth of binary colloidal crystals, Science 296, 106 (2002).

22 V. Kitaev and G. A. Ozin, Self-assembled surface patterns of binary colloidal crystals, Adv. Mater. 15, 75 (2003).

23 F. Burmeister, W. Badowsky, T. Braun, S. Wieprich, J. Boneberg, and P. Leiderer, Colloid monolayer lithography - A flexible approach for nanostructuring of surfaces, Appl. Surf. Sci. 145, 461 (1999).

24 S. Roorda, T. van Dillen, A. Polman, C. Graf, A. van Blaaderen, and B. J. Kooi, Aligned gold nanorods in silica made by ion irradiation of core-shell colloidal particles, Adv. Mater. 16, 235 (2004).

6 Colloidal crystallization induced by optical gradient forces exerted by optical tweezers

Optical tweezers were used to crystallize colloidal dispersions without manipulating colloids on a single particle level. Using "optical gradient" or "high-frequency dielectrophoretic" forces, we demonstrate control over local particle concentration. This control can be used to induce crystallization and melting in two- and three-dimensional colloidal dispersions using single-beam gradient optical tweezers. In our setup, two microscope objectives (one above and one below the sample) allow independent three-dimensional manipulation and imaging of the structure formation inside the sample. We demonstrate crystallization near a wall for a range of particle sizes, refractive index contrasts, and numerical apertures. In a colloidal mixture of tracer particles with a high refractive index core and low refractive index host spheres dispersed in a host refractive index matching solvent, control over the tracers can indirectly lead to controlled crystallization of the host particles.

6.1 Introduction

Colloidal dispersions are widely used in biology, chemistry, physics, and especially where these disciplines meet. Not only is large control over chemical and morphological properties of the colloidal particles possible, but colloids are also easily accessible in experiment.[1] The particles can be followed in real-time, in real-space, and in the bulk at a single particle level. Due to their well-defined statistical-mechanical properties, colloidal dispersions are also used as model systems to investigate condensed matter theories. Colloidal particles have been used to investigate nucleation and growth kinetics of colloidal crystallization[2] and other phase transitions,[3] but also to investigate systems out of equilibrium such as the glass transition.[4] Because of the tunability of their size and optical properties, colloidal particles are also used as building blocks for advanced materials (e.g., photonic crystals).[5] These materials are developed to control, guide, and switch light. For application in devices, control over order in colloidal dispersions is needed.[1, 6] Ordered arrays of colloidal particles were also used as masks for nanolithography,[7, 8] for data storage,[9] and as sensors.[10]

Different methods have been developed to control order in colloidal dispersions. For example, increasing the particle concentration above the freezing volume fraction will result in the self-organization of colloidal particles into crystals. More control over structure and the degree of ordering is possible using external fields.[6] Gravitational,[11, 12] electric,[13-15] and shear[16, 17] fields have been used to control ordering in colloidal dispersions. Optical fields have been used to crystallize two-dimensional colloidal systems: optical substrates were used to trap a small number of particles on lattice sites consisting of two-dimensional arrangements of trapping potentials with different symmetries.[18-21] These potentials were created by interference of multiple laser beam or with arrays of optical tweezers. Brunner *et al.* used a defocused laser beam to confine particles to a plane and subsequently created a corral of trapped particles that was used to control (indirectly) the order of the dispersion inside the corral.[22]

In this chapter, we describe our first results on methods to control order in colloidal dispersions using optical tweezers. We do not rely on control at a single particle level (as in chapter 7), but instead we apply optical gradient forces on collections of particles to create high concentrations of particles. In principle, giving up control over single particles is experimentally simpler and potentially easier for applications to make advanced materials. Ordering

colloids using optical gradient forces is very similar to the method called the "dielectrophoretic bottle", which was recently described by Sullivan *et al.*[15] although it used very different electro-magnetic frequencies. They applied electric field gradients that induced so-called dielectrophoretic forces on polarizable particles to increase the local concentration of colloids. With this approach they have shown colloidal hard sphere crystallization could be induced in a controlled way. It is also possible to use optical binding forces to induce crystallization.[23] In our experiments, optical binding forces can be neglected between most particles.

We used a setup that combines optical tweezers and independent three-dimensional imaging with confocal microscopy of (concentrated) colloidal dispersions using two microscope objectives, one on each side of the sample.[24] In the next section we first briefly describe the experimental setup and subsequently the colloidal dispersions used. Then we show results of control of crystallization of a two dimensional close-packed structure of anisotropic particles (colloidal dumbbells) near a wall. Then, structure formation was investigated in three-dimensional samples. Finally, we show controlled crystallization and melting in a mixture of tracer and host particles. The tracers were strongly influenced by the light while the host particles, which were close to refractive index matching, were only slightly affected by the optical tweezers. We end with conclusions and an outlook for further work.

6.2 Experimental details

6.2.1 Optical tweezers and independent three-dimensional imaging

An infrared laser (Spectra-Physics; 1064 nm, cw) was used as trapping laser. Acousto-optic deflectors (AODs; IntraAction Corp.) were used to control the position of a single optical trap in the sample. An inverted microscope (Leica; DM IRB) was adapted to have a microscope objective positioned on each side of the sample. The upright objective (above the sample) was mounted on a *xyz* translation stage with differential micrometers (Newport) for accurate positioning. Directly behind each objective, a dichroic mirror (ChromaTech) was attached to the microscope. The dichroic mirrors reflected the trapping laser beam, and transmitted light in the visible. This allowed the laser beam to be focused into the sample, while imaging was still possible. A half-lambda plate and a polarization beam splitting cube,

positioned between the AODs and the microscope, were used to send the laser to the upright objective. In this chapter, optical tweezers were always created in upright trapping mode, although inverted and counterpropagating trapping were also possible using this setup. The sample was imaged using the inverted objective that was below the sample. Imaging was either in transmission microscopy, or, when three-dimensional imaging was desired, using the scan head of a confocal microscope (Leica NT) attached to the side port of the microscope. The inverted objective was then positioned on a piezo lens scanner (PIFOC, Physik Instrumente) to be able to make thin two-dimensional optical sections of the sample. We used 100x (0.7-1.4 NA), 63x (1.4 NA), and 40x (0.7-1.4 NA) plan apochromat oil immersion objectives and a 10x (0.3 NA) plan fluotar air objective. All objectives were obtained from Leica. The power of the trapping laser was measured in the back focal plane of the upright objective using a broadband power meter (Melles Griot). The laser beam was linearly polarized. This polarization direction was horizontal in confocal images (xy sections) and vertical in brightfield images. The setup is described in detail in chapter 2 as well as elsewhere.[24]

6.2.2 colloidal dispersions

Colloidal silica particles with a fluorescent core were synthesized using the Stöber process, modified to incorporate a fluorescent dye, followed by a seeded growth. This growth method and particle characterization are described in more detail elsewhere.[25-27] The silica particles used had an average diameter of 1.4 µm and polydispersity of 1.5%. The core had a diameter of 0.4 µm and it was labeled with the fluorescent dye fluorescein isothiocyanate (FITC). We will refer to the fluoresceine labeled silica particles as FITC-SiO_2. Colloidal dumbbell (dimer) particles were synthesized by letting 1.4 µm diameter FITC-SiO_2 particles aggregate under conditions where the dispersion was slightly unstable. The aggregates, mostly dumbbells, were subsequently grown larger using a Stöber growth. Separation of the mixture of aggregates with a density centrifugation method yielded a dispersion with more than 98% dumbbells.[28] The long and short axes of the dumbbells were found to be 3.2 µm and 1.8 µm respectively. ZnS particles were synthesized following a procedure described elsewhere.[29] The ZnS particles had an average diameter of 1.6 µm and a polydispersity of 7%. Anionic polystyrene particles (PS) with a diameter of 0.99 µm and polydispersity of 3% were obtained from Bangs Laboratories.

Tracer particles with a core-shell geometry were synthesized by first coating 0.99 µm diameter PS particles with Poly(allylamine hydrochloride) (PAH; Aldrich).[30, 31] Onto the polyelectrolyte-coated PS particles, polyvinyl pyrrolidone (PVP; Aldrich) was absorbed and a silica shell was grown on them.[32] Finally, the particles were coated with 3-(trimethoxysilyl) propyl methacrylate (TPM; Fluka),[33] transferred to an apolar solvent and sterically stabilized with a 'comb' stabilizer consisting of poly(12-hydroxystearic acid) (PHS) chains grafted on a PMMA backbone.[34] The final diameter of the particles was determined to be 1.1 µm with a polydispersity of less than 3 percent. We will refer to the tracer particles as PS-SiO_2-TPM-PHS. Polymethylmethacrylate (PMMA) particles were synthesized by dispersion polymerization and the particles were sterically stabilized with the same comb-graft stabilizer. The particles were fluorescently labeled with either rhodamine isothiocyanate (RITC)[35] or 1,1'-dioctadecyl-3,3,3',3'-tetra-methylindocarbocyanide (DiIC) as described by Campbell *et al.*,[36] although the stabilizer was not locked to the particles. The RITC-PMMA-PHS and DiIC-PMMA-PHS particles had a diameter of 1.9 µm and 0.9 µm, respectively, with polydispersities of 3%.

The index of refraction (n_d^{20}) of the FITC-SiO_2 and the dumbbell particles was estimated to be n_d^{20} = 1.45. The index of refraction of the ZnS, PS, and PMMA particles was estimated to be 2.0, 1.6, and 1.5, respectively. The particles were dispersed in ethanol (Merck; analytical grade; n_d^{20} = 1.36), water (deionised; n_d^{20} = 1.33), dimethyl formamide (DMF; Merck, analytical grade; n_d^{20} = 1.43), cyclohexyl bromide (CHB; Sigma-Aldrich; n_d^{20} = 1.50), *cis*-decalin (DEC; Sigma-Aldrich; n_d^{20} =1.48), or mixtures of CHB and DEC with tetrabutylammonium chloride (TBAC; Sigma-Aldrich) or tetrabutylammoniumbromide (TBAB; Sigma-Aldrich) added. All chemicals were used as received.

Samples with a thickness of 10 to 15 µm were made by sandwiching a drop of dispersion between a larger and a smaller microscope cover slip (Chance; No. 1; thickness 150 µm). The samples were sealed with candle wax. Samples with a thickness of 50 µm were made by gluing (UV-adhesive; Norland) two microscope cover slips (Chance; No. 1; thickness 150 µm) together with 50 µm thick wires as spacer. Cover slips were coated with PMMA (MicroChem Corp.; 950 PMMA C4) using a spincoater (Speedline Technologies). The samples were filled with dispersion and sealed with UV-adhesive. Thicker samples were made prepared using 0.1 x 2 x 50 mm^3

capillaries (VitroCom; wall thickness 100 µm), which were closed by melting. The optical quality of the microscope cover slips is better than that of the capillaries.

6.3 Results and discussion

6.3.1 Optical gradient forces induced near a wall

In a capillary filled with 1.4 µm diameter FITC-SiO_2 particles in ethanol, the particles sedimented to the bottom of the sample cell. The gravitational height of a particle, defined as the height at which it gains k_bT in the gravitational field, was on the order of a particle diameter. The concentration of particles was low, less than 1 particle per 100 µm^2 at the bottom of the capillary. Using the upright objective (10x; 0.3 NA) the laser beam (600 mW) was first focused in the plane with particles at the bottom of the sample and subsequently focused below the dispersion by bringing the upright objective 100 µm down. This enlarged the area where the particles experienced optical forces. The optical forces on the particles can be decomposed in terms of a "scattering" force and a "gradient" force.[37] The scattering force, present also by illumination with a plane wave, is in the direction of the optical axis and pushes the particles against the bottom wall of the sample cell. As the focus of the tweezers was below the bottom of the sample, the gradient forces also acted partly in the direction of the scattering force. The gradient force pushed the particles towards the optical axis and let them form close-packed structures similarly as in the "dielectrophoretic bottle" experiments described by Sullivan *et al.* where electric field gradients were used.[15] FITC-SiO_2 particles were attracted to the optical axis, where they formed a close-packed two-dimensional crystal. *Figure 6.1a* shows a transmission microscopy image of a two-dimensional crystal at the bottom wall of a sample. The sample was imaged using an inverted objective (100x; 1.4 NA). The particles in the left part of the image were moving towards the crystal. After some time, when a certain number of particles had been trapped near the optical axis, a second layer of particles formed on top of the first layer. As more particles were trapped, the two-layer structure kept growing in size until a third layer of particles formed in three-dimensional registry with the first two layers. Larger crystals were found to form when the laser beams were defocused further, either by lowering the focus further below the dispersion or by lowering the NA of the objective used to create the trap. A wide variety of colloidal dispersions, with particles having different optical properties,

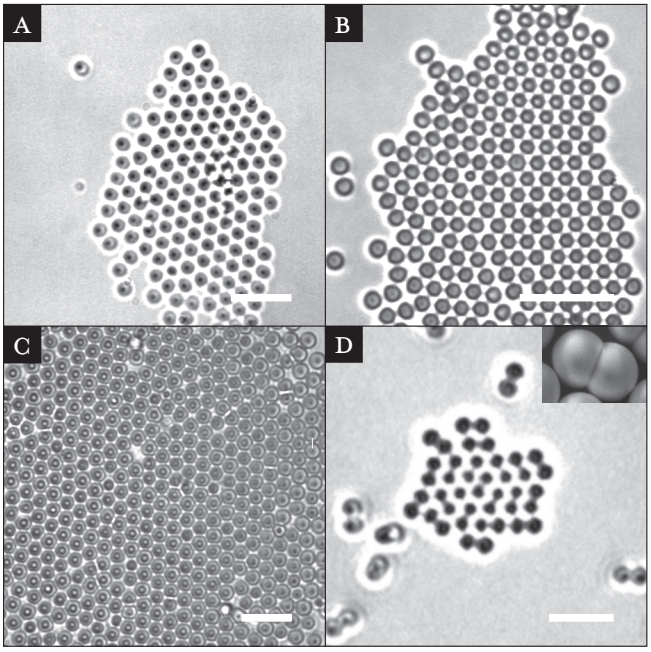

Figure 6.1
Transmission microscopy images of two-dimensional close-packed layers of colloidal particles created using a single optical trap. A laser beam was focused 100 µm below the bottom of the sample cell using an upright objective (10x; NA 0.3).
(a) 1.4 µm diameter FITC-SiO_2 particles in ethanol (600 mW).
(b) 0.99 µm diameter PS particles in water (660 mW).
(c) 1.6 µm diameter ZnS particles in ethanol (600 mW).
(d) A close-packed arrangement of silica dumbbell particles (3.2 µm x 1.8 µm) in water. Here the optical trap (975 mW) was in the bottom plane of the sample.
In (a), (b), and (d), single particles can be seen moving towards a crystal under the influence of the gradient force.
The scale bars are 5 µm.

were found to behave in a similar fashion. *Figure 6.1b* and *6.1c* show images of 0.99 µm diameter PS particles in water (660 mW) and 1.6 µm diameter ZnS particles in ethanol (600 mW) crystallized in a two-dimensional crystal on the bottom of the capillary using a low NA upright objective (10x; 0.3 NA). The optical forces pushed the particles against the bottom wall of the sample. Without the laser turned on, the PS particles were dispersed throughout the whole volume of the capillary, while the ZnS particles were on the bottom of the capillary due to their large negative buoyancy. All dispersions were confined in a layer against the wall. Whether and when a second or third layer formed, depended on the relative strength of the scattering and gradient force on the particles.

Figure 6.1d shows an image of a close-packed structure of colloidal dumbbell particles. Here the optical trap (10x; 0.3 NA; 975 mW) was focused in the plane of the particles on the lower glass wall. The particles were confined around the optical axis and in the bottom plane. Also, as

with the spherical particles, in time the size of the close-packed structure increased, until a critical size was reached when a second layer of dumbbell particles formed on top of the first. Note that while a single dumbbell particle trapped in an optical trap created with a high NA objective would align parallel to the optical axis, here the dumbbell particles were pushed flat on the bottom due to the scattering force. It is interesting to remark that although the structure seen in *Figure 6.1d* looks crystalline, it is not, as the axes of the dumbbells have a "random" orientation.[38] These colloidal dumbbell particles present a new anisotropic model system and it is possible to directly compare their structure formation by optical fields with that of the spheres used to make them.

Ordered regions were also induced in more concentrated dispersions. *Figure 6.2a* shows a fluorescence confocal image of the bottom layer of a sample with 1.4 µm diameter FITC-SiO_2 particles in ethanol. The sample cell consisted of two cover slips spaced 10 µm apart. The particles in the bottom layer were in the fluid state. The sample was imaged with the inverted (100x; 1.4 NA) objective and only the fluorescently labeled cores of the particles are visible. *Figure 6.2b* shows the sample when the laser was focused in the bottom layer using a high numerical aperture objective (100x; 1.4 NA; 500 mW). A crystal formed locally. After the (almost instant) formation of the crystal, its size was constant in time. The particles around it remained in a fluid-like state. Particles from the fluid that were attracted towards the optical axis moved out of the bottom layer, above the crystal, where a three-dimensional structure of particles formed. We also studied the same 1.4 µm diameter FITC-SiO_2 dispersed in DMF in a capillary. Due to smaller refractive index contrast between the spheres and the solvent, better imaging deeper in the sample was possible. *Figure 6.2c* shows a zoomed-in section of the bottom layer of the dispersion with the upright tweezers (100x; 1.4 NA; 1080 mW) focused in the bottom layer. The bottom layer was crystalline, although many defects were present. Due to experimental differences, like solvent, sample cell, and laser power, the size of the crystalline region was larger than in the dispersion in *Figure 6.1b*. The edge of the crystalline region was also more diffuse. *Figure 6.2d* shows an image taken 4.3 µm above the bottom layer. Interestingly, a ring of particles around the optical axis with some particles on the optical axis was seen. The size of the ring increased higher up in the sample. This can also be seen in *Figure 6.2e* where a scan was made perpendicular to the bottom layer. Above the sediment particles

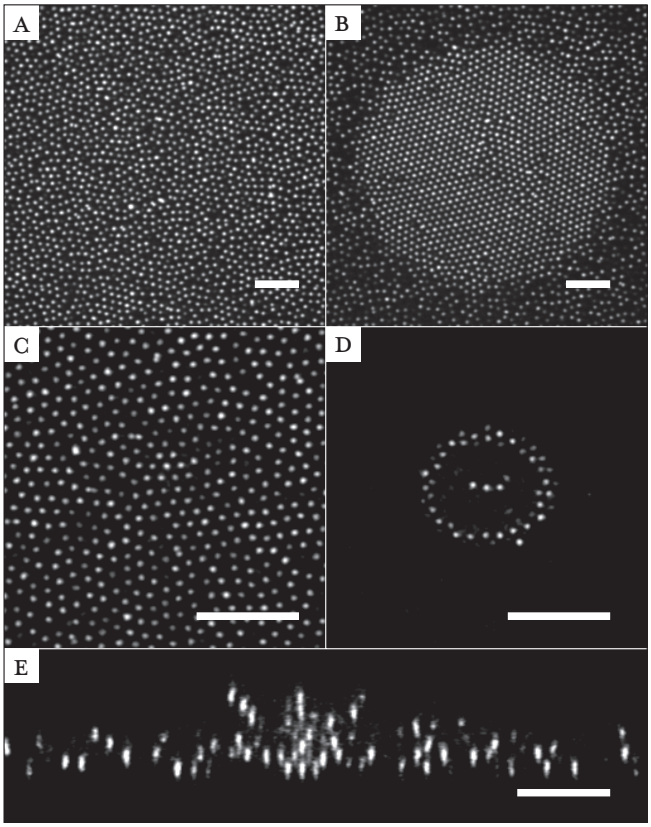

Figure 6.2
Fluorescence confocal images of 1.4 μm diameter FITC-SiO_2 particles.
(a) In the absence of the optical tweezers the particles in the bottom layer were in a liquid-like state.
(b) A crystallite formed when the laser was focused in the bottom layer using a high numerical aperture objective (100x, 1.4 NA, 500mW).
(c) A zoomed-in section of a much larger crystal layer that was formed under different experimental conditions (laser power, solvent, and sample cell).
(d) Image taken 4.3 μm above the bottom layer shows a ring of particles around the optical axis. This image is a cut through a cone of particles formed around the optical axis.
(e) Scan of the sample perpendicular to the bottom layer with the optical trap turned on. The width of the focus was diffraction limited and on the order a few particle diameters. Only the cores of the particles were visible.
The scale bars are 10 μm.

were trapped along the optical axis in a cone around the optical axis. At the moment we do not have a detailed explanation of this effect. It is unlikely, based on numerical calculations with the coupled-dipole method,[39] that a few particle diameters away from the beam waist, the optical binding forces are stronger than $k_b T$.

6.3.2 Optical gradient forces induced in the bulk

To study structure formation away from walls, we focused the laser beam in a capillary filled with 1.9 μm diameter RITC-PMMA-PHS particles in a mixture of CHB and DEC with TBAC-salt added. In this solvent mixture, the particles were almost density matched and did not sediment during the experiments. As the refractive index contrast of the particles with the solvent mixture was small as well, the optical forces were also relatively small. The

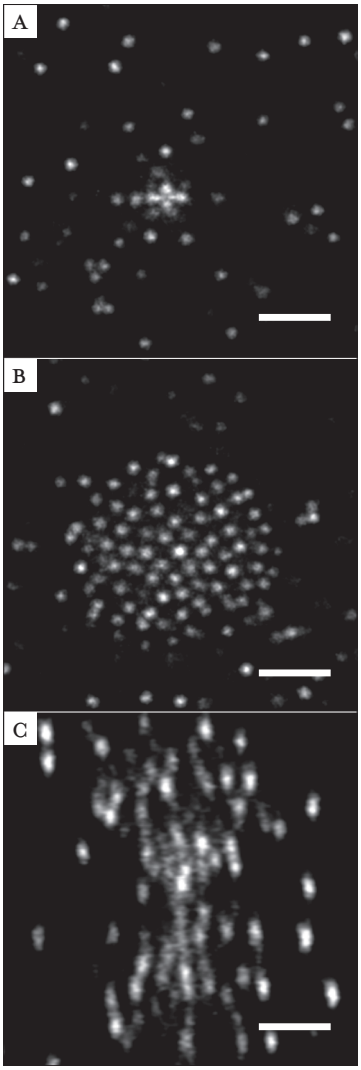

Figure 6.3
Fluorescence confocal images of 2.3 μm diameter RITC-PMMA-PHS particles in a mixture of CHB and DEC with TBAC-salt added.
(a) In the plane were the laser was focused (63x; 1.4 NA, 500 mW), particles were trapped on the optical axis.
(b) Below the trapping plane, particles were confined in a wider area around the optical axis (825 mW).
(c) A scan of the sample parallel to the optical axis shows that particles are confined around the optical axis (825 mW).
The scale bars are 10 μm.

laser was focused in the sample using an upright objective (63x; 1.4 NA). The focus was halfway in the capillary, about 50 μm from both walls. *Figure 6.3a* shows a confocal image of the plane where the tweezers were focused. Only particles in a small region near the optical axis were trapped. *Figure 6.3b* shows an image taken just below the trapping plane. Many more particles were confined close to the optical axis. *Figure 6.3c* shows a scan parallel to the optical axis. It shows the position of the particles in the three-dimensional

optical potential. The power used was 550 mW for *Figure 6.3a* and 825 mW for *Figures 6.3b* and *6.3c*. Under these experimental conditions, we did not observe formation of stable three-dimensional crystal structures. Instead we found particles to move around in the sample in a rather complicated flow profile. For a three-dimensional crystal to form near the focus, the local osmotic pressure has to be balanced by the pressure due to the gradient and scattering forces. Apparently, the asymmetry in the scattering forces made it impossible for a finite number of particles to be stably trapped. Particles were pushed around in the sample by the optical force profile. It is likely that the use of counter propagating tweezers can stabilize structures in three dimensions, which can be studied with our setup as well.

6.3.3 mixtures of tracer and host spheres

A sample cell with a spacing of 50 µm between the PMMA coated walls was filled with a mixture of tracer and host particles. The tracer particles were PS-SiO_2-TPM-PHS particles and the hosts were DiIC-PMMA-PHS particles. The solvent mixture of CHB and DEC had a refractive index slightly lower than that of the host spheres, and TBAB was added to give the particles a hard-sphere like potential.[40] *Figure 6.4a* shows the bottom layer of the sample with the laser beam focused in the bottom layer using an upright objective (63x; 1.4 NA; 900 mW). The sample was imaged using the inverted (100x; 1.4 NA) objective. The tracer and host spheres are displayed with dark and light gray values, respectively. The gradient force on both the tracer and host particles increased the particle concentration around the optical axis and formed a locally crystalline layer. As the force on the tracer particles was larger than the force on the host particles, the tracers were trapped around the optical axis. Although the force on the host spheres was relatively small, the local concentration of host spheres increased, and they crystallized around tracer particles. When the tweezers were turned off, the dispersion melted. *Figure 6.4b* shows the dispersion 2.5 seconds after the tweezers were turned off. The interparticle spacing increased in the crystalline part. *Figure 6.4c* shows the sample 13 seconds after the tweezers were turned off. The crystalline area had melted completely, and the particles were in their original liquid-like state. We want to point out that the force on the slightly mismatched species in a mixture of particles can still be considerable and that this effect can be a potential source of artifacts in delicate force measurements in mixtures of particles.

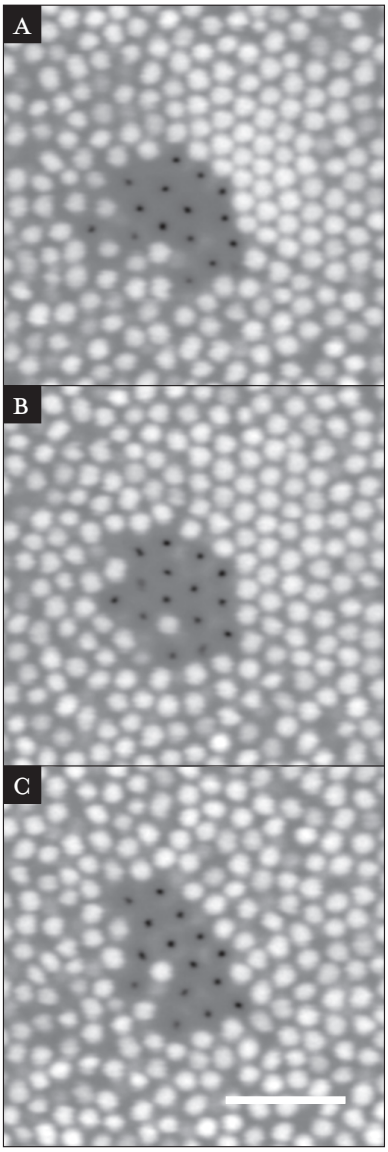

Figure 6.4
Combined fluorescence and reflection confocal images of a mixture of 1 μm diameter DiIC–PMMA–PHS particles (bright, fluorecence) and 1 μm diameter PS–SiO_2–TPM–PHS particles (dark, reflection). The particles were dispersed in a mixture of CHB and DEC with TBAB–salt added.
(a) A crystal of tracer and host particles formed, with the laser turned on (900 mW). The refractive index of the solvent mixture was slightly lower than that of the PMMA particles. The force on the tracer particles was much larger than on the host particles.
(b) Image taken 2.5 seconds after the tweezers were turned off.
(c) Image taken 13 seconds after the tweezers were turned off; now the crystal has molten.
The scale bar is 5 μm.

A system of host and tracer particles as shown here can be used to study crystal nucleation and growth of a colloidal system near a flat wall. Note that by careful tuning of the solvent composition the force on the host spheres can be tuned even and can be set to zero. By turning the laser beam on, the tracers can be made to form a substrate on which the host spheres can

be made to crystallize. The difference between crystallization on a flat wall and on a patterned wall can also be studied using the same dispersion. Also in this case, the possibility of the use of counter propagating tweezers and the induction of crystallization in the bulk still needs to be investigated.

6.4 Conclusions and outlook

We have presented our first results on how to control local densities in a colloidal dispersion using optical tweezers without the need to create traps for single spheres. We demonstrated that optical gradient forces can be used to create two or three-dimensional crystals close to a wall and that crystallization without significant binding forces is possible. We found this to work for a large range of particle sizes and refractive index contrasts. It was also possible to form a close-packed structure of (dimer) dumbbell particles. When we studied three-dimensional manipulation of concentrated colloidal dispersions using a single optical trap, we found that no stable three-dimensional crystals could be formed. Instead, complicated flow profiles were observed. Further work needs to probe the effects of counter propagating tweezers in this respect. We were able to image the effect of structure formation induced by the tweezers in a concentrated dispersion. When a mixture of tracer and host core-shell particles was used, we could trap and manipulate the tracers and through their crystallization influence the host spheres. As the force on the tracer particles was considerably larger than on the host spheres, tracers were pushed against the bottom of the sample cell and acted as a template for crystallization of the host spheres. In chapter 7 we described the manipulation of crystallization in a concentrated dispurtion with optical tweezers at a single particle level.

Acknowledgements

This work has been performed together with Myrthe Plaisier. We gratefully acknowledge the following people for synthesizing colloidal particles: Jacob Hoogenboom (FITC-SiO_2), Patrick Johnson and Carlos van Kats (dumbbells), Krassimir Velikov (ZnS), and Didi Derks (PMMA-PHS).

References

1 A. van Blaaderen, J. P. Hoogenboom, D. L. J. Vossen, A. Yethiraj, A. van der Horst, K. Visscher, and M. Dogterom, Colloidal epitaxy: Playing with the boundary conditions of colloidal crystallization, Faraday Discuss. 123, 107 (2003).

2 U. Gasser, E. R. Weeks, A. Schofield, P. N. Pusey, and D. A. Weitz, Real-space imaging of nucleation and growth in colloidal crystallization, Science 292, 258 (2001).

3 V. J. Anderson and H. N. W. Lekkerkerker, Insights into phase transition kinetics from colloid science, Nature 416, 811 (2002).

4 W. K. Kegel and A. van Blaaderen, Direct observation of dynamical heterogeneities in colloidal hard-sphere suspensions, Science 287, 290 (2000).

5 A. van Blaaderen, K. P. Velikov, J. P. Hoogenboom, D. L. J. Vossen, A. Yethiraj, R. P. A. Dullens, T. van Dillen, and A. Polman, in Photonic crystals and light localization in the 21st century, edited by C. M. Soukoulis (Kluwer, 2001), p. 239.

6 A. van Blaaderen, Colloids under external control, MRS Bulletin 29, 85 (2004).

7 J. C. Hulteen and R. P. Van Duyne, Nanosphere lithography: A materials general fabrication process for periodic particle array surfaces, J. Vac. Sci. Technol. A 13, 1553 (1995).

8 D. L. J. Vossen, D. Fific, J. Penninkhof, T. van Dillen, A. Polman, and A. van Blaaderen, Combined optical tweezers / ion beam technique to tune colloidal masks for nanolithography, Submitted (2004).

9 F. X. Redl, K. S. Cho, C. B. Murray, and S. O'Brien, Three-dimensional binary superlattices of magnetic nanocrystals and semiconductor quantum dots, Nature 423, 968 (2003).

10 J. H. Holtz and S. A. Asher, Polymerized colloidal crystal hydrogel films as intelligent chemical sensing materials, Nature 389, 829 (1997).

11 A. van Blaaderen, R. Ruel, and P. Wiltzius, Template-directed colloidal crystallization, Nature 385, 321 (1997).

12 J. P. Hoogenboom, A. Yethiraj, A. K. van Langen-Suurling, J. Romijn, and A. van Blaaderen, Epitaxial crystal growth of charged colloids, Phys. Rev. Lett. 89, 256104 (2002).

13 A. Yethiraj and A. van Blaaderen, A colloidal model system with an interaction tunable from hard sphere to soft and dipolar, Nature 421, 513 (2003).

14 T. Y. Gong, D. T. Wu, and D. W. M. Marr, Electric field-reversible three-dimensional colloidal crystals, Langmuir 19, 5967 (2003).

15 M. Sullivan, K. Zhao, C. Harrison, R. H. Austin, M. Megens, A. Hollingsworth, W. B. Russel, Z. D. Cheng, T. Mason, and P. M. Chaikin, Control of colloids with gravity, temperature gradients, and electric fields, J. Phys. Cond. Matter 15, S11 (2003).

16 R. M. Amos, J. G. Rarity, P. R. Tapster, T. J. Shepherd, and S. C. Kitson, Fabrication of large-area face-centered-cubic hard-sphere colloidal crystals by shear alignment, Phys. Rev. E 61, 2929 (2000).

17 T. Sawada, Y. Suzuki, A. Toyotama, and N. Iyi, Quick fabrication of gigantic single-crystalline colloidal crystals for photonic crystal applications, Jpn. J. Appl. Phys. Part 2-Lett. 40, L1226 (2001).

18 A. Chowdhury, B. J. Ackerson, and N. A. Clark, Laser-Induced Freezing, Phys. Rev. Lett. 55, 833 (1985).

19 M. M. Burns, J.-M. Fournier, and J. A. Golovchenko, Optical matter: crystallization and binding in intense optical fields, Science 249, 749 (1990).

20 M. Brunner and C. Bechinger, Phase behavior of colloidal molecular crystals on triangular light lattices, Phys. Rev. Lett. 88, 248302 (2002).

21 P. T. Korda, G. C. Spalding, and D. G. Grier, Evolution of a colloidal critical state in an optical pinning potential landscape, Phys. Rev. B 66, 024504 (2002).

22 M. Brunner, C. Bechinger, W. Strepp, V. Lobaskin, and H. H. von Grunberg, Density-dependent pair interactions in 2D colloidal suspensions, Europhys. Lett. 58, 926 (2002).

23 M. M. Burns, J. M. Fournier, and J. A. Golovchenko, Optical Binding, Phys. Rev. Lett. 63, 1233 (1989).

24 D. L. J. Vossen, A. van der Horst, M. Dogterom, and A. van Blaaderen, Optical tweezers and confocal microscopy for simultaneous three-dimensional manipulation and imaging in concentrated colloidal dispersions, Rev. Sci. Instrum. 75, 2960 (2004).

25 A. van Blaaderen and A. Vrij, Synthesis and characterization of colloidal dispersions of fluorescent, monodisperse silica spheres, Langmuir 8, 2921 (1992).

26 *N. A. M. Verhaegh and A. van Blaaderen, Dispersions of Rhodamine-Labeled Silica Spheres - Synthesis, Characterization, and Fluorescence Confocal Scanning Laser Microscopy, Langmuir 10, 1427 (1994).*
27 *H. Giesche, Synthesis of monodispersed silica powders II. Controlled growth reaction and continuous production process, J. Eur. Ceramic Soc. 14, 205 (1994).*
28 *P. Johnson, C. M. van Kats, and A. van Blaaderen, Submitted (2004).*
29 *K. P. Velikov and A. van Blaaderen, Synthesis and characterization of monodisperse core-shell colloidal spheres of zinc sulfide and silica, Langmuir 17, 4779 (2001).*
30 *G. Decher, Fuzzy nanoassemblies: Toward layered polymeric multicomposites, Science 277, 1232 (1997).*
31 *F. Caruso, H. Lichtenfeld, E. Donath, and H. Mohwald, Investigation of electrostatic interactions in polyelectrolyte multilayer films: Binding of anionic fluorescent probes to layers assembled onto colloids, Macromolecules 32, 2317 (1999).*
32 *C. Graf, D. L. J. Vossen, A. Imhof, and A. van Blaaderen, A general method to coat colloidal particles with silica, Langmuir 19, 6693 (2003).*
33 *A. P. Philipse and A. Vrij, Preparation and Properties of Nonaqueous Model Dispersions of Chemically Modified, Charged Silica Spheres, J. Colloid Interface Sci. 128, 121 (1989).*
34 *L. Antl, J. Goodwin, R. Ottewill, and J. Waters, The preparation of poly(methyl methacrylate) latices in non-aqueous media, Colloids and Surfaces 17, 67 (1986).*
35 *G. Bosma, C. Pathmamanoharan, E. H. A. de Hoog, W. K. Kegel, A. van Blaaderen, and H. N. W. Lekkerkerker, Preparation of monodisperse, fluorescent PMMA-Latex colloids by dispersion polymerization, J. Colloid Interface Sci. 245, 292 (2002).*
36 *A. I. Campbell and P. Bartlett, Fluorescent hard-sphere polymer colloids for confocal microscopy, J. Colloid Interface Sci. 256, 325 (2002).*
37 *A. Ashkin, J. M. Dziedzic, J. E. Bjorkholm, and S. Chu, Observation of a single-beam gradient force optical trap for dielectric particles, Opt. Lett. 11, 288 (1986).*
38 *K. W. Wojciechowski, D. Frenkel, and A. C. Branka, Nonperiodic Solid-Phase in a 2-Dimensional Hard-Dimer System, Phys. Rev. Lett. 66, 3168 (1991).*
39 *P. C. Chaumet and M. Nieto-Vesperinas, Optical binding of particles with or without the presence of a flat dielectric surface, Phys. Rev. B 64, 035422 (2001).*
40 *C. P. Royall, M. E. Leunissen, and A. van Blaaderen, A new colloidal model system to study long-range interactions quantitatively in real space, J. Phys. Cond. Matter 15, S3581 (2003).*

7 Colloidal crystallization induced via single particle control with optical tweezers

Preliminary results are presented on the local induction of homogeneous and heterogeneous crystal nucleation in concentrated colloidal dispersions. An array of optical tweezers was used to manipulate individual colloidal tracer particles to create two- and three-dimensional structures of particles that act as nuclei for colloidal crystallization. The symmetry and lattice spacing of the templates were varied inside the host dispersions. The volume fraction of the host spheres was varied, and the interparticle potential was tuned by adding different amounts of salt to the dispersion. The colloidal tracer/host model system, in combination with the optical tweezers/confocal microscopy setup, allows for quantitative and controlled study of the early stages of nucleation and crystal growth using confocal microscopy. Because two microscope objectives were used, one on each side of the sample, optical trapping and imaging in the sample could be completely decoupled. We used a mixture of tracer and host core-shell colloidal particles to selectively trap single particles inside the bulk of a concentrated dispersion. The tracer particles could be trapped because of their high refractive index core, while no optical forces were exerted on the host particles, as they were refractive index matched by the solvent. The host spheres were also nearly density matched by the solvent and therefore did not sediment. We demonstrate the feasibility to determine the critical nucleus size as a function of volume-fraction in a colloidal dispersion. Furthermore, the shape and symmetry of nuclei can be varied, and the effects of this on crystal growth rates and the size of a critical nucleus can be investigated. Because our experimental method is very close to methods used in computer simulations to study crystal nucleation, our results can be directly compared and even linked to such simulations.

7.1 Introduction

Although they are at the basis of many phenomena and important from a fundamental as well as from an applied point of view, (the early stages of) homogeneous and heterogeneous crystal nucleation are relatively poorly understood. In heterogeneous crystallization a liquid nucleates on a piece of foreign material, while in homogeneous nucleation the liquid nucleates itself. Nucleation rates are hard to measure, and microscopic details like the structure of the nuclei formed cannot be determined for molecular systems. This is why a simplified description, like classical nucleation theory (CNT), is often used to fit experimental results. In CNT, the Gibbs free energy difference (ΔG) of a spherical nucleus with radius R in a supersaturated solution is given by

$$\Delta G = \tfrac{4}{3}\pi R^3 \rho_s \Delta\mu + 4\pi R^2 \gamma \ , \qquad (7.1)$$

in which ρ_s is the density of the bulk solid, $\Delta\mu$ the difference in chemical potential between the liquid and the solid, and γ the liquid-solid surface free energy density. The first term in the free energy scales with the volume (R^3) of the nucleus. This term is negative, as free energy is gained when particles go from the fluid to the more stable crystal phase. The second term scales with the surface (R^2) of the nucleus and is positive as it takes into account the free energy it costs to form a fluid-solid interface. For small nuclei the surface term is more important, while for larger ones the bulk term dominates. The critical nucleus size (($R_{critical} = 2\gamma/\rho_s|\Delta\mu|$)) is the size at which the free energy of a nucleus is maximal. In a dense fluid, slightly above the freezing transition, nuclei smaller than $R_{critical}$ continuously form and disappear. Only when a nucleus larger than the critical nucleus size is formed, the nucleus does not disappear and keeps on growing by addition of particles. Although CNT has been used extensively to explain experimental results, it makes several strong simplifying assumptions: the crystal nucleus is treated as spherical and as having the same symmetry as the bulk crystal. Furthermore, parameters like ρ_s, $\Delta\mu$, and γ are assumed to have bulk values and γ is averaged over all crystal orientations.

Recent advances in computer simulations have made it possible to study crystal nucleation in more detail.[1, 2] Predictions of nucleation rates, the critical nucleus size, and the structure of early nuclei became possible.

These simulations have become possible because smart computational methods have been developed to probe the rare event of crystal nucleation. In umbrella sampling, for instance, a local potential is applied which biases unlikely events, resulting in computational effective simulations of homogeneous nucleation.[3]

Due to their well-defined statistical-mechanical temperature, colloidal dispersions can be used as model systems to investigate condensed matter theories. Large control over chemical and morphological properties of the colloidal particles is possible, and, most importantly, due to their time and length scales they are easily accessible in experiments.[4] Colloidal particles can be followed quantitatively in real-time, in real-space, and in the bulk of a three-dimensional system at a single particle level. Colloidal particles have been used to investigate homogeneous and heterogeneous colloidal crystallization,[5, 6] other phase transitions,[7] and to investigate systems (far) out of equilibrium such as the glass transition.[8] Crystallization has been studied extensively using well-defined colloidal model systems,[9] mostly by (light) scattering experiments and analyzed within the framework of CNT. In reciprocal-space experiments, much information on the nucleus in the early stage cannot be extracted, because relatively few particles in the dispersion contribute to the signal.

Although already almost ten years ago, single particle measurements in a colloidal dispersion were obtained using a confocal microscope,[10] there is until now only one paper in which critical nucleation is investigated.[6] Gasser *et al.* studied sub-critical nuclei in a saturated solution and estimated the critical nucleus size using a fast scanning confocal microscope. The disadvantage of microscopy methods is that only a small volume in the sample is investigated and the chance of observing a nucleation event is therefore very small.[3]

In this chapter, we show it is possible to experimentally study nucleation and growth more systematically and in more detail. Arrays of optical tweezers were used to create two- and three-dimensional structures of colloidal particles in the bulk of concentrated dispersions. These structures then acted as nuclei for colloidal crystallization. The symmetry and the lattice spacing of the templates could fully be controlled to mimic different nuclei. Using confocal microscopy we can perform quantitative three-dimensional imaging of individual particles. Imaging and trapping in the sample were completely decoupled because two microscope objectives were

used for imaging and for trapping. To selectively trap particles in the bulk of concentrated dispersions, we used a mixture of tracer and host particles. The tracer particles had a high index core that allowed us to trap them, while the host particles were refractive index matched by the solvent and no optical forces were exerted on them. The host spheres were also nearly density matched by the solvent mixture, allowing experiments to be performed without sedimentation of the host spheres. The core-shell geometry of the tracer particles ensures that all particles in the mixture have similar surface properties. It also reduced distortions of the three-dimensional arrays of optical tweezers, and it eliminated optical binding forces between particles, which are due to scattered light influencing other particles. First results of a SiO_2-based model system, which was not density matched, have been described in chapter 2 and in Ref. 11.

In the next section, we first briefly describe the combined optical tweezers/confocal microscopy setup and the colloidal mixtures we used. In the results and discussion section, we show our first results on nucleation in concentrated colloidal dispersions induced by (two- and three-dimensional) templates of trapped tracer particles. Templates with different symmetries and lattice spacings were studied at several volume fractions. We also show a computer simulation on a system similar to one of our experiments.

7.2 Experimental details

In our setup, an infrared laser (Spectra Physics; 1064 nm; cw) was used for optical trapping.[12] Microscope objectives were positioned on each side of the sample on an inverted microscope (Leica, DM IRB). The upright objective (63x; 1.4 NA) was used for trapping and the inverted objective (100x; 1.4 NA) was used for imaging. The microscope objectives were oil immersion plan apochromats from Leica. The upright objective was mounted on a *xyz* translation stage with differential micrometers (Newport) for accurate alignment with respect to the inverted objective. Dichroic mirrors (ChromaTech), placed directly behind both objectives, reflected the trapping laser beam in the objectives and transmitted light in the visible for imaging. With our setup, optical tweezers can be created in the sample in inverted (from below), upright (from above), or counter propagating (from both sides) trapping modes, depending on whether the upper, the lower or both objectives are used. Acousto-optic deflectors (AODs; IntraAction Corp.) were used to control the position of the optical tweezers in the sample.

By switching the laser beam fast between different positions (up to 220 kHz) in the sample, arrays of optical tweezers were generated. We have demonstrated large two-dimensional arrays (400 traps) that could be changed in real-time.[13] To create three-dimensional structures of trapped tracer particles, two trapping planes at different depths in the sample were created using a Pockels cell (Conoptics; 360-50 LA) in combination with polarizing beam splitters. The Pockels cell and the AODs were synchronized to create different arrays of optical tweezers in each of the two trapping planes.

The sample was imaged in transmission microscopy or, when three-dimensional imaging was desired, using a confocal microscope (Leica NT). To be able to obtain three-dimensional stacks of two-dimensional optical sections, the inverted objective was positioned on a piezo lens scanner (PIFOC, Physik Instrumente). The power of the trapping laser was measured in the back focal plane of the upright objective using a broadband power meter (Melles Griot). The setup is described in detail in chapter 2 as well as in Ref. 13.

Tracer particles with a core-shell geometry were synthesized by coating 0.99 µm diameter polystyrene (PS) particles with Poly(allylamine hydrochloride) (PAH; Aldrich)[14, 15] and absorbing Polyvinyl pyrrolidone (PVP; Aldrich) onto the polyelectrolyte-coated PS particles. Then, a silica shell was grown on them[16] and the particles were coated with 3-(trimethoxysilyl) propyl methacrylate (TPM; Fluka).[17] Finally, the particles were transferred to an apolar solvent and sterically stabilized with a 'comb' stabilizer consisting of poly(12-hydroxystearic acid) (PHS) chains grafted on a PMMA backbone.[18] The final diameter of the tracer particles was determined to be 1.1 µm with a polydispersity of 3%. We will refer to the PS-SiO_2-PMMA-PHS particles as tracers. Polymethylmethacrylate (PMMA) particles were synthesized by dispersion polymerization and also sterically stabilized with PHS. The PMMA particles were fluorescently labeled with 1,1'-dioctadecyl-3,3,3',3'-tetramethylindocarbocyanide perchlorate (DiIC; Molecular Probes) as described by Campbell *et al.*,[19] although the stabilizer was not locked to the particles. We will refer to the DiIC-PMMA-PHS particles as hosts. They had a diameter of 0.93 µm and a polydispersity of 3%. The gravitational height of the (positive buoyant) DiIC-PMMA-PHS spheres was in the order of nine particle diameters. Larger PMMA spheres (2.3 µm diameter) were synthesized as described above and labeled with rhodamine isothiocyanate (RITC).[20] All particle sizes were determined using static light scattering.

The index of refraction (n_d^{20}) of the PS-core and silica-shell, of the tracer particles, as well as of the PMMA particles, was estimated to be 1.59, 1.45, and 1.49 respectively. The mixture of PS-SiO_2-PMMA-PHS and DiIC-PMMA-PHS particles was dispersed in a solvent mixture of cyclohexyl bromide (CHB; Sigma-Aldrich, n_d^{20} = 1.50) and *cis*-decalin (DEC; Sigma-Aldrich, n_d^{20} =1.48) of 96% CHB and 4% DEC by weight. The solvent composition was chosen such that the refractive index of the CHB/DEC mixture matched the refractive index of the DiIC-PMMA-PHS spheres at 1064 nm.[13] It also nearly matched the density of the PMMA spheres. The interactions between the particles were tuned to be hard-sphere like, by adding tetrabutylammonium bromide (TBAB; Sigma-Aldrich) to the CHB (260 µM). We determined the average interparticle distance (a_o) for the DiIC-PMMA-PHS particles in a close-packed crystal to be 1.05 µm. The crystal had a volume fraction of 52 vol-% and it was at coexistence with a fluid. Hard sphere particles in a crystal at coexistence (55 vol-%) have an average interparticle spacing of 1.104 particle diameters. The DiIC-PMMA-PHS particles (0.93 µm diameter) can be scaled to an effective hard sphere diameter of 0.95 µm. We convert all distances to the average interparticle distance in the DiIC-PMMA-PHS crystal at coexistence (a_o). The mixture of PS-SiO_2-PMMA-PHS and RITC-PMMA-PHS particles was dispersed in a mixture of CHB/DEC (96/4 wt-%) with no salt added. The RITC-PMMA-PHS particles were almost refractive index matched, but the optical forces on the spheres were not zero. All chemicals were used as received.

Samples were made by gluing (UV-adhesive; Norland Optical Products Inc. no 68) microscope cover slips (Chance; No. 1; thickness 150 µm) together with ±50 µm thick wires as spacers. The samples were filled with dispersion and sealed with UV-adhesive. The tracer particles were trapped at least 20 µm from the upper sample wall.

Monte Carlo (NPT) computer simulations were performed on a system of about 6000 hard sphere colloids at crystal-fluid coexistence in the presence of a template. The template was composed of 36 particles on a square lattice with a lattice spacing of 1.7 particle diameters.[3, 21]

7.3 Results and discussion

A mixture of PS-SiO_2-PMMA-PHS tracer particles (< 10^{-3} vol-%) and DiIC-PMMA-PHS host particles (32 vol-%) was dispersed in a solvent mixture of CHB and DEC. *Figure 7.1a* shows a brightfield image (Köhler

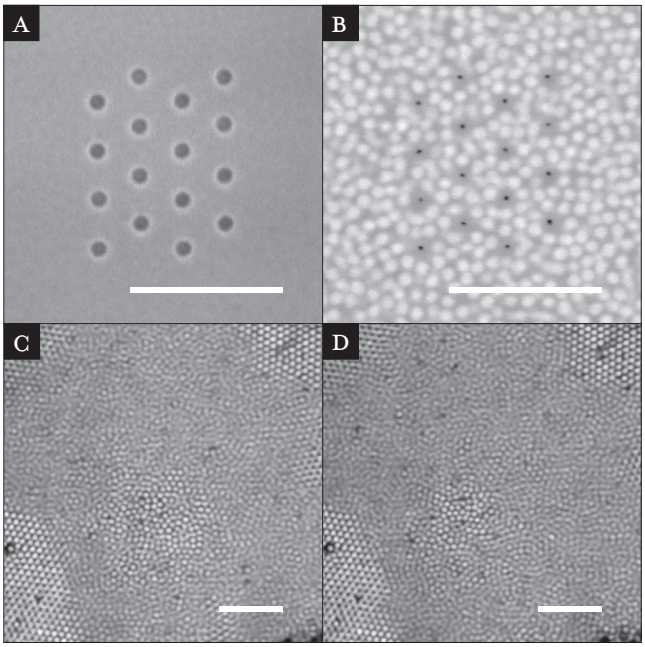

Figure 7.1
(a) Brightfield transmission image of sixteen PS-SiO_2-PMMA-PHS tracer particles in a hexagonal array of optical tweezers. The lattice spacing was 3.0 times the average interparticle distance (a_o) in a DiIC-PMMA-PHS crystal at coexistence. The tracers were trapped in a concentrated dispersion of DiIC-PMMA-PHS host spheres that are not visible because the host spheres were refractive index matched by the solvent.
(b) Confocal microscopy allows imaging of both the tracer (dark gray, reflection) and host spheres (light gray, fluorescence).
(c) Averaged confocal image of a dispersion of host spheres at fluid-crystal coexistence. Self-organized crystals are visible at the edges with a fluid in between. Immobile particles were imaged sharply while moving particles were blurred.
(d) Averaged confocal image of the same dispersion of host spheres at coexistence, but now with an empty array of optical tweezers. The array had sixteen traps in hexagonal symmetry with a lattice spacing of $3.0a_o$. No ordering of the host spheres due to the array of optical traps was observed, showing successful matching of the host spheres by the solvent (at 1064 nm).
The scale bars are 10 µm.

illumination) of sixteen tracer particles trapped in the dispersion of host particles using optical tweezers. The array of optical traps with hexagonal symmetry had a lattice spacing of 3.2 µm, which is 3.0 times the average interparticle distance (a_o) in a crystal of host spheres at coexistence. Only the tracer particles are clearly visible. The host spheres are not because they were refractive index matched by the solvent and they were therefore transparent in transmission microscopy. *Figure 7.1b* shows the same configuration but now imaged using confocal microscopy. The tracer particles (dark gray) were

imaged using reflected light while the host spheres (light gray) were imaged using fluorescence. The concentrated fluid of host spheres surrounding (and penetrating) the trapped tracer particles is now also visible. Due to their complex core-shell geometry with layers of different refractive index, the tracer particles act as tiny lenses and appear smaller when imaged in reflection microscopy.

To investigate whether the samples were really well index matched by the solvent, such that no optical forces were exerted on the host spheres, we created an array of empty optical traps in a dispersion. The sample with host spheres that was at fluid-crystal coexistence is shown in *Figure 7.1c*, before the optical tweezers were turned on. The image is an average over 50 confocal frames that were taken 1.70 seconds apart. In the corners of the image, self-organized crystals of host spheres are visible. In the rest of the sample the host spheres were in a fluid-state. Particles in the fluid are not confined to a lattice position such as in the crystal and appear therefore more blurred than the particles in the crystal. *Figure 7.1d* shows an average of again 50 frames (Δt = 1.7 s), with an array of empty optical tweezers turned on (hexagonal symmetry, $3.0a_o$). No change in structure in the host particles was observed. In case of a mismatch between the refractive index (at 1064 nm) of the host spheres and the solvent, particles would have been trapped (or repelled, see *Figure 8.1c* in chapter 8) by the traps and locally a higher (or lower) intensity would have been visible.

Figure 7.2a shows an average over 50 images (Δt = 0.87 s) of a time-series of frames taken of the configuration already shown in *Figures 7.1a* and *7.1b*. The tracer particles were imaged sharply because they were confined in the optical traps. The host particles (32 vol-%) in between the template showed more structure than the host spheres surrounding the template of tracer particles. However, the order of the host spheres between the tracer particles was not commensurate with the symmetry of the template. Outside the template, the structure in the host spheres remained liquid-like and was therefore almost averaged out. *Figure 7.2b* shows the sample when the lattice spacing of the template was reduced to $2.2a_o$. The order of the host particles between the tracer particles was now commensurate with the symmetry of the template. Three host spheres fitted between three tracer particles. When the lattice spacing was further reduced to $1.9a_o$ *(Figure 7.2c)*, only one host sphere fitted between three tracer particles. When the lattice spacing was reduced to $1.5a_o$ *(Figure 7.2d)*, the host spheres between the tracer particles in the

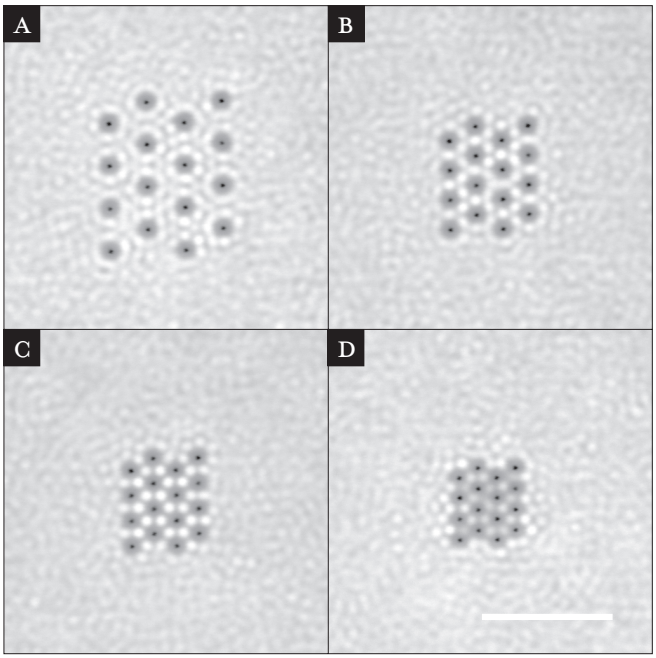

Figure 7.2
Combined confocal reflection and fluorescence images of sixteen tracer particles trapped in an optical tweezers array with hexagonal symmetry. The tracer particles were surrounded by refractive index matched host particles. (a) Array with lattice spacing of $3.0a_o$. The host spheres ordered between the trapped tracer particles, but no order commensurate with the symmetry of the tracers was observed. (b) Array with $2.2a_o$, (c) $1.9a_o$, and (d) $1.5a_o$. The images were averaged over 50 images with 0.87 seconds between the frames. The volume fraction of the host particles was 32 vol-%.
The scale bar is 10 µm.

template were partially expelled from the imaging plane. The surrounding host dispersion was relatively far from the freezing volume fraction and ordering of host spheres occurred only locally near the template.

Figure 7.3 shows the same sample, but the template was changed to a square symmetry. For a lattice spacing of $3.0a_o$ *(Figure 7.3a)*, there was some order of the host spheres induced between the tracer particles. The order increased for a spacing of $2.2a_o$ *(Figure 7.3b)*, although it was still incommensurate with the structure of the template. For the template spacing of $1.9a_o$ *(Figure 7.3c)*, the host spheres ordered in a more complex way between the tracer particles. Finally, for a spacing of $1.5a_o$ *(Figure 7.3d)*, the host spheres ordered perfectly in the template.

Extending these experiments, it is possible to study homogeneous nucleation of a colloidal dispersion. It will be interesting to study different template symmetries, host volume fractions, and interparticle potentials. From a comparison between *Figures 7.2* and *7.3*, it might be concluded that for this set of experimental parameters (particle sizes and lattice spacings) the hexagonal symmetry shows stronger ordering than the square symmetry.

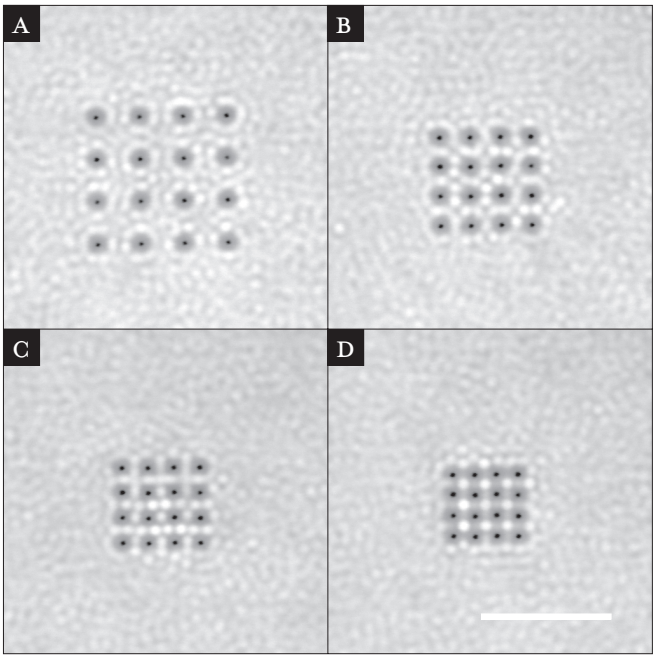

Figure 7.3
Tracer particles trapped in an array with square symmetry in the same sample as in Figure 7.2. Lattice spacings were the same as in Figure 7.2: (a) 3.0a_o, (b) 2.2a_o, (c) 1.9a_o, and (d) 1.5a_o. Images were averaged over 50 images with 0.87 seconds between the frames.
The scale bar is 10 μm.

We have plans for a more detailed investigation of the relative number of particles ordered in and on different templates. It should be noted that a lattice mismatch of only a few percent in a fixed template with square symmetry (a wall with holes) already results in reconstruction of the first crystal layer to hexagonal packing.[22, 23] Although averaging images taken with the confocal microscope does not give quantitative information, it does capture the qualitative information in the image and is easy to interpret. We will perform a more quantitative analysis using local bond order parameters calculated from the coordinates retrieved from our measurements.

Figure 7.4 shows a density plot calculated from a simulation with parameters close to the ones in our experiments.[21] In the simulation, the host to tracer particle size ratio was 1, the interparticle spacing was 1.7 particle diameters, a template of 6 x 6 particles was used, and the dispersion was at coexistence. Although this simulation did not have exactly the same parameters as our experiments, it qualitatively showed the same behavior as the experiments shown in *Figure 7.3d*. We are currently working on a more detailed and quantitative comparison.

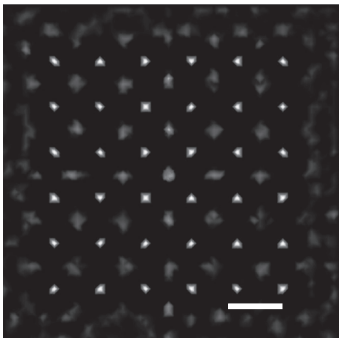

Figure 7.4
Local particle density obtained from a computer simulation of a system of about 6000 hard spheres in the presence of a 6 x 6 template of square symmetry (bright spots) with a lattice spacing of 1.7 particle diameters. The particles were found to order between the template particles.
The scale bar is 2 particle diameters.

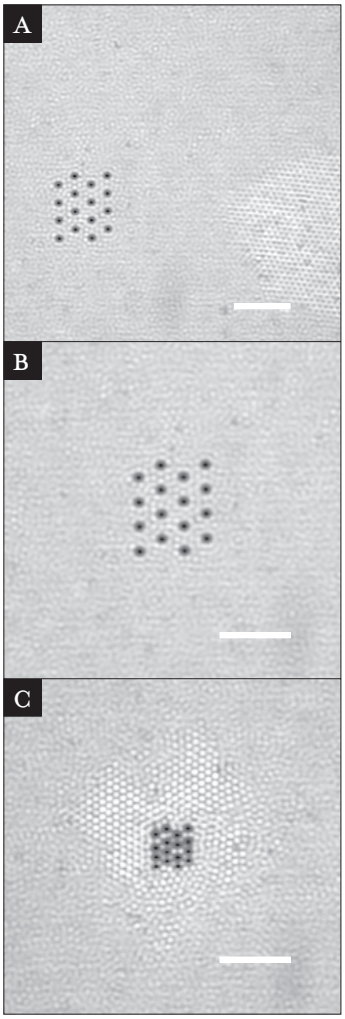

Figure 7.5
Combined confocal reflection and fluorescence images of a template of tracer particles in a concentrated dispersion of host particles. The dispersion of host particles was at fluid-crystal coexistence.
(a) 16 tracer particles in a square symmetry with a lattice spacing of $3.0a_o$. Around the trapped tracer particles, the host dispersion remained fluid-like. A crystal coexisting with the fluid is visible in the lower-right corner. This crystal had formed before the optical tweezers were turned on.
(b) Zoomed-in on the tracer particles of Figure 7.5a.
(c) When the lattice spacing of the template was reduced to $1.5a_o$, a crystal nucleated on the edge of the template. Images were averaged over 100 frames with 0.85 seconds in between them.
The scale bars are 10 µm.

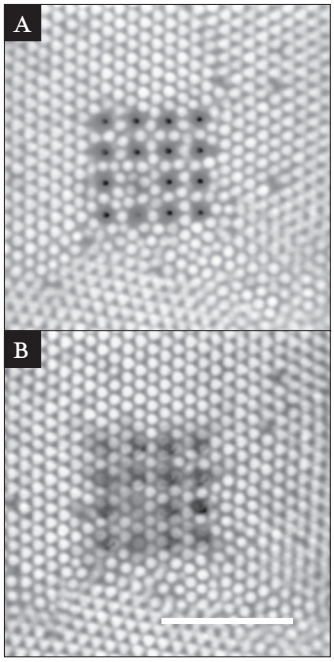

Figure 7.6
Combined confocal reflection and fluorescence images of an array with square symmetry with 15 tracer particles. The lattice spacing between the tracers was $2.2a_o$. The host particles were ordered in a hexagonal symmetry.
(a) The layer with the array was imaged. As can be seen, even between the tracer spheres the host spheres did not order into a square symmetry. This is attributed to a mismatch between the lattice spacing of the template and the equilibrium spacing of the host spheres.
(b) Above the array the host spheres had the hexagonal order of a close-packed plane. Images were averaged over 100 images with 1.70 seconds between the frames.
The scale bar is 10 μm.

Figure 7.5a shows an image (averaged over 100 frames, Δt = 1.70 s) of an array of tracer particles trapped in a sample in which the host particles were at fluid-crystal coexistence. The same sample was used in *Figures 7.1c* and *7.1d* to test the refractive index matching of the host spheres. On the right of the image, a self-organized crystal of host spheres is visible, while in the rest of the image a fluid can be seen. Sixteen tracer particles were trapped in a hexagonal symmetry with a lattice spacing of $3.0a_o$. *Figure 7.5b* shows a zoomed-in image, and, although there was some ordering of host spheres between the tracer particles in the template, no crystal formed on or in the template. When we reduced the lattice spacing of the template to $1.5a_o$, a crystal of host spheres nucleated at the template. *Figure 7.5c* shows an averaged image of the nucleated crystal and the template. The edge of the template acted as a seed for heterogeneous nucleation of host spheres. The particles in and on top of the template did not follow the template, as it was incommensurate with the crystal structure.

Using our setup, it is possible to study the sample in three dimensions. *Figure 7.6a* shows an image of fifteen tracer particles in a template with square symmetry ($2.2a_o$ spacing). The template is incorporated in a crystal of host spheres that filled the complete field of view of the confocal microscope.

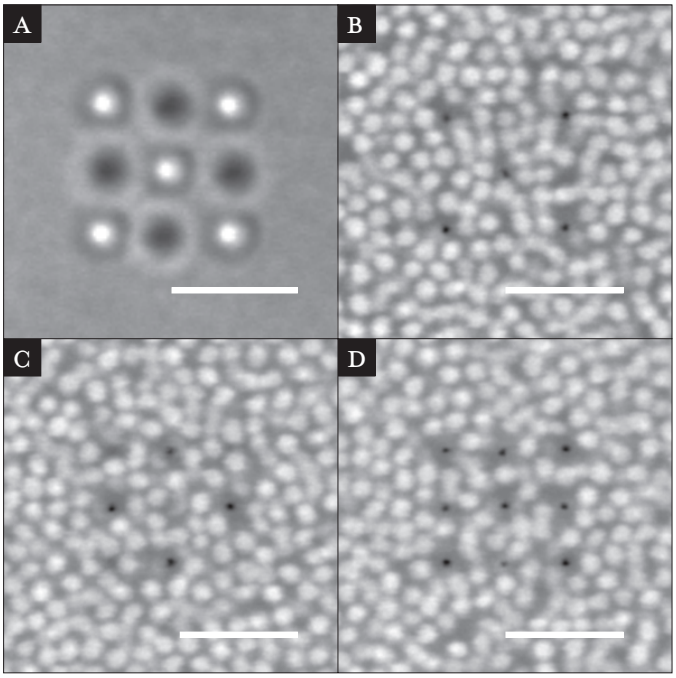

Figure 7.7
A three-dimensional array of traps was created by synchronizing the Pockels cell with the AODs.
(a) Image in brightfield with five tracer particles (white) in the upper plane and four tracer particles (dark gray) in the lower plane. The host particles were well index matched and not visible around the trapped tracer particles.
(b)-(d) Combined confocal reflection and fluorescence images of the three-dimensional structure of tracer particles in the host dispersion, with (b) the upper plane, (c) the lower plane, and (d) a plane in between. The height difference between the two trapping planes was $1.1a_o$.
The scale bars are 5 µm.

The crystal had nucleated on the template. The host spheres ordered between the tracer particles, but the structure of the template was incommensurate with the close-packed crystal. Note that where one tracer is missing, the packing of host spheres is hexagonal. Below the template *(Figure 7.6b)*, the host spheres were hexagonally ordered and commensurate with the rest of the crystal. The fact that tracer particles can be manipulated in a crystal of host spheres is used for experiments in chapter 8.

Figure 7.7a shows a brightfield image of a three-dimensional structure of tracer particles created using the Pockels cell synchronized with the AODs to trap particles in two planes. Five tracer particles (above the focal plane and imaged in white) were trapped in the upper trapping plane and four tracer particles (below the focal plane and imaged in dark gray) were trapped in the lower trapping plane. The distance between the traps in each plane was $3.4a_o$ and the distance between the trapping planes was $1.1a_o$. The host particles are not visible around the tracer particles as they were well index matched. When the sample was imaged using the confocal microscope, both the tracer particles and the host spheres were visible. *Figures 7.7b, 7.7c,* and *7.7d* show confocal images of the upper and lower trapping plane and a plane

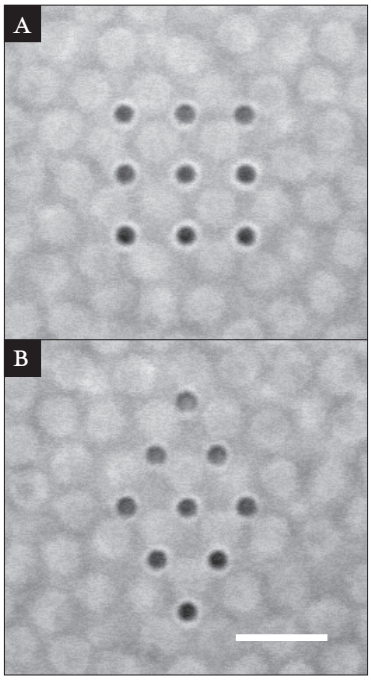

Figure 7.8
(a) Brightfield image of nine PS-SiO_2-PMMA-PHS tracer particles in a square array of optical tweezers. The tracers were trapped in a dispersion of FITC-PMMA-PHS host spheres (R_{tracer} / R_{host} = 1/2.1). The host spheres are visible as they were not perfectly matched. The particles were soft repulsive as no salt was added. They ordered in between the tracer particles trapped in the template.
(b) Array changed to hexagonal order.
The scale bar is 5 μm.

between the two trapping planes, respectively. The volume fraction of the host spheres (32 vol-%) was not high enough to observe nucleation induced by the tracer spheres. We are currently investigating the influence of three-dimensional nuclei in more concentrated dispersions.

Templates of tracer particles can also be used to induce nucleation and growth of binary crystals. *Figure 7.8a* shows a brightfield image of a mixture of PS-SiO_2-PMMA-PHS tracer and RITC-PMMA-PHS host particles in a solvent that was close to refractiveindex matching. The size ratio of the tracer and host spheres was 2.1. The optical forces on the host spheres were small, but the sample could be better refractiveindex matched. *Figure 7.8b* shows the template after it had been changed to a hexagonal structure. Note that here we only demonstrate that it is possible to create a binary nucleus. For a binary crystal to nucleate on this template, a mixture of small and large host spheres combined with tracer spheres has to be used.

7.4 Conclusions and outlook

In conclusion, we have demonstrated the feasibility to nucleate colloidal crystals by manipulating particles with optical tweezers. Arrays of optical

tweezers were used to create two- and three-dimensional structures of colloidal particles that acted as nuclei for colloidal crystallization. The crystal symmetry and lattice spacing of the nuclei could be controlled. Quantitative three-dimensional imaging of individual particles was possible using a confocal microscope. Imaging was decoupled from optical trapping because two microscope objectives were used. A mixture of tracer and host particles allowed selective trapping and imaging of individual particles in the bulk of a concentrated dispersion. The tracer particles could be trapped because of a high refractive index core. No optical forces were exerted on the host particles, as they were refractive index matched by the solvent. The host particles were also nearly density matched by the solvent. The core-shell geometry gave the particles in the mixture similar surface properties, reduced distortions of the three-dimensional arrays of optical tweezers, and removed the optical binding forces between the tracer particles. We demonstrated first results on nucleation on several templates (with different symmetry and spacing) in colloidal dispersions. The influence of the geometry and size of the templates on the ordering of the host spheres can be studied systematically and in more detail. The volume fraction and the interparticle potential are experimental parameters that can be tuned as well. We plan to combine our experiments with a "dielectrophoretic" bottle to control the volume fraction of host spheres accurately.[24] With this method, electromagnetic field gradients are used to tune the volume fraction. With our colloidal model system in combination with the setup, it is possible to determine the critical nucleus size for different volume fractions. The shape and symmetry of nuclei can be varied and their influence on the size of a critical nucleus and crystal-growth rates can be investigated. Our experimental method is very close to methods used in computer simulations to study crystal nucleation. We have compared our results to such simulations.

Acknowledgements
We gratefully acknowledge Christina Christova and Didi Derks for RITC- and DiIC- PMMA synthesis, respectively, and Astrid van der Horst for help with measurements with the Pockels cell. Angelo Cacciuto is thanked for performing the computer simulations.

References

1 S. Auer and D. Frenkel, Prediction of absolute crystal-nucleation rate in hard-sphere colloids, Nature 409, 1020 (2001).

2 A. Cacciuto, S. Auer, and D. Frenkel, Onset of heterogeneous crystal nucleation in colloidal suspensions, Nature 428, 404 (2004).

3 S. Auer and D. Frenkel, Quantitative prediction of crystal-nucleation rates for spherical colloids: A computational approach, Annu. Rev. Phys. Chem. 55, 333 (2004).

4 A. van Blaaderen, J. P. Hoogenboom, D. L. J. Vossen, A. Yethiraj, A. van der Horst, K. Visscher, and M. Dogterom, Colloidal epitaxy: Playing with the boundary conditions of colloidal crystallization, Faraday Discuss. 123, 107 (2003).

5 A. van Blaaderen, R. Ruel, and P. Wiltzius, Template-directed colloidal crystallization, Nature 385, 321 (1997).

6 U. Gasser, E. R. Weeks, A. Schofield, P. N. Pusey, and D. A. Weitz, Real-space imaging of nucleation and growth in colloidal crystallization, Science 292, 258 (2001).

7 V. J. Anderson and H. N. W. Lekkerkerker, Insights into phase transition kinetics from colloid science, Nature 416, 811 (2002).

8 W. K. Kegel and A. van Blaaderen, Direct observation of dynamical heterogeneities in colloidal hard-sphere suspensions, Science 287, 290 (2000).

9 T. Palberg, Colloidal crystallization dynamics, Curr. Opin. Colloid Interface Sci. 2, 607 (1997).

10 A. van Blaaderen and P. Wiltzius, Real-space structure of colloidal hard-sphere glasses, Science 270, 1177 (1995).

11 M. M. Burns, J. M. Fournier, and J. A. Golovchenko, Optical Binding, Phys. Rev. Lett. 63, 1233 (1989).

12 A. Ashkin, J. M. Dziedzic, J. E. Bjorkholm, and S. Chu, Observation of a single-beam gradient force optical trap for dielectric particles, Opt. Lett. 11, 288 (1986).

13 D. L. J. Vossen, A. van der Horst, M. Dogterom, and A. van Blaaderen, Optical tweezers and confocal microscopy for simultaneous three-dimensional manipulation and imaging in concentrated colloidal dispersions, Rev. Sci. Instrum. 75, 2960 (2004).

14 G. Decher, Fuzzy nanoassemblies: Toward layered polymeric multicomposites, Science 277, 1232 (1997).

15 F. Caruso, H. Lichtenfeld, E. Donath, and H. Mohwald, Investigation of electrostatic interactions in polyelectrolyte multilayer films: Binding of anionic fluorescent probes to layers assembled onto colloids, Macromolecules 32, 2317 (1999).

16 C. Graf, D. L. J. Vossen, A. Imhof, and A. van Blaaderen, A general method to coat colloidal particles with silica, Langmuir 19, 6693 (2003).

17 A. P. Philipse and A. Vrij, Preparation and Properties of Nonaqueous Model Dispersions of Chemically Modified, Charged Silica Spheres, J. Colloid Interface Sci. 128, 121 (1989).

18 L. Antl, J. Goodwin, R. Ottewill, and J. Waters, The preparation of poly(methyl methacrylate) latices in non-aqueous media, Colloids and Surfaces 17, 67 (1986).

19 A. I. Campbell and P. Bartlett, Fluorescent hard-sphere polymer colloids for confocal microscopy, J. Colloid Interface Sci. 256, 325 (2002).

20 G. Bosma, C. Pathmamanoharan, E. H. A. de Hoog, W. K. Kegel, A. van Blaaderen, and H. N. W. Lekkerkerker, Preparation of monodisperse, fluorescent PMMA-Latex colloids by dispersion polymerization, J. Colloid Interface Sci. 245, 292 (2002).

21 A. Cacciuto, S. Auer, and D. Frenkel, In preparation, (2004).

22 J. P. Hoogenboom, A. K. van Langen-Suurling, J. Romijn, and A. van Blaaderen, Hard-sphere crystals with hcp and non-close-packed structure grown by colloidal epitaxy, Phys. Rev. Lett. 90, 138301 (2003).

23 J. P. Hoogenboom, A. K. van Langen-Suurling, J. Romijn, and A. van Blaaderen, Epitaxial growth of a colloidal hard-sphere hcp crystal and the effects of epitaxial mismatch on crystal structure, Phys. Rev. E 69, 051602 (2004).

24 M. Sullivan, K. Zhao, C. Harrison, R. H. Austin, M. Megens, A. Hollingsworth, W. B. Russel, Z. D. Cheng, T. Mason, and P. M. Chaikin, Control of colloids with gravity, temperature gradients, and electric fields, J. Phys. Cond. Matter 15, S11 (2003).

8 Defect formation induced by a particle driven through a three-dimensional colloidal crystal

We present experiments on a single particle driven through a three-dimensional colloidal crystal. Using optical tweezers a tracer particle was trapped in the bulk of a colloidal crystal of host spheres. The crystal was moved past the trapped particle at constant velocities. Only the tracer particle was trapped because it had a high refractive index core, while no optical forces were exerted on the host spheres in the crystal as they had the same refractive index as the solvent. The tracer and host particles were imaged using quantitative three-dimensional confocal microscopy. Particle interactions were tuned to hard-sphere like by adding salt to the dispersion. At low driving speed of 0.27 particle diameters per second (a_o/s), defects were only formed within a few diameters from the tracer. Occasionally, a defect survived and lived for some time before it was annealed out by the crystal. At higher driving speed of 2.1 a_o/s, many more defects were introduced behind the trapped particle, which were not annealed out within the field of view of the microscope. Host particles were sometimes observed to be pushed in front of the tracer particle for a while. Similar behavior was reported in recent computer simulations on a two-dimensional version of our experiment.

8.1 Introduction

Colloidal particles can be used as model systems to test condensed matter theories.[1, 2] Due to their Brownian motion, colloidal particles have an equilibrium behavior that is thermodynamically equivalent to that of atoms. This strict analogy does not hold for the dynamics. Nevertheless, because the dynamics of colloids are simpler, colloids are also used as model systems for molecular systems in which the dynamics are important; e.g. the glass transition.[3] One of the big advantages of colloidal dispersions is their accessibility in experiments. Real-time and real-space position information of individual particles can be obtained using confocal microscopy.[4]

It is possible to manipulate single particles using optical tweezers. Pertsinidis *et al.* removed a particle from a two-dimensional colloidal crystal using optical tweezers and studied equilibrium properties as well as the dynamics of the defects formed.[5, 6] Particle movement close to the glass transition has been studied using a magnetic particle dragged through a two-dimensional crystal using magnetic tweezers.[7] Using computer simulations, the defect formation and the drag on a tracer particle driven through a two-dimensional crystal has been studied as well.[8, 9]

Here we extend these experiments to three-dimensional systems using a setup we recently developed, in which a confocal microscope is combined with optical tweezers. Independent (three-dimensional) imaging and trapping of individual particles is possible because two microscope objectives are used. In combination with a specially developed colloidal dispersion, selective optical trapping and imaging was possible inside concentrated colloidal dispersions (see also chapters 2 and 7).

In this chapter, we describe experiments on a single tracer particle trapped inside a three-dimensional colloidal crystal of host particles using optical tweezers. Once a particle was trapped, we moved the crystal of host spheres past the tracer particle at several speeds. The interparticle potential was modified to be hard-sphere like. In the next section we describe our experimental setup and the colloidal dispersions used. We then describe and discuss our experiments and end with conclusions and an outlook.

8.2 Experimental details

Optical tweezers were created by focusing an infrared laser (Spectra Physics; cw; 1064 nm) to a diffraction-limited spot using a microscope objective. A second microscope objective, positioned on the other side of the sample,

allowed for independent optical trapping and three-dimensional imaging using a confocal microscope (Leica; TSC NT). The upright objective (63x; 1.4 NA) was used for trapping. For imaging we used the inverted objective (100x; 1.4 NA) mounted on a piezo lens scanner (PIFOC, Physik Instrumente) to obtain three-dimensional stacks of two-dimensional optical sections. The combined optical tweezers/confocal microscopy setup is described in detail in chapter 2 and in Ref. 10.

Colloidal tracer particles with a core-shell geometry were synthesized by coating 0.99 µm diameter polystyrene particles with a silica shell.[11] The particles were then coated with 3-(trimethoxysilyl) propyl methacrylate (TPM; Fluka),[12] transferred to an apolar solvent, and sterically stabilized with a 'comb' stabilizer consisting of poly(12-hydroxystearic acid) (PHS) chains grafted on a PMMA backbone.[13] The final diameter of the tracer particles was determined to be 1.1 µm with a polydispersity of 3%. We will refer to the PS-SiO_2-PMMA-PHS particles as tracers. Polymethylmethacrylate (PMMA) particles were synthesized by dispersion polymerization and also sterically stabilized with PHS. The PMMA particles were fluorescently labeled with 1,1'-dioctadecyl-3,3,3',3'-tetramethylindocarbocyanide perchlorate (DiIC; Molecular Probes) as described by Campbell *et al.*,[14] although the stabilizer was not locked to the particles. They had a diameter of 0.93 µm with a polydispersity of 3%. We will refer to the DiIC-PMMA-PHS particles as hosts. Particle sizes were determined using static light scattering.

The indices of refraction (n_d^{20}) of the PS-core and silica-shell, of the tracer particles, and of the PMMA particles were estimated to be 1.59, 1.45, and 1.50 respectively. The particles were dispersed in a mixture of cyclohexyl bromide (CHB; Sigma-Aldrich, n_d^{20} = 1.50) and *cis*-decalin (DEC; Sigma-Aldrich, n_d^{20} = 1.48) consisting of 96% CHB and 4% DEC by weight. The solvent composition was chosen such that the refractive index of the CHB/DEC-mixture matched the refractive index of the host spheres at 1064 nm. The solvent mixture also closely matched the density of the PMMA spheres. The interactions between the particles were tuned to be hard-sphere like, by adding tetrabutylammonium bromide (TBAB; Sigma-Aldrich) to the CHB (260 µM) used in the solvent mixture. We determined the average interparticle distance for the host particles in an FCC (rHCP) crystal to be a_o = 1.10 µm. The crystal was at coexistence with a fluid, and its volume fraction was 45 vol-%. Hard sphere particles in a crystal at coexistence (55 vol-%) have an average interparticle spacing of 1.104 particle diameters.

The host particles (0.93 µm) can be scaled to an effective hard-sphere diameter of 1.0 µm. We convert all distances to the average interparticle distance in the host crystal at coexistence (a_o). All chemicals were used as received.

Sample cells with a thickness of 50 µm were made by gluing (UV-adhesive; Norland; no. 68) microscope cover slips (Chance; No. 1; thickness 150 µm) together using 50 µm thick wires as spacers. The sample cells were filled with dispersion and sealed with UV-adhesive. A tracer particle was trapped 4 µm from the bottom wall of the sample. The power of the trapping laser was measured to be 250 mW in the back focal plane of the upright objective using a broadband power meter (Melles Griot). The sample was moved at constant velocities using a translation stage (Rolyn) with motorized actuators (Newport, accuracy better than 1 µm). Confocal images were analyzed using software routines for finding particle coordinates that are described in Refs. 15, 16. Two-dimensional Voronoi diagrams were constructed from the particle coordinates.

8.3 Results and discussion

A sample was made containing a mixture of PS-SiO_2-PMMA-PHS tracer and DiIC-PMMA-PHS host spheres in a mixture of CHB and DEC. The host spheres formed a random hexagonal close-packed crystal (rHCP) as expected for a (physical) hard-sphere crystal.[17, 18] Using optical tweezers, a single tracer particle was trapped inside the three-dimensional crystal. Then, a series of images was recorded using the confocal microscope with the colloidal crystal at rest with respect to the trapped tracer particle. *Figure 8.1a* shows a combined confocal reflection and fluorescence image of the optically trapped tracer particle (black) in the crystal of the host spheres (white). Due to the complex core-shell geometry of the tracer particle, the size of the particle in the image appears to be much smaller than its real size. The crystal of host spheres was oriented with its hexagonally close-packed layers parallel to the bottom wall. From the particle coordinates determined from the image we constructed a Voronoi diagram *(Figure 8.1b)*. It displays the image as a set of polygons that are defined as those points that are closer to the particle in the center of the polygon than to all other particles.

To investigate the possibility of significant optical forces being exerted on the host particles by the optical tweezers, we focused an optical trap in the host dispersion. Without trapping a tracer particle, the crystal of

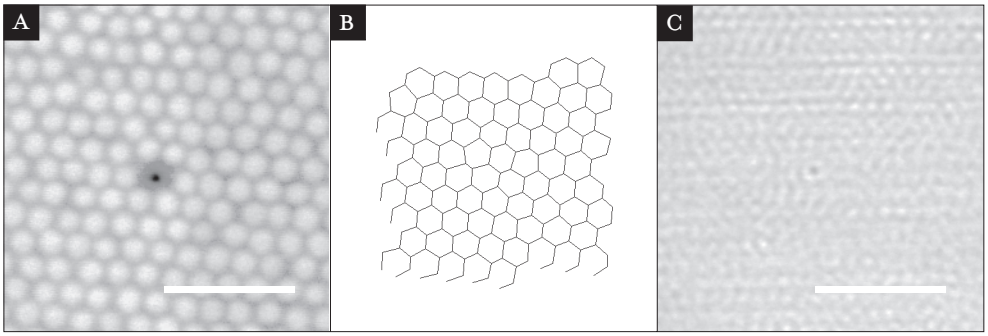

Figure 8.1
(a) Combined confocal reflection and fluorescence image of a two-dimensional plane in a three-dimensional crystal. A tracer particle (black) was trapped inside a crystal of host spheres (white) using optical tweezers. The crystal was at rest with respect to the tracer particle. Due to the complex core-shell geometry of the tracer particle, the size of the particle in the image appears to be much smaller than its real size.
(b) A Voronoi diagram of the image in Figure 8.1a shows close-packed hexagonal order in the crystal plane.
(c) An average over 100 images (Δt = 1.0 s) was taken when the crystal was moved past an empty optical trap (1.18 a_o/s). The optical trap expelled the host spheres slightly from the center of the image. As the optical forces decay strongly with distance, the optical force on the host spheres was negligible when a tracer particle was trapped.
The scale bars are (a) 5 µm and (c) 10 µm.

host spheres was then moved past the empty optical trap at 1.18 a_o/s. A time series of confocal images was recorded, and from the average of 100 images *(Figure 8.1c)* it is visible that the host spheres were slightly depleted from the optical trap, which was is the center of the image. This indicates that the refractive index of the solvent was slightly higher (~ order 10^{-3}) than that of the host spheres. However, when a tracer particle was trapped, the optical forces on the host dispersion were negligible, as the optical forces on the host spheres decay strongly with distance from the (diffraction-limited) optical trap. Complete refractive index matching of the host spheres is possible, as described in chapters 2 and 7.

We then trapped a tracer particle and moved the crystal of host spheres from left to right *(in Figure 8.2)* at a speed of 0.27 a_o/s. Defects induced by the tracer particle were observed within a few diameters of the tracer particle. However, defects induced by the tracer particle were on occasion observed to survive for some time behind the tracer particle. These defects annealed out in the field of view of the confocal microscope. An example is shown in *Figure 8.2a*. In the confocal image two defects (vacancies) can be seen behind (to the right of) the tracer particle. In the corresponding Voronoi diagram,

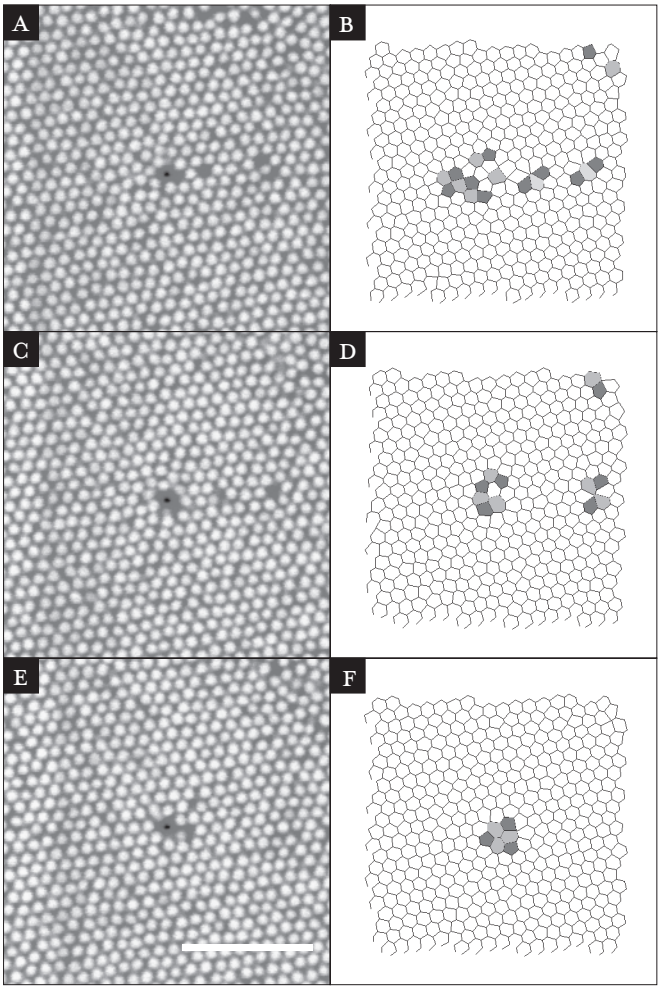

Figure 8.2
The crystal of host spheres was driven (from left to right) past the trapped tracer particle at a speed of 0.27 a_o/s.
(a) Image of the plane in which the tracer particle was trapped
(b) A Voronoi diagram of the same image. Two defects are visible in the crystal behind the tracer particle.
(c)(d) Confocal image and Voronoi diagram after the sample was translated over 1.4a_o and (e)(f) 3.0a_o respectively. The defects behind the tracer particle have been annealed out of the crystal.
The scale bar is 10 μm.

shown in *Figure 8.2b*, the defects can also clearly be seen. The cells are shaded according to the number of nearest neighbors: dark-gray for five, white for six, and light-gray seven nearest neighbors. The *Figures 8.2c-d* and *8.2e-f* show the sample after it was translated over 1.4a_o and 3.0a_o, respectively, with respect to *Figures 8.2a-b*. The defects visible in *Figure 8.2a* were annealed out of the crystal in *Figure 8.2e*.

Figures 8.3a-f show confocal images and Voronoi diagrams of the sample at a driving speed of 2.1 a_o/s. At this higher velocity the tracer induced many more defects in the crystal. The sample was displaced 0.28a_o and 0.56a_o between (a)-(c) and (c)-(e) respectively. A region of defects is

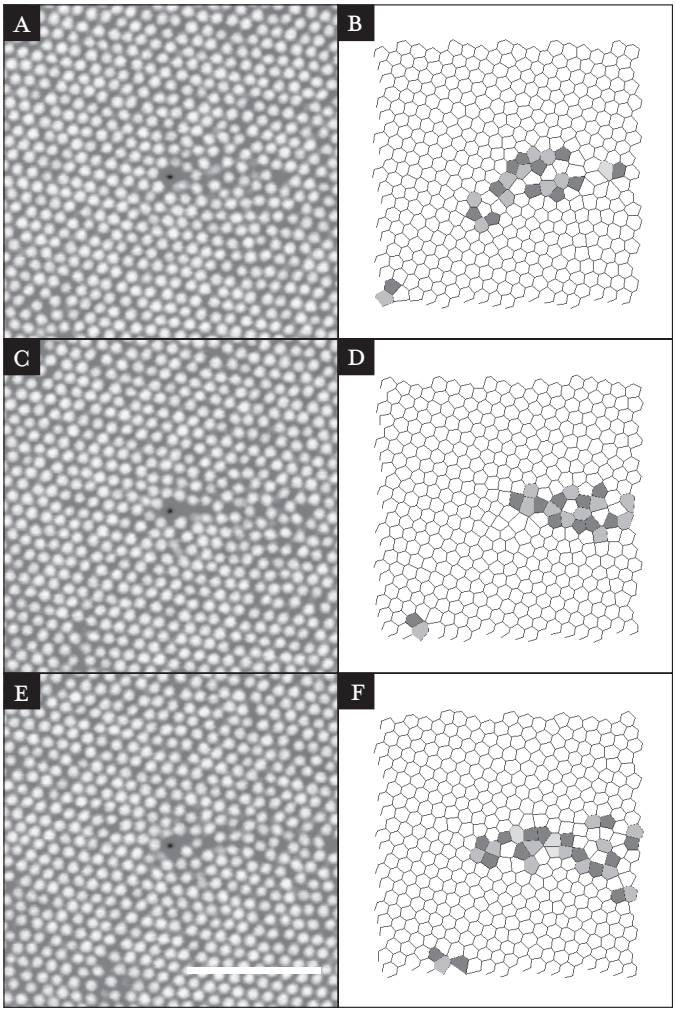

Figure 8.3
The crystal of host spheres was driven (from left to right) past the trapped tracer particle at a speed of 2.1 a_o/s.
(a) Confocal image and
(b) Voronoi diagram of the sample. The tracer particle induced many defects in the host crystal.
(c)(d) The sample after it was translated 0.28a_o and
(e)(f) 0.56a_o respectively.
At this driving speed, the wake of defects behind the tracer particle was always observed. It did not anneal out in the field of view of the microscope.
The scale bar is 10 μm.

visible behind the tracer particle. This wake was not seen to anneal out in the field of view of the microscope. We observed host particles being pushed in front of the tracer particle for several particle diameters. The response of the crystal to the tracer particle was qualitatively similar to that observed in computer simulations on two-dimensional crystals.[8] In those simulations, a strong dependence of defect generation on the crystal orientation with the driving direction was observed.[9] We expect this dependence also for our three-dimensional system, but we have not investigated it yet.

8.4 Conclusions and outlook

In this chapter we have presented initial experiments on a particle driven through a three-dimensional colloidal crystal. Optical tweezers were used to trap a tracer particle inside a three-dimensional colloidal crystal of host spheres. The host spheres had nearly the same refractive index as the solvent and negligible optical forces were exerted on them. The crystal was dragged past the trapped tracer particle at constant velocities. Both tracer and host spheres were imaged using confocal microscopy. Although we have only shown results in a two-dimensional plane, full three-dimensional quantitative imaging was possible and will be used in future experiments.

The optical forces on the tracer particle were large enough to introduce defects in the host crystal without loosing the tracer particle from the trap. At low driving speed (0.27 a_o/s), the tracer particle generated defects in the crystal within a few particle diameters. Sometimes a defect lived longer and was observed behind the tracer particle. These defects were seen to anneal out in the field of view of the microscope. At higher speed (2.1 a_o/s), many more defects were generated. Behind the tracer particle a defect-rich wake was observed, similar to the locally molten region behind the particle as seen in two-dimensional simulations.[8] At this speed, host particles were observed to be pushed in front of the tracer sphere for several particle diameters. The response of the crystal to the tracer particle was qualitatively similar to that observed in simulations on two-dimensional crystals.[8] At the moment we are investigating defect formation in three-dimensional crystals quantitatively and in much more detail. Different interparticle potentials, crystal orientations, and driving speeds will be investigated. We are currently implementing a high-speed scanning-disk confocal (Yokogawa) on the optical tweezers setup. With this faster imaging system, the sample can be imaged at video rates and higher, and much higher driving speeds of the tracer are accessible.

Local friction of single particle(s) in a crystal can also be studied. Using a quadrant photo diode, available on our setup, it is possible to measure the force that the crystal exerts on the tracer particle. The accuracy and time resolution achievable is sub-pN and tens of kHz, respectively. Finally, we plan to investigate the elastic properties of colloidal crystals. For hard-sphere crystals, differences in elastic properties of FCC and HCP crystals have been predicted,[19] while highly charged BCC colloidal crystals

have been predicted to have a negative Poisson's ratio.[20] Both predictions should be verifiable using our colloidal model system in combination with the optical tweezers/confocal microscopy setup.

Acknowledgements

We gratefully acknowledge Didi Derks for synthesis of the DiIC particles and Paddy Royall for calculating the Voronoi diagrams.

References

1 *U. Gasser, E. R. Weeks, A. Schofield, P. N. Pusey, and D. A. Weitz, Real-space imaging of nucleation and growth in colloidal crystallization, Science 292, 258 (2001).*
2 *A. van Blaaderen, J. P. Hoogenboom, D. L. J. Vossen, A. Yethiraj, A. van der Horst, K. Visscher, and M. Dogterom, Colloidal epitaxy: Playing with the boundary conditions of colloidal crystallization, Faraday Discuss. 123, 107 (2003).*
3 *W. K. Kegel and A. van Blaaderen, Direct observation of dynamical heterogeneities in colloidal hard-sphere suspensions, Science 287, 290 (2000).*
4 *A. van Blaaderen, R. Ruel, and P. Wiltzius, Template-directed colloidal crystallization, Nature 385, 321 (1997).*
5 *A. Pertsinidis and X. S. Ling, Equilibrium configurations and energetics of point defects in two-dimensional colloidal crystals, Phys. Rev. Lett. 8709, 098303 (2001).*
6 *A. Pertsinidis and X. S. Ling, Diffusion of point defects in two-dimensional colloidal crystals, Nature 413, 147 (2001).*
7 *P. Habdas, D. Schaar, C. Levitt, and E. R. Weeks, Forced motion of a probe particle near the colloidal glass transition, Europhys. Lett. 67, 447 (2004).*
8 *C. Reichhardt and C. J. O. Reichhardt, Local melting and drag for a particle driven through a colloidal crystal, Phys. Rev. Lett. 92, 108301 (2004).*
9 *C. Reichhardt and C. J. O. Reichhardt, Directional locking effects and dynamics for particles driven through a colloidal lattice, Phys. Rev. E 69, 041405 (2004).*
10 *D. L. J. Vossen, A. van der Horst, M. Dogterom, and A. van Blaaderen, Optical tweezers and confocal microscopy for simultaneous three-dimensional manipulation and imaging in concentrated colloidal dispersions, Rev. Sci. Instrum. 75, 2960 (2004).*
11 *C. Graf, D. L. J. Vossen, A. Imhof, and A. van Blaaderen, A general method to coat colloidal particles with silica, Langmuir 19, 6693 (2003).*
12 *A. P. Philipse and A. Vrij, Preparation and Properties of Nonaqueous Model Dispersions of Chemically Modified, Charged Silica Spheres, J. Colloid Interface Sci. 128, 121 (1989).*
13 *L. Antl, J. Goodwin, R. Ottewill, and J. Waters, The preparation of poly(methyl methacrylate) latices in non-aqueous media, Colloids and Surfaces 17, 67 (1986).*
14 *A. I. Campbell and P. Bartlett, Fluorescent hard-sphere polymer colloids for confocal microscopy, J. Colloid Interface Sci. 256, 325 (2002).*
15 *A. van Blaaderen and P. Wiltzius, Real-space structure of colloidal hard-sphere glasses, Science 270, 1177 (1995).*
16 *J. C. Crocker and D. G. Grier, Methods of Digital Video Microscopy for Colloidal Studies, J. Colloid Interface Sci. 179, 298 (1996).*
17 *S. Pronk and D. Frenkel, Can stacking faults in hard-sphere crystals anneal out spontaneously?, J. Chem. Phys. 110, 4589 (1999).*
18 *J. P. Hoogenboom, D. Derks, P. Vergeer, and A. van Blaaderen, Stacking faults in colloidal crystals grown by sedimentation, J. Chem. Phys. 117, 11320 (2002).*
19 *S. Pronk and D. Frenkel, Large difference in the elastic properties of fcc and hcp hard-sphere crystals, Phys. Rev. Lett. 90, 255501 (2003).*
20 *R. H. Baughman, S. O. Dantas, S. Stafstrom, A. A. Zakhidov, T. B. Mitchell, and D. H. E. Dubin, Negative Poisson's ratios for extreme states of matter, Science 288, 2018 (2000).*

Summary

Using a laser beam that is focused down to a diffraction-limited spot, particles with a size ranging from several nanometers up to tens of micrometers can be trapped and manipulated. This technique, called optical tweezers, has become an important tool in fields like biology, physical chemistry, and (bio)physics. Optical tweezers are ideally suited to manipulate colloidal particles. They have been used to exert and measure forces between them. Colloidal particles can be tuned in size, shape, and chemical composition. Like atoms, they have a well-defined thermodynamical temperature because of their Brownian motion, and colloidal systems are used as a model system for atoms and to test statistical mechanical theories. Colloids also find application in the development of advanced materials like, for example, photonic crystals. Until now, selective manipulation of particles in a concentrated dispersion was not possible. Optical tweezers have been used in colloidal systems that had a very low particle concentration or were (almost) two-dimensional.

The work described in this thesis can, roughly, be divided into three parts. In *part I* the two main methodological advancements in this thesis are introduced. *Chapter 2* describes the setup developed for simultaneous three-dimensional manipulation and imaging of individual particles inside a concentrated colloidal dispersion. Manipulation is done using optical tweezers, while imaging is done using confocal microscopy. The use of two microscope objectives, one above and one below the sample, enables imaging to be completely decoupled from trapping. Different trapping (inverted, upright, and counter-propagating) and imaging modes are possible. Time-shared optical tweezers arrays, dynamically changeable and capable of trapping several hundreds of micrometer-sized particles, were created using acousto-optic deflectors (AODs). The setup can be used to trap three-dimensional colloidal structures with optical tweezers. Arrays of tweezers in two planes were created using a Pockels cell and polarizing beam splitters. The chapter also introduces the use of mixtures of tracer and host core-shell particles for selective trapping and manipulation of individual tracer particles inside a concentrated dispersion of host particles. The tracer particles could be trapped because of their high refractive index core, while no optical forces were exerted on the host particles, as they were refractive

index matched by the solvent. The core-shell geometry ensures the same interaction between all particles in the mixture. The host spheres could also be nearly density matched by the solvent and therefore did not sediment.

In *part II* of the thesis, optical tweezers and colloids are used to create arrays of nanoparticles on substrates. In *chapter 3*, a method is described for patterning substrates with colloidal particles in any designed two-dimensional structure. Using optical tweezers, particles are moved from a reservoir to a surface. Chemical surface modification or polyelectrolyte coating, of either the substrate or the colloids, makes the method generally applicable. Using this technique, large two-dimensional patterns can be fabricated, with full control over the position of each individual particle. The patterned structures can be dried without distortions due to surface tension forces using critical point drying. As examples we have shown positioning of 79 nm radius metallodielectric particles, and we used two-dimensional patterns to direct three-dimensional epitaxial crystal growth. High refractive index particles, interesting for photonic applications, that cannot be trapped in three dimensions with conventional single-beam optical tweezers, can be manipulated using counterpropagating tweezers. The method is inexpensive, relatively fast, and can be fully automated. Some first results of three-dimensional structures created by repeating the procedure of patterning were shown.

In *chapter 4*, the method described in chapter 3 to pattern surfaces was used to create structures of colloidal particles for nanolithography. In nanosphere lithography, a mask of colloidal particles is used for a deposition or etching step, which after mask removal, yields large arrays of nanoparticles. We resolve the two main limitations of nanosphere lithography. First, using optical tweezers, we extended the possible geometries of the colloidal masks from, self-organized, hexagonal to any desired symmetry and spacing. The size of the holes in the mask was controlled by MeV ion irradiation, which caused the colloids to expand in the in-plane direction and thus reduced the size of the holes. Modified masks were used for nanolithography, and after metal deposition and mask removal, large arrays of nanoparticles were created. Evaporation at different angles with respect to the mask gives additional control over structure and interparticle distance, allowing nanoparticles of different materials to be deposited next to each other. We have demonstrated large arrays of metal nanoparticles with dimensions

in the 15-30 nm range and with complete control over the interparticle distance and in-plane ordering.

In *chapter 5*, an alternative method is described to modify the size of the holes in colloidal masks for nanolithography. Using a wet-chemical method, a thin layer of silica is grown on masks of colloidal silica particles. The growth mechanism of the silica coating was found to be diffusion-limited, and the size of the holes can be controlled accurately using calibration and a seed dispersion. Using modified arrays of colloidal particles, nanoparticles with sizes down to tens of nanometers were created.

In *part III* of this thesis, optical tweezers have been used to manipulate crystallization in concentrated colloidal dispersions. In *chapter 6* a single optical trap was used to crystallize and melt colloidal dispersions without manipulating colloids on a single particle level. Crystallization was demonstrated near a wall for a range of particles sizes, refractive index contrasts, and numerical apertures. When a mixture of tracer and host core-shell particles was used, we could trap and manipulate the tracers and through their crystallization influence the host spheres. This technique to manipulate the concentration of particles can be used to study the critical nucleus size in a colloidal fluid close to crystallization as well.

In *chapter 7*, the first results on the local induction of homogeneous and heterogeneous crystal nucleation in concentrated colloidal dispersions have been demonstrated. An array of optical tweezers was used to manipulate individual colloidal tracer particles to create two- and three-dimensional structures of particles that acted as nuclei for colloidal crystallization. The symmetry and lattice spacing of the templates were varied inside the host dispersions. The volume fraction of the host spheres was varied, and the interparticle potential was tuned by adding different amounts of salt to the dispersion. The colloidal core-shell mixture in combination with the optical tweezers and confocal microscopy setup, allows detailed and controlled study of the early stages of nucleation and crystal growth. We demonstrated the feasibility to determine the critical nucleus size as a function of volume-fraction in a colloidal dispersion. Furthermore, the shape and symmetry of nuclei can be varied, and the effects of this on crystal growth rates and the size of a critical nucleus can be investigated. Because our experimental method is very close to methods used in computer simulations to study crystal nucleation, our results can be directly compared and even linked to such simulations.

Finally, *chapter 8* describes experiments on a single particle driven through a three-dimensional colloidal crystal. Using optical tweezers a tracer particle was trapped in the bulk of a three-dimensional colloidal crystal of host spheres. The crystal was moved past the trapped particle at constant velocities. The tracer and host particles were imaged using quantitative three-dimensional confocal microscopy. At low driving speed, defects were only formed within a few diameters from the tracer. Sometimes, a defect survived and lived for some time before it was annealed out by the crystal. At higher driving speed, many more defects were introduced behind the trapped particle, which were not annealed out within the field of view of the microscope. Similar behavior was reported in recent computer simulations on a two-dimensional version of our experiment.

Samenvatting

Colloïdale deeltjes, met een grootte van enkele nanometers tot tientallen micrometers, kunnen worden vastgepakt en verplaatst met een sterk gefocusseerde laserbundel. Zulke "optical tweezers" (of "pincet van licht") worden veel gebruikt in de biologie, de fysische chemie en de (bio)fysica. Je kunt niet alleen colloïdale deeltjes vastpakken en manipuleren, maar je kunt ook de krachten tussen de deeltjes meten.

Het is mogelijk om colloïdale deeltjes te maken met verschillende grootte, vorm, structuur en chemische samenstelling. Vanwege hun Brownse beweging hebben colloïden, net als atomen, een thermodynamische temperatuur. Daarom worden ze gebruikt als modelsysteem voor atomen en om statistisch mechanische theorieën te testen. Daarnaast gebruikt men colloïden bij het maken van geavanceerde materialen met bijvoorbeeld fotonische eigenschappen.

Tot nu toe was niet mogelijk om individuele deeltjes in een geconcentreerde dispersie selectief te manipuleren. Optical tweezers zijn alleen gebruikt in colloïdale dispersies met een zeer lage deeltjes concentratie of in dispersies met een tweedimensionale geometrie.

Het onderzoek beschreven in dit proefschrift kan verdeeld worden in drie delen. *Deel één* beschrijft de twee belangrijkste nieuwe methodes die we ontwikkeld hebben. *Hoofdstuk 2* introduceert de opstelling die we ontworpen en gebouwd hebben om colloïdale deeltjes te manipuleren en te bekijken in een geconcentreerde dispersie. Met een combinatie van optical tweezers en een confocale microscoop kunnen we dit in drie dimensies doen. We gebruiken twee microscoop objectieven, één boven en één onder het sample, zodat we de deeltjes kunnen vastpakken en tegelijkertijd het hele sample kunnen bekijken. Dit kan op verschillende manieren, bijvoorbeeld in een rechtopstaande, geïnverteerde of gecombineerde geometrie. We kunnen grote aantallen optical tweezers maken door een enkele laserbundel te verdelen over meerdere plaatsen in het sample. Dit doen we door de bundel snel door het sample te bewegen met zogenaamde acousto-optic deflectors (AODs). We hebben ook driedimensionale structuren van colloïden gecreëerd door op twee verschillende hoogtes in een sample optical tweezers te maken. Dit hebben we gedaan door de AODs te combineren met een Pockels cell.

Hoofdstuk 2 beschrijft ook het gebruik van mengsels van colloïdale "tracer" en "host" deeltjes. Hiermee kunnen we deeltjes individueel manipuleren in een geconcentreerde dispersie. De tracer deeltjes hebben een kern met hoge brekingsindex en daarom kunnen we ze vastpakken. Tegelijkertijd oefenen de optical tweezers geen krachten uit op de host deeltjes omdat die dezelfde brekingsindex hebben als het oplosmiddel. Bovendien zijn de onderlinge interacties hetzelfde omdat de verschillende deeltjes een zelfde oppervlak hebben. De host deeltjes kunnen we ook nog vrijwel gewichtsloos maken door ze in een oplosmiddel te brengen met dezelfde dichtheid als zij zelf.

In *deel twee* van dit proefschrift presenteren we structuren van nanodeeltjes die we met behulp van optical tweezers gemaakt hebben. In *hoofdstuk 3* beschrijven we een methode om colloïden vanuit een reservoir op een oppervlak te plaatsen. Het oppervlak is van tevoren gecoat zodat de deeltjes op het oppervlak blijven zitten door elektrostatische krachten. De gebruikte coating-technieken maken onze methode algemeen toepasbaar.

We kunnen grote tweedimensionale structuren maken waarbij we controle hebben over de positie van ieder deeltje afzonderlijk. Door middel van "kritisch punt drogen" is het mogelijk de structuren te drogen zonder verstoring door oppervlaktespanningkrachten. We laten structuren zien van (metallo)dielectrische deeltjes. Ook demonstreren we de mogelijkheid om op een tweedimensionale structuur een driedimensionaal kristal epitaxiaal te laten groeien. Daarnaast is het mogelijk om met twee tegen elkaar ingaande optical tweezers, deeltjes met een hoge brekingsindex vast te pakken en op een oppervlak te plaatsen. Deze hoge index deeltjes zijn interessant voor toepassingen in fotonische materialen, maar kunnen met normale, "enkelvoudige" optical tweezers niet vastgepakt worden. De methode is relatief goedkoop, snel en kan volledig worden geautomatiseerd. We tonen aan dat het in beginsel mogelijk is om zo, laag voor laag, driedimensionale structuren te maken.

In *hoofdstuk 4* beschrijven we een methode om maskers van colloïden te maken voor nanolithografie. We bieden daarbij een oplossing voor de twee grootste nadelen van het gebruik van colloïdale maskers voor nanolithografie. Met optical tweezers hebben we de mogelijke masker symmetrieën uitgebreid van hexagonaal-dichtstgepakt naar elke gewenste symmetrie. Verder veranderen we de grootte van de gaten tussen de colloïden door de maskers

te bestralen met hoog-energetische ionen. Deze gemodificeerde maskers gebruiken we vervolgens voor nanolithografie: na depositie van een metaal en verwijderen van het masker kunnen we structuren van nanodeeltjes maken. Door onder verschillende hoeken ten opzichte van het masker materialen te deponeren, hebben we complexe structuren gemaakt. In deze structuren zitten nanodeeltjes van verschillende materialen naast elkaar. We geven voorbeelden waarbij we volledige controle over de afstand tussen de nanodeeltjes en de symmetrie van de structuren hebben. De kleinste nanodeeltjes hadden een grootte van 15 tot 30 nm.

In *hoofdstuk 5* beschrijven we een andere methode om colloïdale maskers voor nanolithografie te bewerken. Hierbij brengen we met een natchemische methode een dun laagje glas aan op de maskers. Tijdens het coaten voegen we een oplossing met gekarakteriseerde colloïden toe. Omdat het groeimechanisme diffusie-gelimiteerd is, is het mogelijk om de dikte van de aangegroeide laag op de maskers zeer nauwkeurig te beheersen. Daardoor kan ook de grootte van de nanodeeltjes nauwkeurig gekozen worden. Op deze manier hebben we deeltjes van enkele tientallen nanometers gemaakt.

In *deel drie* van dit proefschrift tonen we hoe je met optical tweezers de kristallisatie van geconcentreerde colloïdale dispersies kunt beïnvloeden. In *hoofdstuk 6* gebruiken we een enkele optical trap om geconcentreerde dispersies te bevriezen en te laten smelten. We laten zien dat kristallisatie bij een wand mogelijk is voor veel verschillende deeltjesgroottes, brekingsindices en openingshoeken van microscoop objectieven. In een mengsel van deeltjes, konden we indirect de kristallisatie van host deeltjes beïnvloeden door de tracer deeltjes te laten kristalliseren. Op deze wijze is het mogelijk om de kritische kiemgrootte voor kristallisatie in een colloïdale dispersie bepalen.

In *hoofdstuk 7* laten we onze eerste resultaten zien waarbij we lokaal homogene en heterogene kristalnucleatie induceren. Dit doen we door met de optical tweezers tracers vast te pakken en deze vervolgens als kiem te laten dienen voor colloïdale kristallisatie. We hebben de invloed van de symmetrie en deeltjesafstand in de kiem onderzocht. Ook varieerden we de concentratie van de host deeltjes en pasten we de interactie tussen de deeltjes aan door zout toe te voegen aan de dispersies. Met de optical tweezers opstelling en het mengsel van colloïden is het mogelijk om op een gecontroleerde manier de vroege fases van nucleatie en kristalgroei te bestuderen. We demonstreren de mogelijkheid om de kritische kiemgrootte voor kristallisatie te bepalen

in dispersies met verschillende concentraties van host deeltjes. Daarnaast kun je de vorm en de symmetrie van de kristalkiemen variëren en het effect hiervan op de grootte van de kritische kiem en de kristalgroeisnelheid bestuderen. Omdat onze techniek lijkt op computersimulatiemethoden om kristalgroei te bestuderen, zijn onze resultaten direct te vergelijken met dergelijke simulaties.

Tot slot beschrijven we in *hoofdstuk 8* experimenten waarbij we een enkel deeltje vast pakken met optical tweezers en het dan door een driedimensionaal kristal van host deeltjes trekken. Bij lage snelheden ontstaan alleen defecten op korte afstand van het tracer deeltje. Soms bleef een defect enige tijd bestaan voordat het kristal zich weer herstelde. Bij hogere snelheden veroorzaakte het tracer deeltje veel meer defecten en bleven deze ook langer bestaan. Het kristal herstelde zich niet meer binnen het gezichtsveld van de confocale microscoop. Recent zijn vergelijkbare resultaten gepubliceerd voor computersimulaties aan een deeltje dat door een tweedimensionaal colloïdaal kristal werd gedreven.

Dankwoord

Aan dit proefschrift hebben veel mensen een bijdrage geleverd en ik ben hen daar erg dankbaar voor. Aan het eind van elk hoofdstuk noem ik met wie is samengewerkt en wie daarbij geholpen heeft. Hier wil ik nog een aantal mensen met naam noemen.

Als eerste wil ik Alfons van Blaaderen bedanken: zijn inbreng is op vrijwel elke pagina in dit proefschrift terug te vinden. Alfons, bedankt voor de vrijheid en het vertrouwen dat ik van je gekregen heb en voor mijn opleiding tot wetenschapper in dit interessante, interdisciplinaire onderzoek. Je creativiteit, je volledige toewijding aan de wetenschap en je "search for excellence" hebben me enorm geïnspireerd.

Aan de ontwikkeling van de opstelling met optical tweezers en confocale microscoop heb ik met Astrid van der Horst met heel veel plezier gewerkt. Astrid, je hebt een grote bijdrage aan dit proefschrift geleverd en ik ben je daar heel dankbaar voor. Door discussies met Cendrine Faivre-Moskalenko, Koen Visscher en Marileen Dogterom heb ik de optical tweezers pas goed leren begrijpen. Veel onderdelen van de opstelling zijn ontworpen door Dick Glastra van Loon en Joop van Dorsselaer, en gemaakt door Henk Neerings. Waarschijnlijk is er niemand in de werkplaats of tekenkamer op Amolf die niet een onderdeel van de opstelling in handen heeft gehad. Sjoerd Wouda, Marco Konijnenburg, Marco Seynen, Duncan Verheijde en Hans Wisman hebben veel bijgedragen op het gebied van software en elektronica. Henk den Hartog van Leica wil ik ook bedanken voor zijn toewijding aan de confocale microscoop.

Colloïden zijn een ander belangrijk ingrediënt van dit proefschrift. De synthese van deze fascinerende en onvolprezen systemen is een ware kunst. In mijn onderzoek heb ik gebruik gemaakt van dispersies van Jacob Hoogenboom, Peter Vergeer, Krassimir Velikov, Didi Derks, Christina Graf, Christina Christova, Arnout Imhof en Alfons van Blaaderen. Verder wil Arnout Imhof en Carlos van Kats bedanken voor hun hulp bij de synthese van de tracer deeltjes. Voor de TEM en EDX ondersteuning ben ik Carlos van Kats, Teun van Dillen, Hans Meeldijk, Katrien Keune en Carmen Zoldesi erg dankbaar.

Dit onderzoek ben ik begonnen op het FOM instituut Amolf in Amsterdam. Amolf is een bijzondere plek waar ik met veel plezier heb gewerkt. De (technische) ondersteuning is zeer waardevol geweest voor

mijn onderzoek en heb ik erg gewaardeerd. Een aantal mensen wil ik met (voor)naam noemen: Michiel, Anne-Marie, Miranda, Johan, Willem, Ed, Els, Trees, Grace en Wouter, bedankt. Op Amolf heb ik veel gediscussieerd en samengewerkt met (de groepen van) Daan Frenkel, Marileen Dogterom en Albert Polman. Verschillende hoofdstukken in dit proefschrift zijn daar uit voortgekomen. Ik wil hier de volgende mensen bedanken: Anna Tchebotareva, Michiel de Dood, Lenneke Sloof, Teun van Dillen, Joan Penninkhof en Jan van der Elsken, Sander Pronk, Angelo Cacciuto, Gerbrand Koster, Wouter Roos, Cendrine Faivre-Moskalenko, Marcel Janson, Jacob Kerssemakers, Chris Retif, Annebeth Kraij, Jan Verhoeven en Martin Jak. Met Anand Yethiraj, Jacob Hoogenboom en Krassimir Velikov heb ik de eerste jaren Alfons' groep gevormd en van hen heb ik veel geleerd.

Halverwege ben ik met opstelling en al naar Alfons' groep in Utrecht verhuisd. Ik wil de volgende mensen bedanken voor discussies, hulp en gezelligheid: Christina Christova, Didi Derks, Andrea Fortini, Antti-Pekka Hynninen, Dannis 't Hart, Astrid van der Horst, Mirjam Leunissen, Carlos van Kats, Joan Penninkhof, Svytoslav Savenko, Job Thijssen, Esther Vermolen, Yu Ling Wu, Carmen Zoldesi, María Delgado Flores, Arnout Imhof, Marjolein Dijkstra, Andrew Campbell, Paddy Royall, Matthias Schmidt, Johan Keijzer, Gerard van Lingen, Hans Wisman, Anand Yethiraj, Jacob Hoogenboom, Krassimir Velikov, Christina Graf, Patrick Johnson, Alexander Moroz en Hans Gerritsen.

Ik wil de studenten bedanken die me geholpen hebben tijdens dit onderzoek: Karin Overgaag, Damir Fific, Myrthe Plaisier en Floor van der Pavert: ik heb het met veel plezier gedaan, jullie werk heeft me veel opgeleverd.

Astrid van der Horst, Job Thijssen en Esther Vermolen bedankt voor het lezen van het manuscript. Floris Peeters heeft het ontwerp van dit proefschrift prachtig verzorgd.

Ook mijn familie en vrienden en alle lieve mensen om me heen wil ik bedanken voor jullie (indirecte) bijdrage aan dit proefschrift. Ik wil Jeanne, Joep en Marieke bedanken omdat ze er altijd voor me zijn. En tenslotte Jos-marien: dank je wel voor je steun, coaching en geduld gedurende de afgelopen jaren. We hebben al veel meegemaakt maar dit is nog maar het begin.

Curriculum Vitae

Dirk Leo Joep Vossen was born on January 29th 1975 in Weert, The Netherlands. The first four years of his life were spent in Nigeria. After returning to The Netherlands (Venray), he attended first primary and subsequently high school at the "Scholengemeenschap Jerusalem", where he obtained the Atheneum degree in 1993.

From 1993 onwards he studied experimental physics at Utrecht University. His M.Sc. project, on molecular biophysics, was carried out under supervision of dr. Marc van Zandvoort. During this project he had the opportunity to spend five weeks at the "European Laboratory for Non-linear Spectroscopy" in Florence, Italy. During his studies, he worked also on a research project in the groups of prof. dr. Albert Polman and prof. dr. Alfons van Blaaderen at the FOM institute AMOLF in Amsterdam. In 1999, he started his PhD-project in Alfons van Blaaderen's soft condensed matter group, initially at FOM-AMOLF and from 2002 onwards at Utrecht University. The results described in this thesis were published in scientific journals, and presented as invited oral presentations at international conferences.

Besides his scientific works, he was active in other fields. In 1996 he was a member of the lightweight freshmen's eight at Utrecht's student rowing club Orca. In 1997-98 he was president of Orca, for which he received a full-time grand from the Utrecht University. In that year, he also founded the "Bussinessclub Orca" to finance the (golden) Olympic goals of the ambitious rowing club. In 2001 he got an honorary award for his work at Orca. He was also member of the board of the national student rowing federation, president of the "Instituutsraad" at FOM-AMOLF, and vice-president of the "Centrale Ondernemings Raad" (COR) at FOM.

His spare time is spent in sports (squash, skiing, and scuba diving), literature, cooking, and traveling. His passion for science is threefold: fundamental science, its applications, and its connection with and impact on society.

List of publications

Publications related to the work described in this thesis:

1. *D. L. J. Vossen, A. van der Horst, M. Dogterom, and A. van Blaaderen, Optical tweezers and confocal microscopy for simultaneous three-dimensional manipulation and imaging in concentrated colloidal dispersions, Rev. Sci. Instrum. 75, 2960 (2004). (Chapter 2)*
2. *J. P. Hoogenboom, D. L. J. Vossen, C. Faivre-Moskalenko, M. Dogterom, and A. van Blaaderen, Patterning surfaces with colloidal particles using optical tweezers, Appl. Phys. Lett. 80, 4828 (2002). (Chapter 3)*
3. *D. L. J. Vossen, J. P. Hoogenboom, K. Overgaag, and A. van Blaaderen, Building two- and three-dimensional structures of colloidal particles on surfaces using optical tweezers and critical point drying, Materials Research Society Symposium Proceedings, 705, Y 6.8.1 (2002). (Chapter 3)*
4. *D. L. J. Vossen, D. Fific, J. Penninkhof, T. van Dillen, A. Polman, and A. van Blaaderen, Combined optical tweezers / ion beam technique to tune colloidal masks for nanolithography, Submitted (2004). (Chapter 4)*
5. *D. L. J. Vossen, J. Penninkhof, and A. van Blaaderen, Chemically modified colloidal masks for nanolithography, In preparation (2004). (Chapter 5)*
6. *D. L. J. Vossen, M. A. Plaisier, and A. van Blaaderen, Colloidal crystallization induced by optical gradient forces exerted by optical tweezers, accepted for publication in Proceedings of the Int. Soc. Opt. Eng. - SPIE, (2004). (Chapter 6)*
7. *D. L. J. Vossen et al., Colloidal crystallization induced via single particle control with optical tweezers, In preparation (2004). (Chapter 7)*
8. *D. L. J. Vossen et al., Defect formation induced by a particle driven through a three-dimensional colloidal crystal, In preparation (2004). (Chapter 8)*
9. *A. van der Horst, D. L. J. Vossen, K. Visscher, M. Dogterom, and A. van Blaaderen, 3D manipulation and imaging on single particle level in concentrated dispersions, To appear in "Microscopy and Analysis", (2005).*
10. *C. Graf, D. L. J. Vossen, A. Imhof, and A. van Blaaderen, A general method to coat colloidal particles with silica, Langmuir 19, 6693 (2003).*
11. *A. van Blaaderen, J. P. Hoogenboom, D. L. J. Vossen, A. Yethiraj, A. van der Horst, K. Visscher, and M. Dogterom, Colloidal epitaxy: Playing with the boundary conditions of colloidal crystallization, Faraday Discuss. 123, 107 (2003).*
12. *A. van Blaaderen, K. P. Velikov, J. P. Hoogenboom, D. L. J. Vossen, A. Yethiraj, R. P. A. Dullens, T. van Dillen, and A. Polman, in Photonic crystals and light localization in the 21st century, edited by C. M. Soukoulis (Kluwer, 2001), p. 239.*

Other publications:

1. *M. J. A. de Dood, L. H. Slooff, T. M. Hensen, D. L. J. Vossen, A. Moroz, T. Zijlstra, E. W. J. M. van der Drift, A. van Blaaderen, and A. Polman, in Photonic crystals and light localization in the 21st century, edited by C. M. Soukoulis (Kluwer, 2001), p. 555.*
2. *D. L. J. Vossen, M. J. A. de Dood, T. van Dillen, T. Zijlstra, E. van der Drift, A. Polman, and A. van Blaaderen, Novel method for solution growth of thin silica films from tetraethoxysilane, Adv. Mater. 12, 1434 (2000).*
3. *M. van Zandvoort, D. L. J. Vossen, G. van Ginkel, R. Torre, P. Bartolini, M. Ricci, J. Thomas-Oates, and H. Zuilhof, Spectral characterization of fluorescent 5-iodoacetamidotetramethylrhodamine and its N-acetylcysteine derivative, Physical Chemistry Chemical Physics 1, 4571 (1999).*

COLOFON
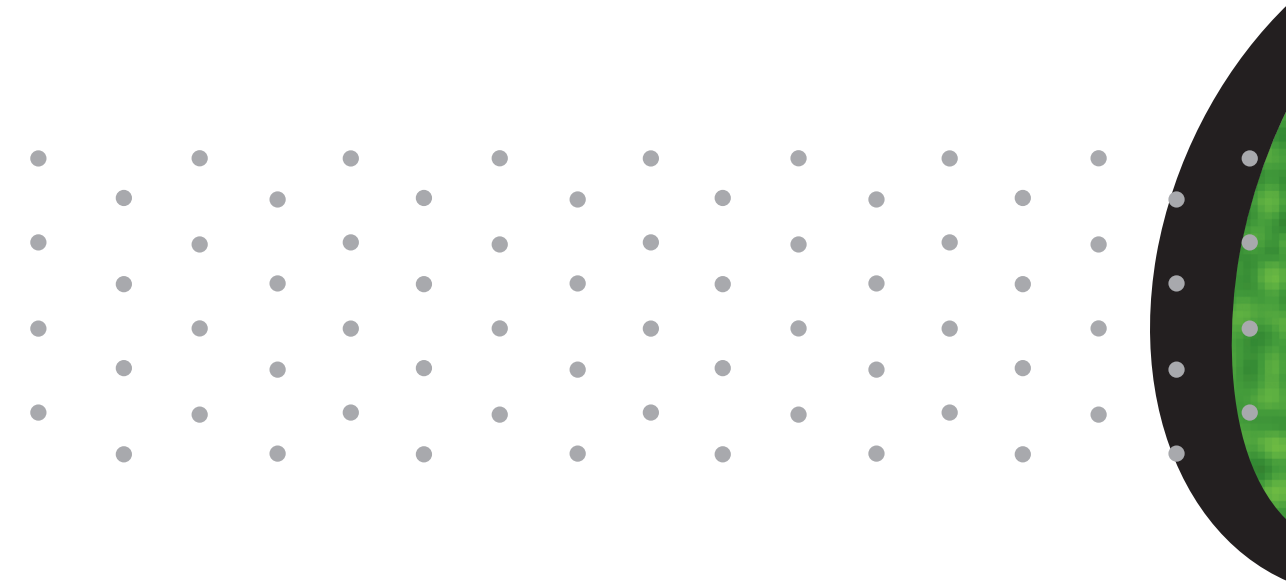
Ontwerp: Floris Peeters
Druk: Labor Grafimedia BV, Utrecht
Papier: het binnenwerk is gedrukt op 100 grs. Oxford. Het omslag is gedrukt op Oxford, 300 grs.
Oplage: 500 stuks
© Dirk Vossen, 2004